AD

USAAVLABS TECHNICAL REPORT 68-49C

AN INVESTIGATION OF THE DYNAMIC STABILITY CHARACTERISTICS OF A QUAD CONFIGURATION, DUCTED-PROPELLER V/STOL MODEL

VOLUME III

FINAL DATA REPORT
PHASE III - LATERAL/DIRECTIONAL DYNAMICS AT HIGH DUCT INCIDENCES

By

William F. Putman
Joseph J. Traybar
Howard C. Curtiss, Jr.
John P. Kuhon

November 1968

U. S. ARMY AVIATION MATERIEL LABORATORIES
FORT EUSTIS, VIRGINIA

CONTRACT DAAJ02-67-C-0025
PRINCETON UNIVERSITY
PRINCETON, NEW JERSEY

This document has been approved for public release and sale; its distribution is unlimited.

Disclaimers

The findings in this report are not to be construed as an official Department of the Army position unless so designated by other authorized documents.

When Government drawings, specifications, or other data are used for any purpose other than in connection with a definitely related Government procurement operation, the United States Government thereby incurs no responsibility nor any obligation whatsoever; and the fact that the Government may have formulated, furnished, or in any way supplied the said drawings, specifications, or other data is not to be regarded by implication or otherwise as in any manner licensing the holder or any other person or corporation, or conveying any rights or permission to manufacture, use, or sell any patented invention that may in any way be related thereto.

Trade names cited in this report do not constitute an offical endorsement or approval of the use of such commercial hardware or software.

Disposition Instructions

Destroy this report when no longer needed. Do not return it to the originator.

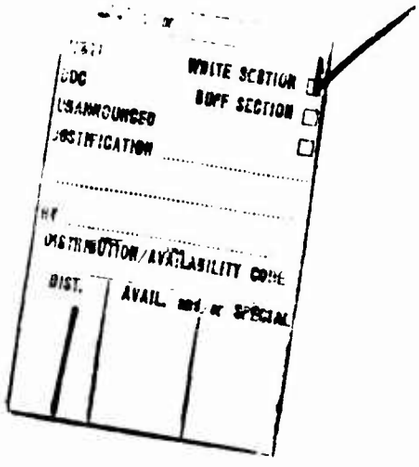

DEPARTMENT OF THE ARMY
U. S. ARMY AVIATION MATERIEL LABORATORIES
FORT EUSTIS, VIRGINIA 23604

This report has been reviewed by the U. S. Army Aviation Materiel Laboratories, the Naval Air Systems Command, and the Air Force Flight Dynamics Laboratories. It is considered to be technically sound.

This work, which was performed under Contract DAAJ02-67-C-0025, was undertaken to determine experimentally the lateral/directional dynamic stability characteristics of a quad configuration, four-duct V/STOL aircraft similar to the X-22A configuration at low speeds and high duct incidences. The Princeton Dynamic Model Track was utilized to perform the investigation.

This report is published for the exchange of information and the stimulation of ideas.

Task 1F162204A14233
Contract DAAJ02-67-C-0025
USAAVLABS Technical Report 68-49C
November 1968

AN INVESTIGATION OF THE DYNAMIC STABILITY CHARACTERISTICS OF A QUAD CONFIGURATION, DUCTED-PROPELLER V/STOL MODEL

Volume III

Final Data Report
Phase III - Lateral/Directional Dynamics at High Duct Incidences

Aerospace Sciences Report 847

By

William F. Putman
Joseph J. Traybar
Howard C. Curtiss, Jr.
John P. Kukon

Prepared by

Department of Aerospace and Mechanical Sciences
Princeton University
Princeton, New Jersey

for

U. S. ARMY AVIATION MATERIEL LABORATORIES
FORT EUSTIS, VIRGINIA

SUMMARY

The results of experiments to determine the lateral/directional dynamic stability characteristics of a quad configuration, ducted-propeller V/STOL aircraft at four low-speed/high-duct-incidence trim conditions (i_d = 80°, 70°, 60°, and 50°) are presented. Lateral/directional transient responses in various degrees of freedom were measured using a dynamic model on the Princeton Dynamic Model Track. The data presented include time histories of the model motions in various lateral/directional degrees of freedom that occur when the model is disturbed from trimmed flight.

The dynamic model employed in these experiments is a generalized research model arranged to represent closely the Bell X-22A V/STOL aircraft.

The data presented in this report comprise the third phase of a three-phase investigation of the dynamic stability characteristics of a quad configuration, ducted-propeller V/STOL aircraft at low speeds and high duct incidences. The other two phases pertain to the lateral and longitudinal hovering stability characteristics, presented in Reference 1, and the longitudinal characteristics at four low-speed/high-duct-incidence trim conditions presented in Reference 2.

FOREWORD

This research was performed by the Department of Aerospace and Mechanical Sciences, Princeton University, under the sponsorship of the United States Army Aviation Materiel Laboratories Contract DAAJ02-67-C-0025, with financial support from the United States Naval Air Systems Command and the Air Force Flight Dynamics Laboratory. The research was monitored by Mr. Robert P. Smith of the United States Army Aviation Materiel Laboratories.

The research was directed by Associate Professor H. C. Curtiss, Jr., and was conducted by Messrs. W. F. Putman, J. J. Traybar, and J. P. Kukon, all of Princeton University.

TABLE OF CONTENTS

LIST OF ILLUSTRATIONS

LIST OF SYMBOLS

b	propeller blade chord, feet
c	duct chord, feet
cg	center of gravity of pivoting mass of model
d	propeller blade diameter, feet
FS	fuselage station (horizontal reference), inches
g	acceleration due to gravity, feet per second squared
I_x	model moment of inertia in roll about principal axis, slug-feet squared
I_z	model moment of inertia in yaw about principal axis, slug-feet squared
i_d	duct incidence, degrees
k_{ϕ_m}	mechanical spring constant in roll, foot-pounds per radian (positive for normal spring restoring moment sense)
k_{ψ_m}	mechanical spring constant in yaw, foot-pounds per radian (positive for normal spring restoring moment sense)
L	vertical aerodynamic force of model in trimmed flight, pounds
L_p, L_r, L_v	stability derivatives, rate of change of rolling moment divided by inertia I_x with variable indicated in subscript
m	equivalent aerodynamic mass of model, slugs ($m = \frac{L}{g} = 1.60$ slugs)
m_ℓ	mass of lateral travel link, slugs ($m_\ell = 0.17$ slug)
m_p	pivoting mass of model, slugs ($m_p = 1.48$ slugs)
m_t	total mass accelerated by the model when translating laterally, slugs ($m_t = m_p + m_\ell = 1.65$ slugs)

$\frac{m}{m_t}$	ratio of equivalent aerodynamic mass of model to lateral translating mass ($\frac{m}{m_t} = 0.970$)
N_p, N_r, N_v	stability derivatives, rate of change of yawing moment divided by inertia I_z with variable indicated in subscript
p	model angular velocity in roll about principal axis, radians per second or degrees per second ($p = \dot{\phi}$)
R	propeller blade radius, feet
r	distance along propeller radius (measured from axis of rotation), feet; or model angular velocity in yaw about principal axis, radians per second or degrees per second ($r = \dot{\Psi} \cos \phi \approx \dot{\Psi}$)
$\frac{r}{R}$	propeller blade radial station
rpm	model propeller rotational speed, revolutions per minute
t	propeller blade thickness, feet
U	aircraft velocity along body-fixed X″-axis (principal axis system), feet per second
U_o	aircraft initial velocity along X″-axis (principal axis), feet per second
U_{o_f}	aircraft initial horizontal velocity (space-fixed axis system), feet per second
V_f	aircraft lateral velocity (space-fixed axis system), feet per second
V_{o_f}	aircraft initial lateral velocity (space-fixed axis system), feet per second
v	aircraft lateral perturbation velocity along body-fixed Y″-axis (principal axis system), feet per second
v_f	aircraft lateral perturbation velocity (space-fixed axis system), feet per second
W	model weight, pounds; or aircraft velocity along body-fixed Z″-axis (principal axis system), feet per second

W_f	aircraft vertical velocity (space-fixed axis system), feet per second
W_p	model pivoting weight, pounds (W_p = 47.5 lb)
W_{o_f}	aircraft initial vertical velocity (space-fixed axis system), feet per second
W_o	aircraft initial velocity along body-fixed Z″-axis (principal axis system), feet per second
WL	fuselage water line (vertical reference station), inches
X″	body-fixed longitudinal axis (principal axis system), coincides with model gimbal axis
X_f	longitudinal horizontal axis (space-fixed axis system
$\bar{X}_f$	longitudinal space axis
x_{cg}	longitudinal distance of cg from pivot axis, inches
x_{PIVOT}	longitudinal position of model pivot axis referenced to FS 0, inches (model scale unless noted)
$\bar{x}$	axial coordinate distance from duct leading edge, inches (full scale)
Y_f	lateral axis (space-fixed axis system)
$\bar{Y}_f$	lateral space axis
Y_v	stability derivative, rate of change of lateral horizontal force divided by mass m with lateral velocity, per second
$\bar{y}$	radial coordinate distance from duct center line, inches (full scale)
Z″	body-fixed vertical axis (principal axis system)
Z_f	vertical axis (space-fixed axis system), aligned with gravity
$\bar{Z}_f$	vertical space axis, coincides with model gimbal axis
z_{cg}	vertical distance of cg from pivot axis, inches

z_{PIVOT}	vertical position of model pivot axis referenced to WL 0, inches (model scale unless noted)
β	local propeller blade angle, degrees
β_F	average propeller blade angle on the two front propellers, degrees
β_R	average propeller blade angle on the two rear propellers, degrees
$\beta_{.75R}$	average propeller blade angle required for vertical force trim (collective pitch), measured at the three-quarter radius and averaged for four propellers, degrees
$\Delta L_{\dot{v}_{cg}}$	additional stability derivative due to vertical displacement of cg from pivot axis, per foot
ΔL_{ϕ_m}	additional stability derivative due to mechanical spring in roll, per second squared
$\Delta L_{\phi_{cg}}$	additional stability derivative due to vertical displacement of cg from pivot axis, per second squared
$\Delta N_{\dot{v}_{cg}}$	additional stability derivative due to horizontal displacement of cg from pivot axis, per foot
ΔN_{Ψ_m}	additional stability derivative due to mechanical spring in yaw, per second squared
$\Delta\beta_o$	longitudinal control required for pitching moment trim (differential collective pitch), degrees or radians
δ	elevon deflection, degrees (positive for elevon trailing edge forward with duct at 90 degrees incidence)
η	angle between model principal axis and fuselage reference line, degrees (positive for principal axis inclined downward) (6.1 degrees)
λ	linear scale factor $\lambda = \frac{\text{model length}}{\text{full-scale length}}$
ϕ	roll angle about model gimbal roll axis, degrees or radians
Ψ	yaw angle about model gimbal yaw axis, degrees or radians
$(\dot{})$	differentiation with respect to time

$( )'$ perturbed locations of axes

$\bar{( )}$ vector

INTRODUCTION

A series of experiments to determine the lateral/directional dynamic stability characteristics of a quad configuration, ducted-propeller V/STOL aircraft at low speeds and high duct incidences were conducted in the Princeton Dynamic Model Track. The data presented in this report, Phase III of a three-part test program, consist of time histories of the lateral/directional transient response characteristics of a dynamic model at four low-speed trim conditions in transition flight. Reference 1 presents experimental data from Phase I, an investigation of the hovering stability characteristics, and Reference 2 presents data from Phase II, concerned with the longitudinal dynamics at the same trim conditions as those of Phase III.

The dynamic model employed in these tests is shown in Figures 1 and 2. The model, described in Reference 3, was designed as a general research model with variable geometry and lifting system configuration such that a variety of quad V/STOL designs could be simulated. In the configuration selected for the tests described here, the model closely resembles a 0.145-scale dynamic model of the Bell Aerosystems X-22A V/STOL research aircraft. The model differs from actual aircraft (as given in Reference 4) in certain minor details, which are described in the section entitled DESCRIPTION OF APPARATUS, under MODEL.

The test program consisted of measurement of the transient response characteristics of the dynamic model in various lateral/directional degrees of freedom when disturbed from trimmed level flight at constant flight velocity. One of the features of the Princeton Dynamic Model Track (described in detail in Reference 5) is the ability to use the servo carriage to restrict the degrees of freedom of the model, such that response measurements can be conducted in various combinations of degrees of freedom as well as the three-degree-of-freedom lateral/directional motion. These restricted degree-of-freedom tests greatly assist in the analysis of the data for stability derivatives of the vehicle. Therefore, response measurements in this investigation included three-degree-of-freedom experiments (roll angle/yaw angle/lateral velocity), two-degree-of-freedom measurements (roll angle/yaw angle and roll angle/lateral velocity), and single-degree-of-freedom measurements (roll angle only and yaw angle only). The single-degree-of-freedom measurements are particularly useful for a direct determination of the angular damping characteristics of the vehicle.

The test conditions covered are given in Table I.

All data are presented in model scale and may be interpreted in terms of the full-scale vehicle (which the model closely resembles), using the conversion factors given in Table II.

DESCRIPTION OF APPARATUS

TEST FACILITY

The Princeton University Dynamic Model Track is a facility designed expressly for the study of the dynamic motions of helicopter and V/STOL models at equivalent flight speeds of up to 60 knots (for a one-tenth scale model). Basic components of the facility include a servo-driven carriage riding on a track 750 feet long, located in a building with a cross section of 30 by 30 feet; the carriage has an acceleration potential of 0.6g and a maximum speed of 40 feet per second. A detailed description of the facility and the testing techniques employed may be found in Reference 5.

A model can be attached to the carriage by one of several booms. The mount used to conduct lateral/directional investigation is shown in Figure 1. This mount permits lateral motion of the model in a direction perpendicular to the plane of the vertical and the carriage velocity vector. The model is supported on a three-axis gimbal system that allows selection of any or all of the three angular degrees of freedom. Lateral relative motion of the model with respect to the model-mount carriage is sensed and used to command this carriage to follow the lateral motion of the model in a closed-loop fashion. Thus the mass of the mount carriage does not influence the motions of the model. This method of testing may be considered to be similar to dynamic flight testing, but considerably more control over the experiment is possible.

The dynamic tests conducted during this program included one-, two-, and three-degree-of-freedom motion measurements. The transient behavior of the model was dominated in general by an unstable oscillation, so no predetermined control inputs were used to excite the model motions.

MODEL

The model is shown in Figure 2, and a three-view drawing is presented in Figure 3. The model's pertinent dimensions and inertia characteristics are listed in Table III, and the model reference stations are defined and compared with full-scale X-22A reference stations in Figure 4.

This dynamic model is powered by a 200-volt, 400-cycle, 3-phase electric motor. The motor drives the four ducted propellers through a central transmission and various right-angle gearboxes. The aerodynamic shape of the model is obtained through the use of a Fiberglas skin with Styrofoam stiffeners. The propeller blades are made with a plastic foam core and Fiberglas skin. The geometric characteristics of the propeller are shown in Figure 5, and the duct geometry is shown in Figure 6. The duct shape is identical to that of the Bell Aerosystems X-22A aircraft.

Model control positions are set from a control console on the carriage. The blade pitch angles on each of the four propellers are electrically controllable. Also, the deflection angles of the elevons are electrically controllable. All of these control systems are closed-loop position controls and are used as such in the portions of the experiments involving feedback to alter the transient motions of the model. The dynamic characteristics of these feedback loops are such that the time response of the controls is negligible in the frequency range of interest. Although the control servo loops are nonlinear, using polarized relays for power amplification, they can be characterized as having a closed-loop natural frequency of approximately 10 cycles per second with a damping ratio of approximately seven-tenths. The servo gear ratios were selected so that the rate limits arising from the rpm limitations of the control drive motors were equal to, or greater than, scaled rate limits determined from full-scale X-22A values.

This research model differs from the Bell Aerosystems X-22A flight aircraft in the following particulars:

1. The elevon on the model differs from that on the full-scale aircraft. The model elevon has no movable surface forward of the hinge line, and its hinge line is located below the trailing edge of the duct, as shown in Figure 7. While these differences would affect the control effectiveness and the control loads, they would not be expected to have any significant effect on the dynamic motions.

2. The duct rotation point is at a different location on the model (84 percent c) than on the full-scale aircraft (55 percent c).

   With the ducts at 90 degrees incidence, the propeller hubs are in the same relative position on the model as on the full-scale aircraft. The center of gravity of the model is higher (by 1.2 percent c) on the model with respect to the propeller hubs than on the full-scale aircraft.

3. As noted in Table I, the vertical tail used on the model for some single-degree-of-freedom experiments was smaller than the scaled X-22A vertical tail. A comparison of the two tail sizes tested is shown in Figure 3.

The only one of these differences that may influence the lateral/directional stability characteristics is the vertical tail size. Therefore the single degree of freedom in yaw experiments were done with both tail sizes at all but the lowest speed trim condition. All multiple-degree-of-freedom experiments were performed with the large (scale size) vertical tail.

EXPERIMENTAL RESULTS AND DISCUSSION

The experimentally determined trim conditions are shown in Figure 8 as graphs of trim velocity U_f and average propeller pitch $\beta_{.75R}$ as a function of duct incidence. The elevons were set at zero deflection angle for all tests. All experiments were conducted with the vertical aerodynamic force produced by the model equal to 51.5 pounds in trimmed flight, corresponding to a full-scale vehicle gross weight of 16,700 pounds at sea level. Strain gages were employed on the model mounting system to determine longitudinal force trim. By observing the strain gage readings, the model controls were set such that the vertical aerodynamic force was equal to the desired value of 51.5 pounds and the horizontal aerodynamic force was equal to zero (corresponding to level flight) at all trim conditions investigated. The trim conditions are identical to those of Reference 2. To eliminate extraneous moments from the gimbal mounting system, as were present in the tests described in Reference 6, all tests were conducted with the model free about the pitch axis. The pitch angle was maintained at its trim value by attitude and rate feedback about the pitch axis. The performance of this system was such that the pitch angle may be considered to be constant for all of the data presented here.

Transient response characteristics are presented about a gimbal axis system, as discussed in the Appendix. Time histories of the lateral/directional transient responses of the quad configuration V/STOL aircraft model from the level flight trim conditions at four duct incidences (i_d = 80°, 70°, 60°, and 50°) are presented in Figures 9 through 30. In most test conditions repeat data runs have been presented to aid in the analysis of the data and to indicate the repeatability of the experiments.

The responses shown include one-, two-, and three-degree-of-freedom time histories as discussed previously. The single-degree-of-freedom responses are presented to permit a direct determination of the angular damping characteristics of the model. These runs are presented in Figures 9 and 10, 14 through 16, 20 through 22, and 25 through 27. For the single-degree-of-freedom tests with the small vertical tail, mechanical springs were added to the model to provide a restoring moment about the model roll and yaw axes, such that the single-degree-of-freedom motions will be oscillatory. In this way the time histories are more readily analyzed for angular damping derivatives. The angular spring constants and the inertia characteristics of the model are given in Table III. Data are presented with the model motor off and the rpm equal to zero so that the mechanical damping of the model mounting system may be determined. This damping, due to friction, is very small compared to the total damping with the model running, but should be subtracted from the damping measured with the model running to determine the aerodynamic damping. For testing convenience the single- and multiple-degree-of-freedom experiments were performed at different pivot axis locations.

In contrast to the data of References 1 and 2, no feedback was used about the roll and yaw axes in these experiments. The lateral/directional motions of the model were dynamically unstable at all test conditions investigated.

All of the transient response time history data presented in Figures 9 through 30 have been conditioned by second-order filters with natural frequencies of 5 Hz and damping ratios of 0.7. However, in some of the model data channels, particularly the rate gyros and linear velocity tachometer, residual signals in the bandwidth of 2 to 10 Hz can still be seen. These signals are due to the flexible modes of motion of the model and/or gyro support structures or the high frequency transient response of the lateral servo and are not associated with the natural model rigid-body dynamic motions under investigation. In some cases, as for example in Figure 17, where there is a possibility that these spurious signals could be misinterpreted as data, a line has been faired to represent the model's true dynamic motions in the absence of the high frequency signals. In other cases, the transient response of the filters to momentary data loss within the telemetry system has produced data "drop-outs" which have also been faired to avoid misinterpretation.

The model angular velocity initial conditions at release are occasionally masked by the high frequency noise content of the rate gyro signals prior to release. Again, these data should not be interpreted as the rigid-body initial conditions; however, these portions of the time histories were not faired since the first portion of the transient response is of little value for analysis purposes due to the random excitation of the model transient motion. In general, all of the time histories of Figures 9 through 30 start at time zero minus, prior to release, and the initial conditions are as indicated on the data record. Exceptions to this are some single-degree-of-freedom data with model rpm equal to zero where time zero has been deleted because the initial excursions are of no value for analysis purposes.

TABLE I. SUMMARY OF TEST CONDITIONS

Tests conducted at model lift = 51.5 lb (except where rpm = 0).
All tests conducted without stability augmentation.

Duct Incidence i_d (deg)	Average Propeller $\theta_{.75R}$ (deg)	Propeller Speed (rpm)	Trim Velocity U_{o_f} (ft/sec)	Run Nos.	Fig. Nos.	Degrees of Freedom
80	25.2	6780	11	705 706	9**	ϕ*
		0	0	710		
		6780	12	715 718	10**	ψ*
		0	0	719		
		6780	10	1131	11	ϕ-ψ
				1122 1123 1125 1128 1129 1130	12	ϕ-v_f
				1136 1137 1138	13	ϕ-ψ-v_f
70	26.4	6780	21	733 736	14**	ϕ*
		0	0	737		
		6780	21	739 740	15**	ψ*
		0	0	742		
		6780	21	1239 1242	16	ψ
	25.6	6780	21	1164 1165	17	ϕ-ψ
	26.4	6780	21	1142 1156	18	ϕ-v_f
	25.6	6780	21	1157 1162	19	ϕ-ψ-v_f

TABLE I - Continued

Tests conducted at model lift = 51.5 lb (except where rpm = 0).
All tests conducted without stability augmentation.

Duct Incidence i_d (deg)	Average Propeller $\beta_{.75R}$ (deg)	Propeller Speed (rpm)	Trim Velocity U_{o_f} (ft/sec)	Run Nos.	Fig. Nos.	Degrees of Freedom
60	26.4	6780	27	753 756	20**	ϕ*
		0	0	758		
		6780	27	759 761	21**	ψ*
		0	0	763		
		6780	27	1224	22	ψ
	25.5	6780	29	1171 1172 1173 1174	23	ϕ-v_f
				1177 1180 1181 1184	24	ϕ-ψ-v_f
50	26.4	6780	36	773 775	25	ϕ*
		0	0	778		
		6780	36	779 782	26**	ψ*
		0	0	783		
		6780	36	1206 1208	27	ψ
	24.8	6780	38	1199	28	ϕ-ψ
				1191 1192	29	ϕ-v_f
				1193 1195	30	ϕ-ψ-v_f

*Mechanical spring in place.
**Small vertical tail.

TABLE II. SCALE FACTORS FOR DYNAMIC MODEL SIMILARITY

Multiply full-scale property by scale factor to obtain model property.

		For λ_L = 0.1453
Linear dimension	λ_L	0.1453
Area	λ_L^2	2.112×10^{-2}
Volume, mass, force	λ_L^3	3.071×10^{-3}
Moment	λ_L^4	4.463×10^{-4}
Moment of inertia	λ_L^5	6.487×10^{-5}
Linear velocity	$\lambda_L^{0.5}$	0.3812
Linear acceleration	λ_L^0	1.000
Angular velocity	$\lambda_L^{-0.5}$	2.623
Angular acceleration	λ_L	0.1453
Time	$\lambda_L^{0.5}$	0.3812
Frequency	$\lambda_L^{-0.5}$	2.623
Reynolds number	$\lambda_L^{1.5}$	5.541×10^{-2}
Mach number	$\lambda_L^{0.5}$	0.3812

$$\text{where } \lambda_L = \frac{\text{model linear dimension}}{\text{full-scale linear dimension}}$$

TABLE III. MODEL GEOMETRIC AND INERTIA CHARACTERISTICS

All tests conducted with model translating mass m_t = 1.65 slugs.

Duct Incidence i_d (deg)	Pivot Axis Location		Location of cg		Moment of Inertia About Pivot Axis		Mechanical Spring Rate		Figure Numbers
	x_{PIVOT} (FS)	z_{PIVOT} (WL)	x_{cg} (in.)	z_{cg} (in.)	I_x (slug-ft^2)	I_z (slug-ft^2)	k_{ϕ_m} (ft-lb/rad)	$k_{\dot{\psi}_m}$ (ft-lb/rad)	
80	44.45	20.10	0	0	1.41	2.97	9.1	0	9
							0	7.7	10
	45.70	20.10	2.47	0.37	1.57	3.84	none		11 thru 13
70	44.45	20.10	0	0	1.41	2.97	9.1	0	14
							0	7.7	15
	45.70	20.10	2.55	0.48	1.57	3.59	none		16 thru 19
60	43.95	20.05	0	0	1.41	2.97	9.1	0	20
							0	7.7	21
	45.70	20.10	2.47	0.60	1.54	3.72	none		22 thru 24
50	43.95	20.05	0	0	1.41	2.97	9.1	0	25
							0	7.7	26
	45.70	20.10	2.56	0.67	1.49	3.88	none		27 thru 30

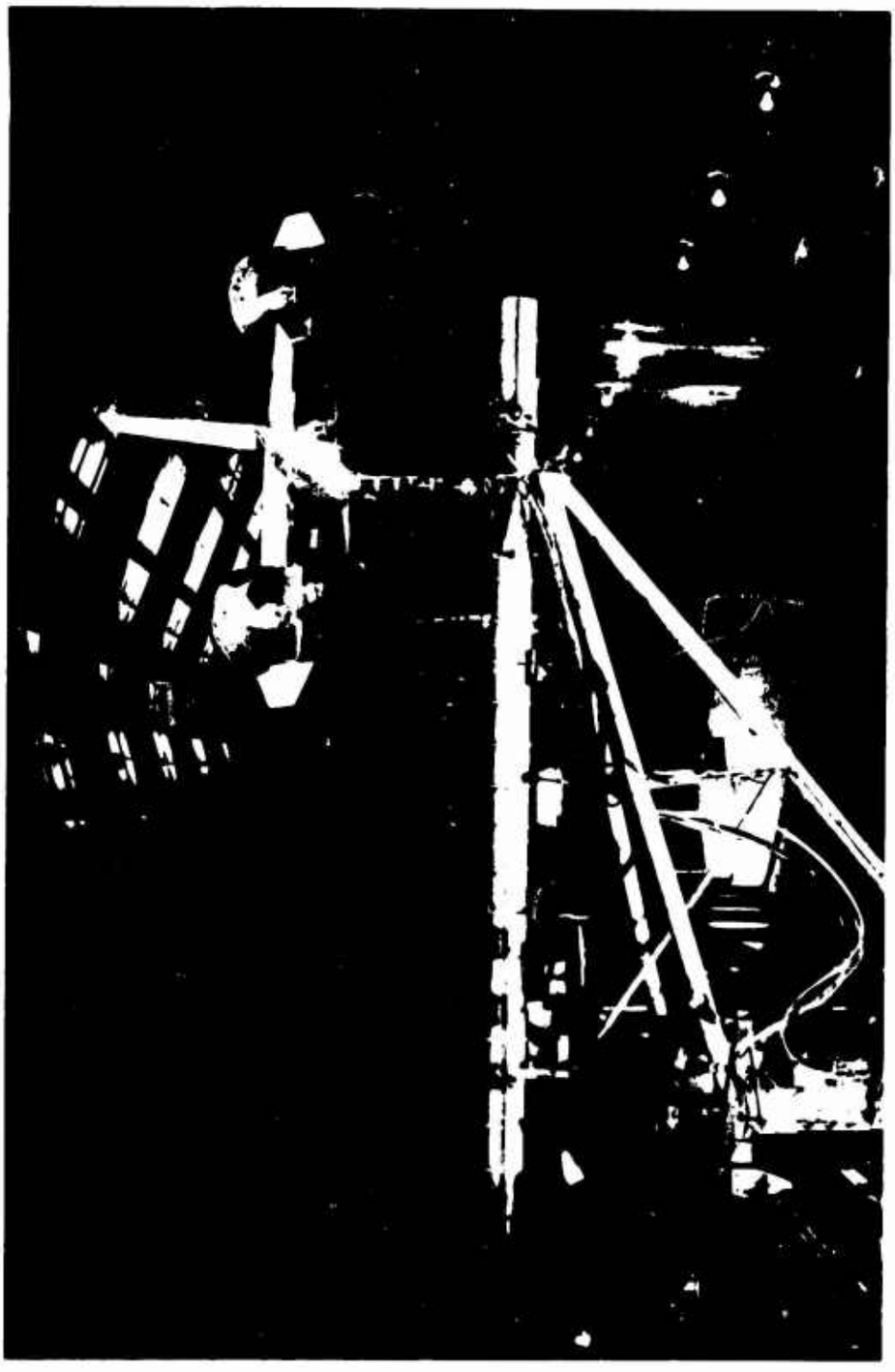

Figure 1. Princeton Dynamic Model Track, Showing Model Mounted on Lateral/Directional Dynamic Testing Apparatus.

Figure 2. 0.145-Scale Quad Configuration Dynamic Model.

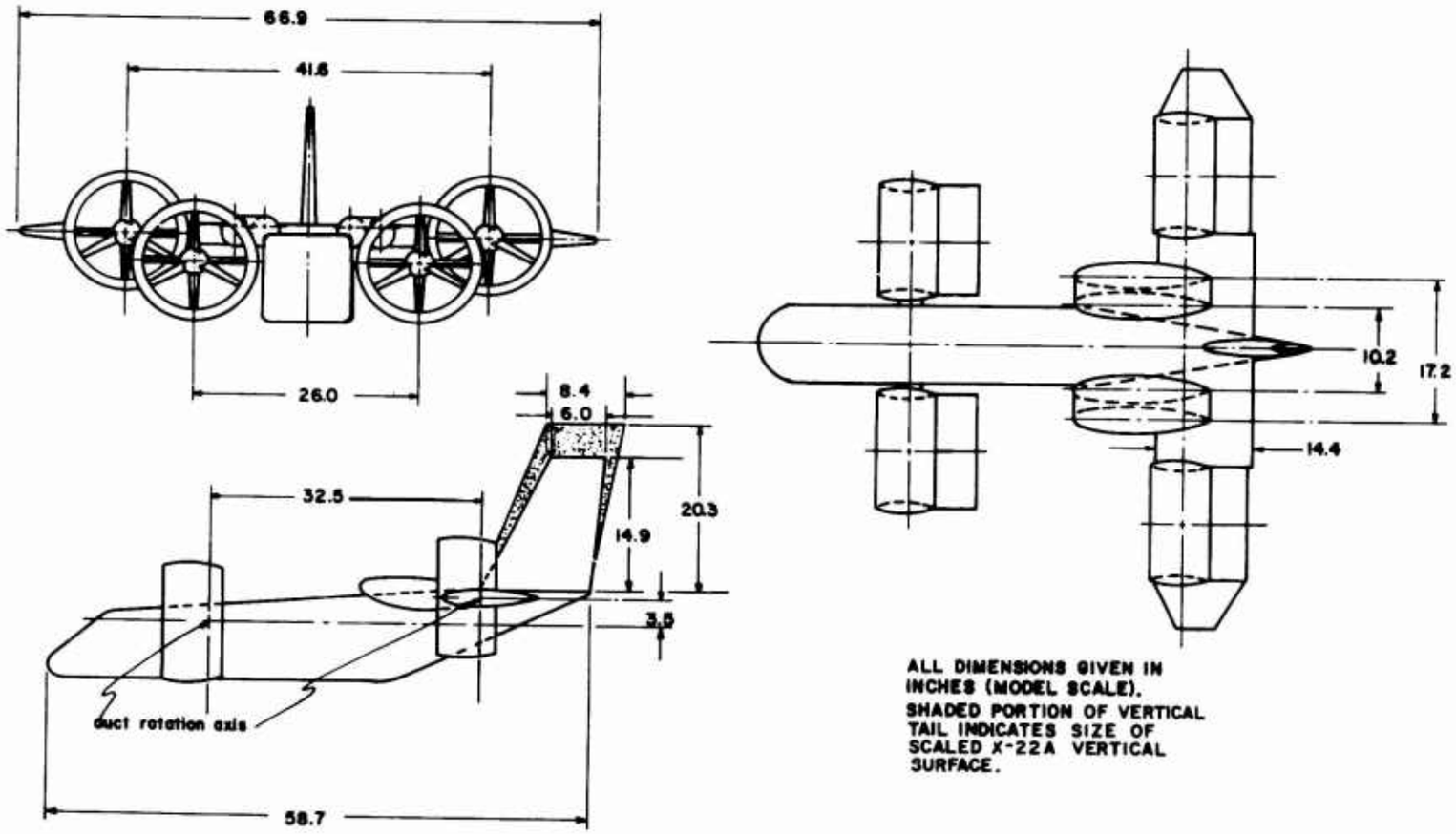

Figure 3. General Arrangement, Quad Configuration Dynamic Model.

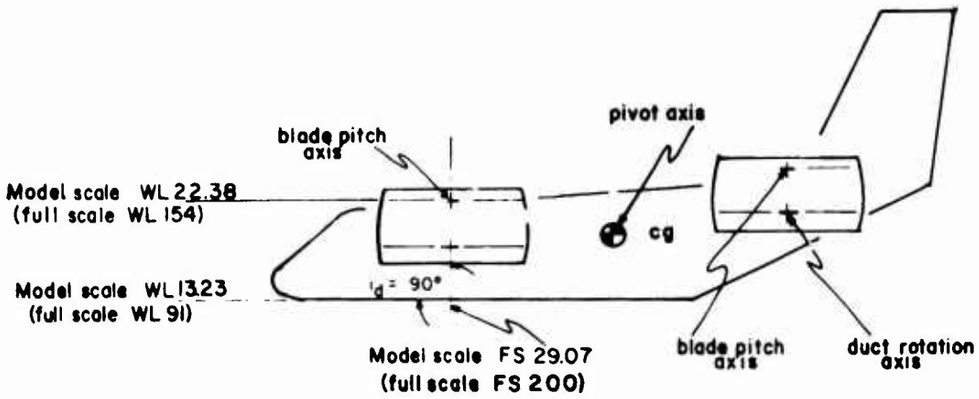

Note: 1.) Reference FS and WL locations shown do not change with duct rotation.

2) Pivot point is reference point for aerodynamic measurements of complete aircraft.

3) Model angular motions measured about pivot point.

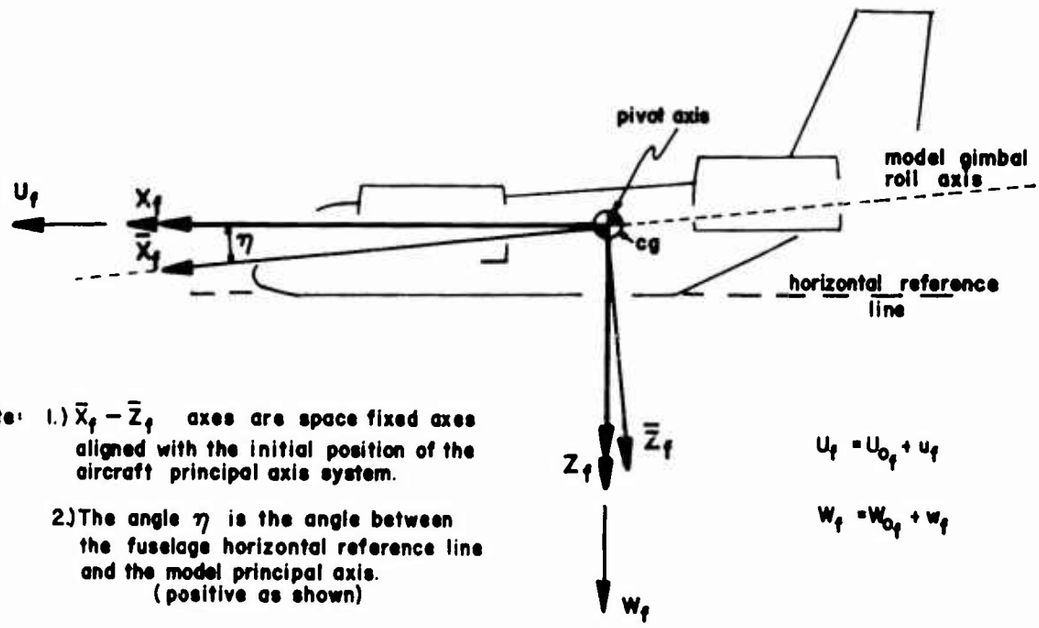

Note: 1.) $\bar{X}_f - \bar{Z}_f$ axes are space fixed axes aligned with the initial position of the aircraft principal axis system.

2.) The angle η is the angle between the fuselage horizontal reference line and the model principal axis. (positive as shown)

Figure 4. Model Reference Stations, Location of Model Center of Gravity and Axes Systems.

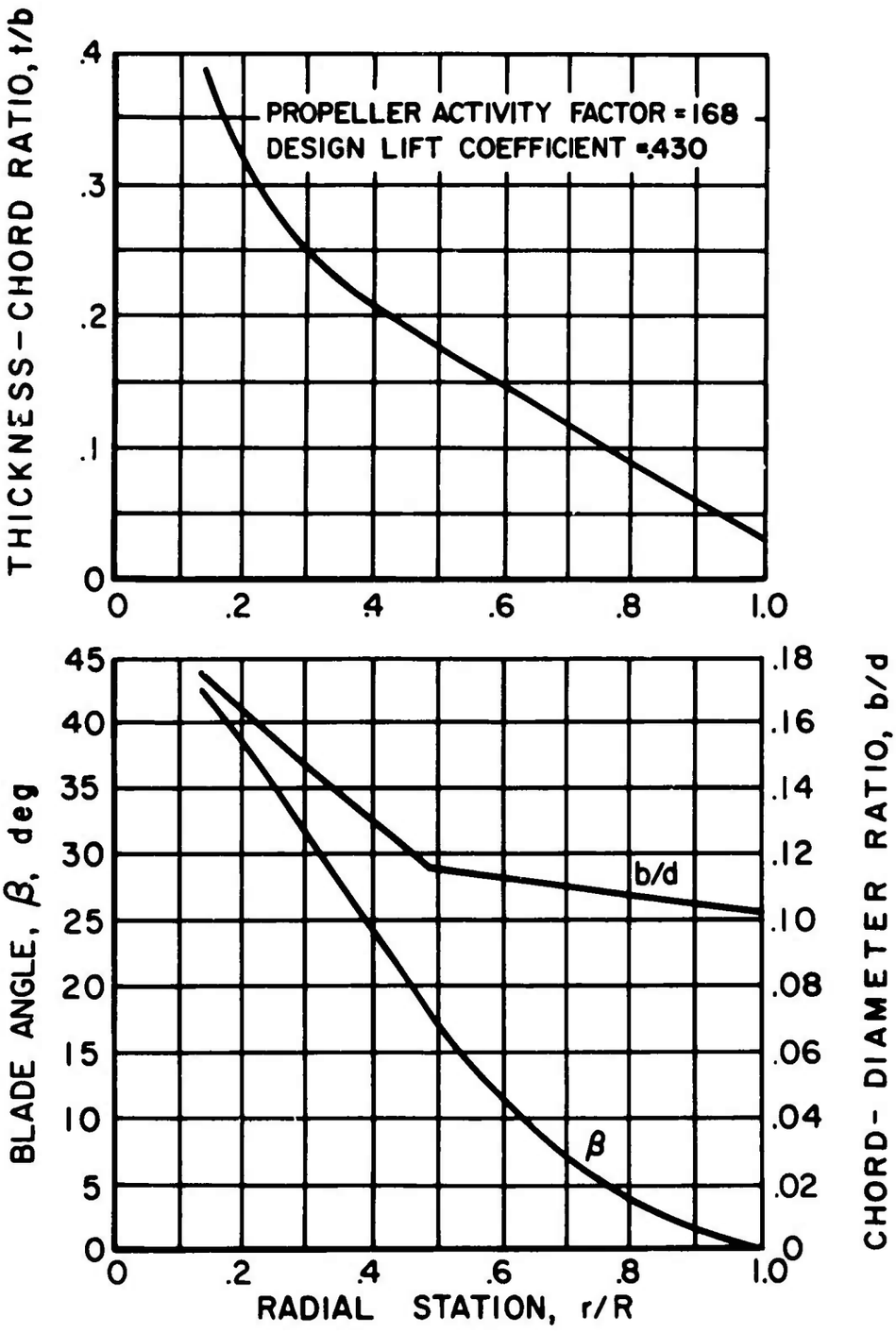

Figure 5. Geometric Characteristics of Three-Bladed Model Propellers.

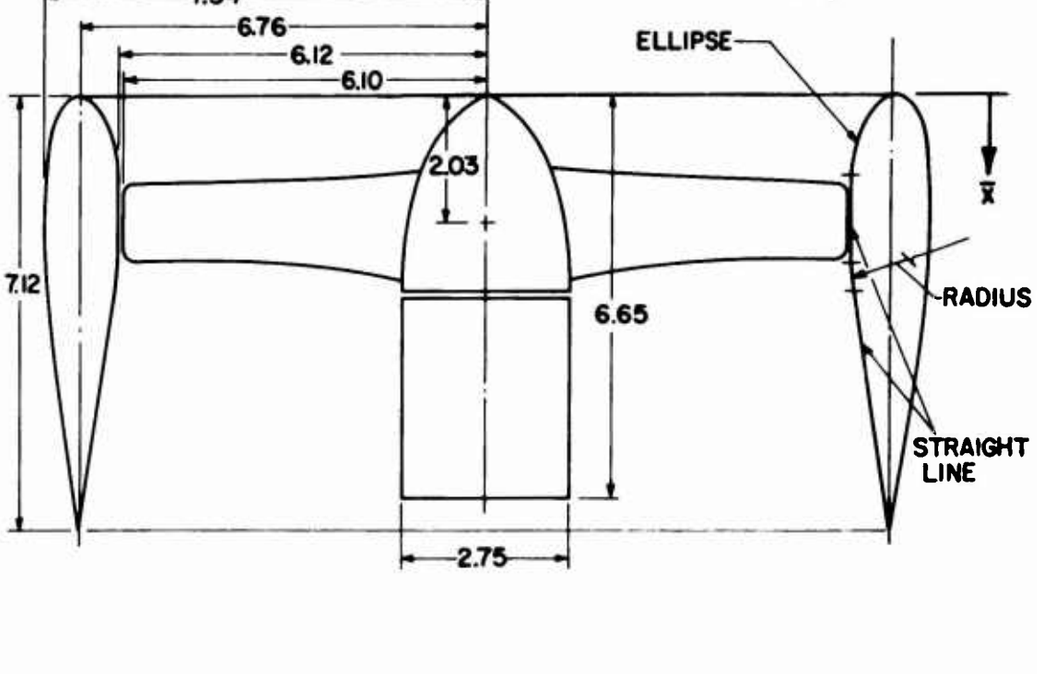

ALL DIMENSIONS ON ABOVE DRAWING IN INCHES (MODEL SCALE)

X-22A DUCT OUTER ORDINATES (FULL SCALE)	
x̄	ȳ
0	47.625
0.613	48.695
1.225	49.096
2.450	49.609
3.675	49.953
4.900	50.205
7.350	50.535
9.800	50.710
10.250	—
12.250	50.779
14.700	50.763
17.750	—
19.600	50.552
23.700	—
24.500	50.164
29.400	49.649
34.300	49.038
39.200	48.344
44.100	47.576
46.550	47.160
49.000	46.722

Figure 6. Geometric Characteristics of Scaled Model Ducts.

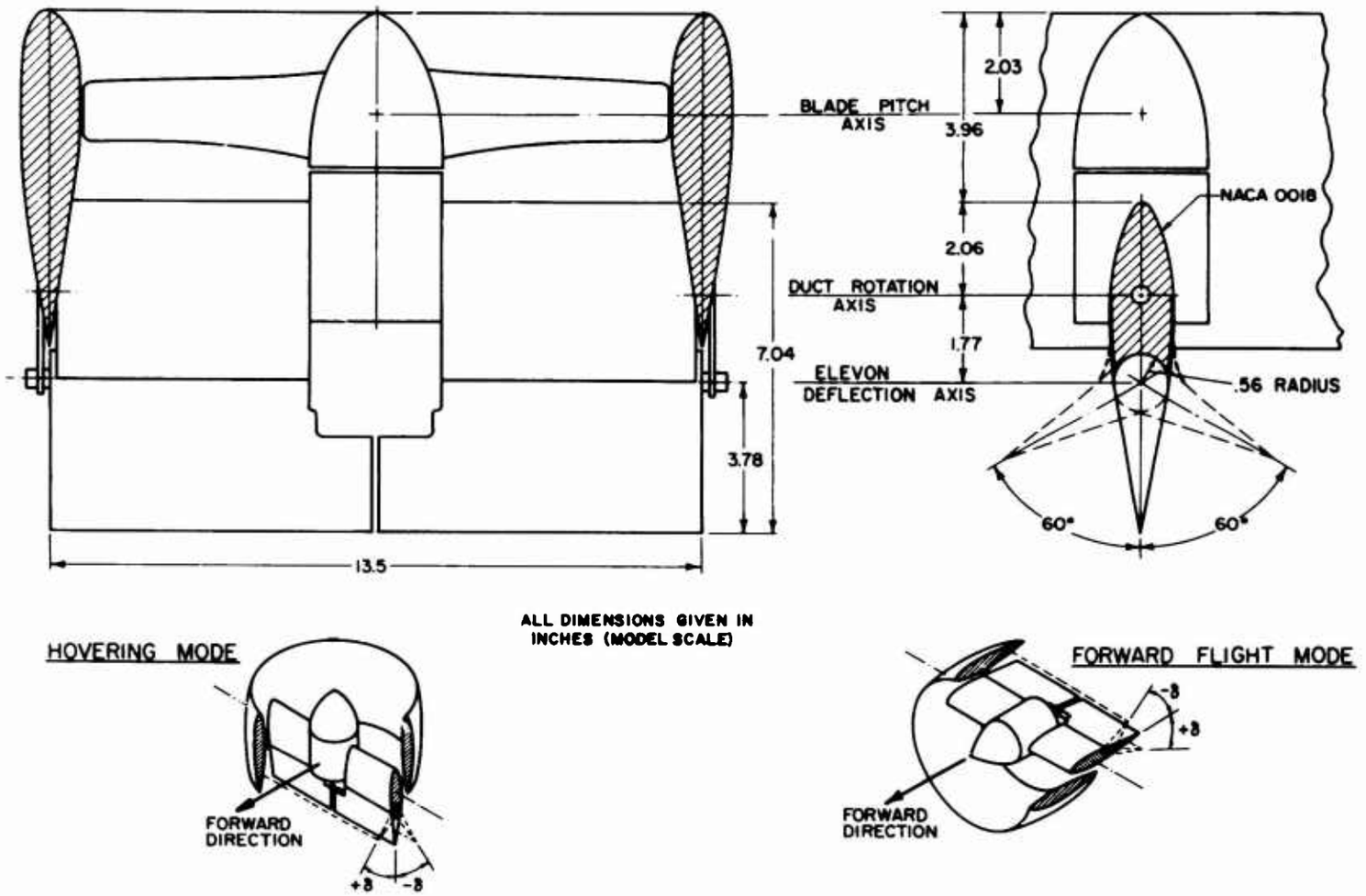

Figure 7. Geometric Characteristics and Reference Locations for Model Duct System.

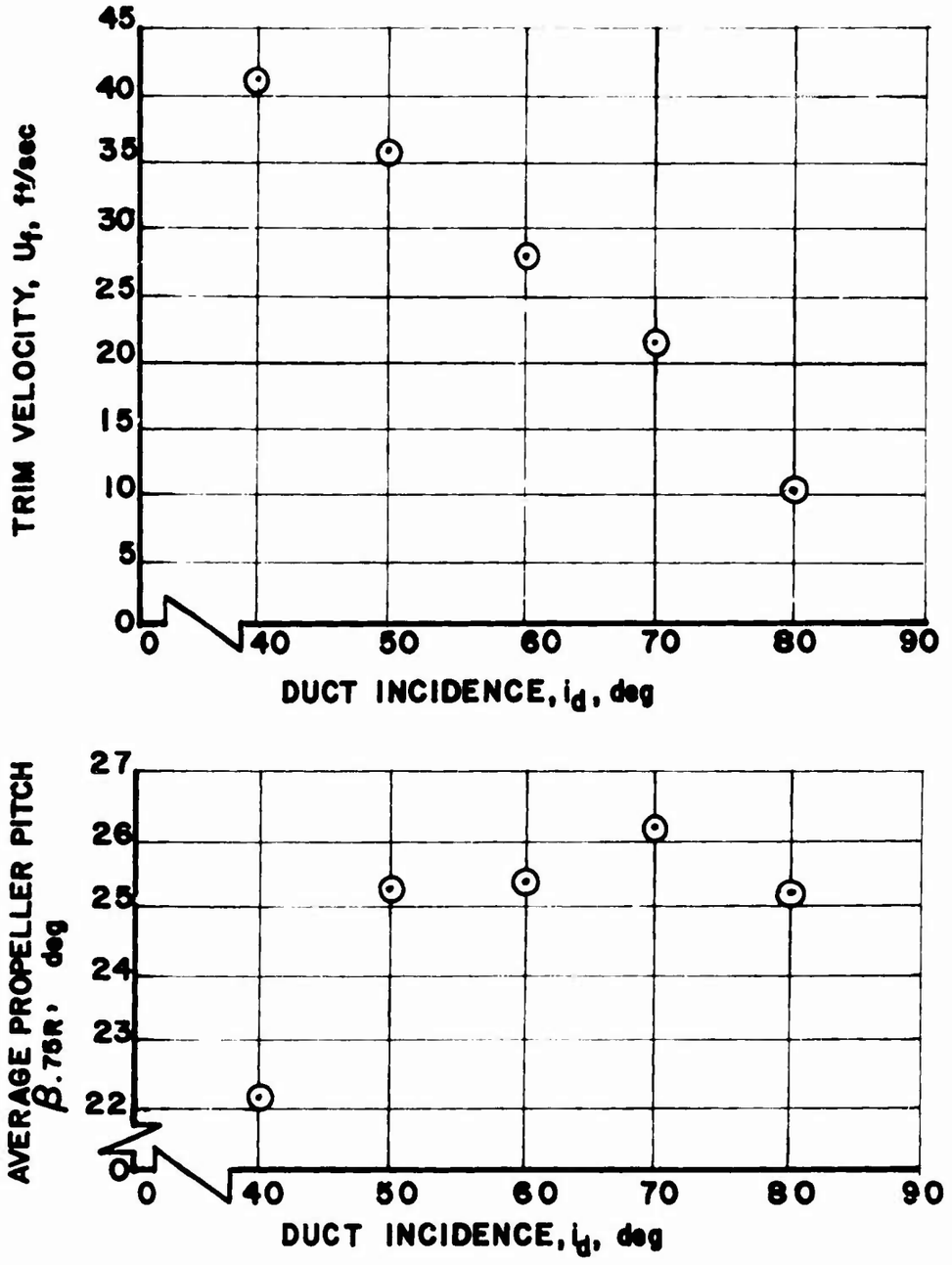

Figure 8. Experimental Data, Model Trim Conditions.
Model Lift = 51.5 lb, rpm = 6780.

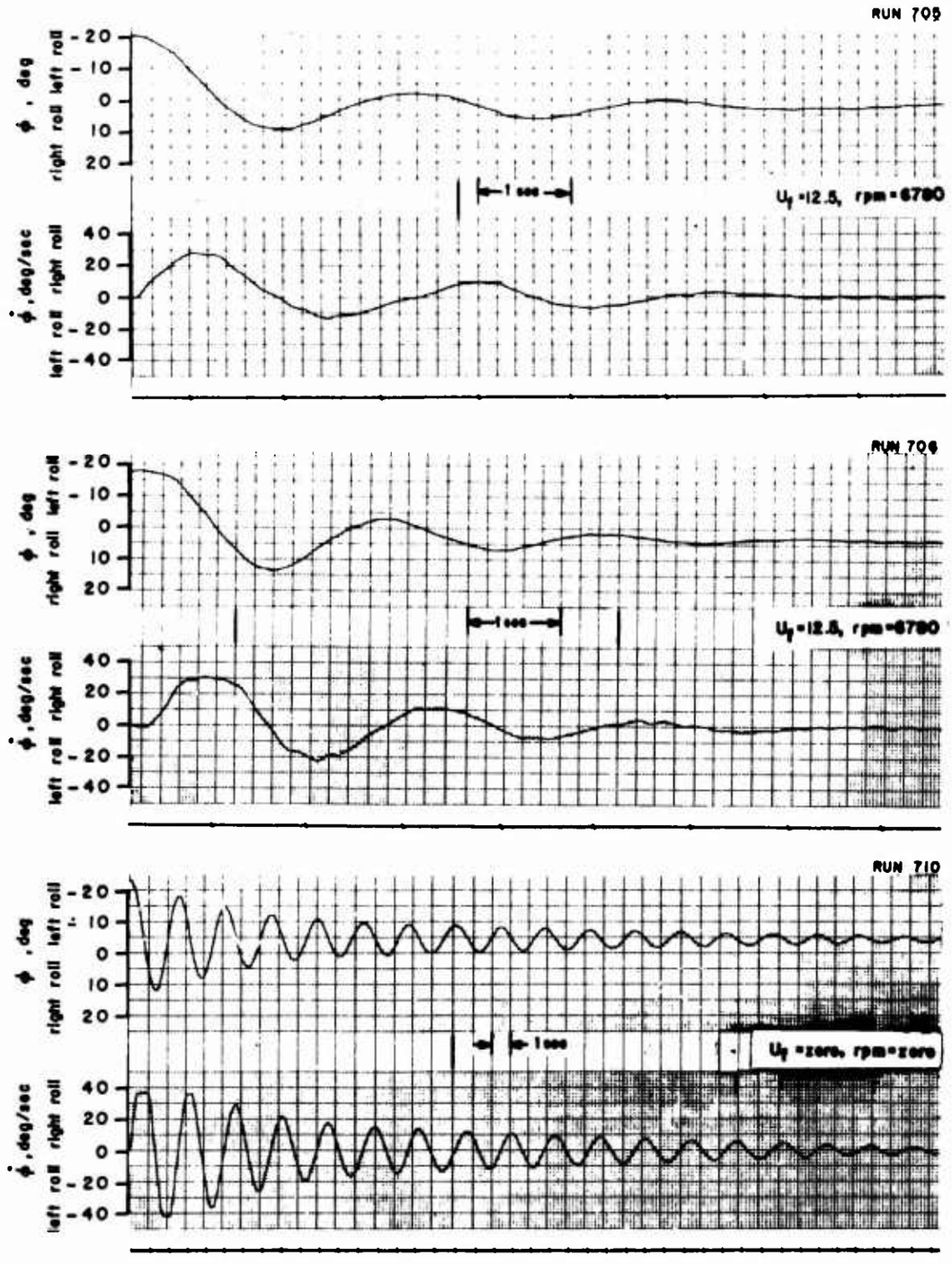

Figure 9. Lateral Transient Response. One Degree of Freedom, ϕ.
$i_d = 80^\circ$, $\beta_{.75R} = 25.2^\circ$, $\Delta\beta_o = 1.6^\circ$,
Small Vertical Tail, Spring Restrained

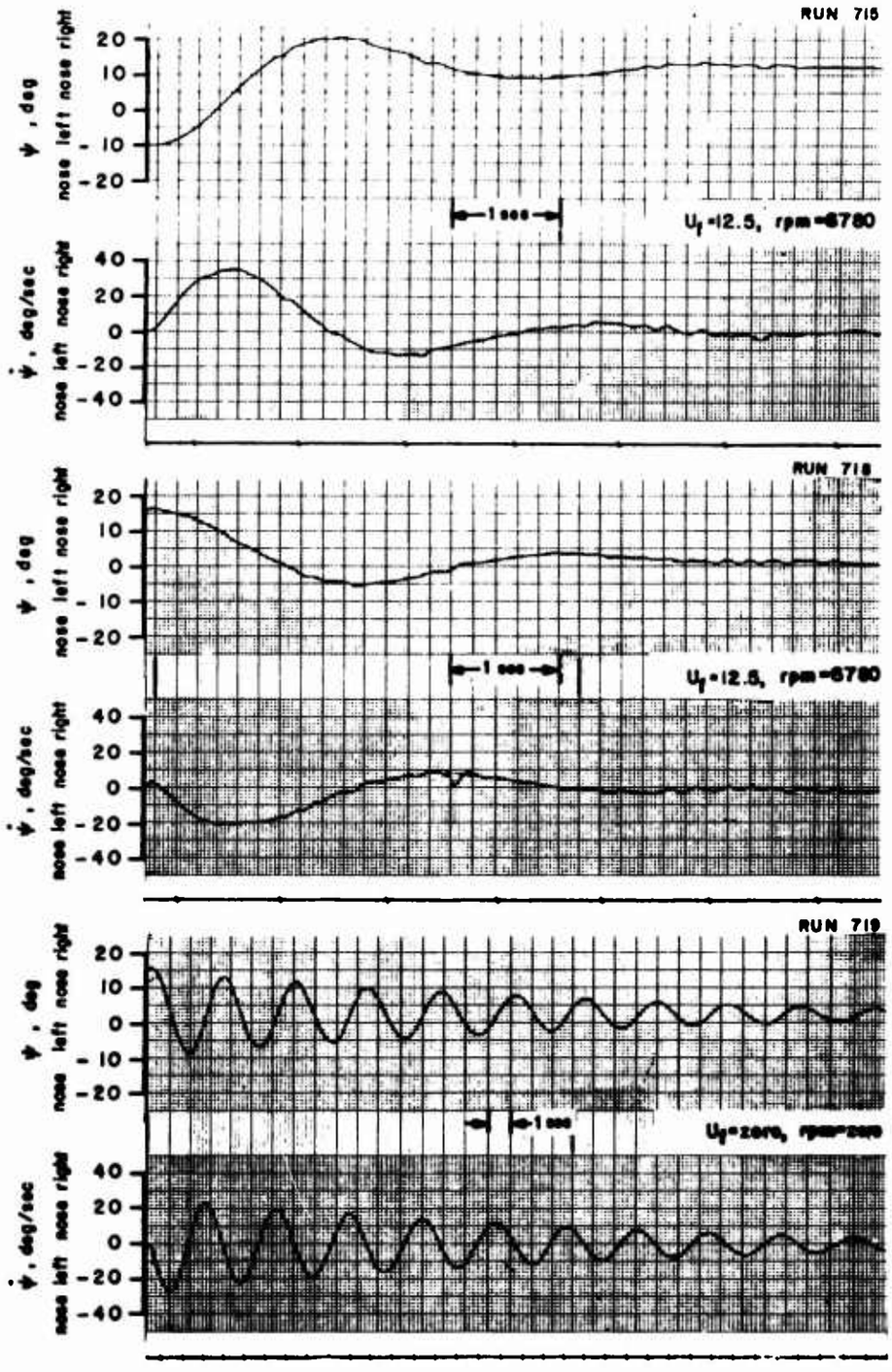

Figure 10. Directional Transient Response. One Degree of Freedom, Ψ.
$i_d = 80^\circ$, $\beta_{.75R} = 25.2^\circ$, $\Delta\beta_o = 1.5^\circ$,
Small Vertical Tail, Spring Restrained.

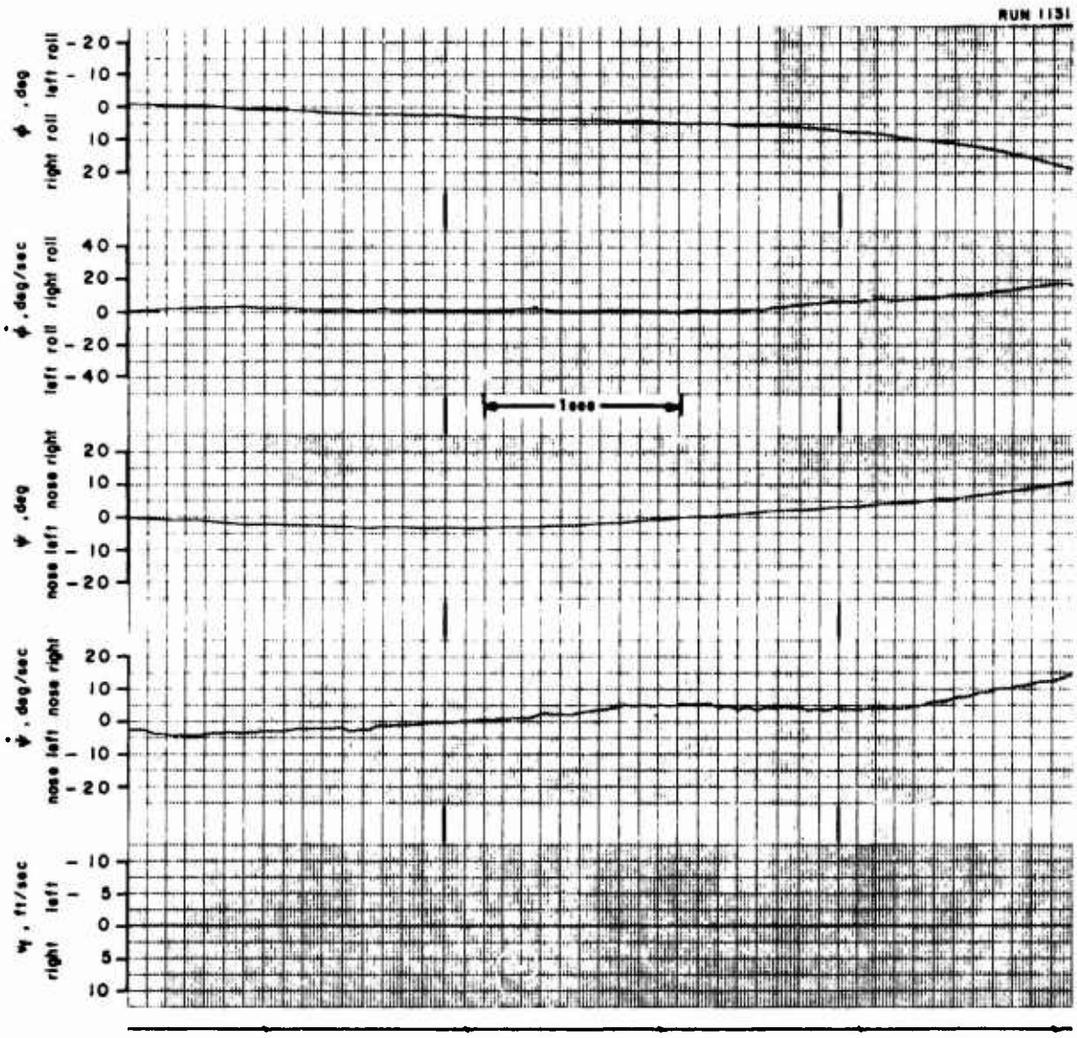

Figure 11. Lateral/Directional Transient Response. Two Degrees of Freedom, ϕ-Ψ. $i_d = 80^\circ$, U_{o_f} = 10 ft/sec, $\beta_{.75R} = 25.2^\circ$, rpm = 6780, $\Delta\beta_o = 0.5^\circ$, Large Vertical Tail.

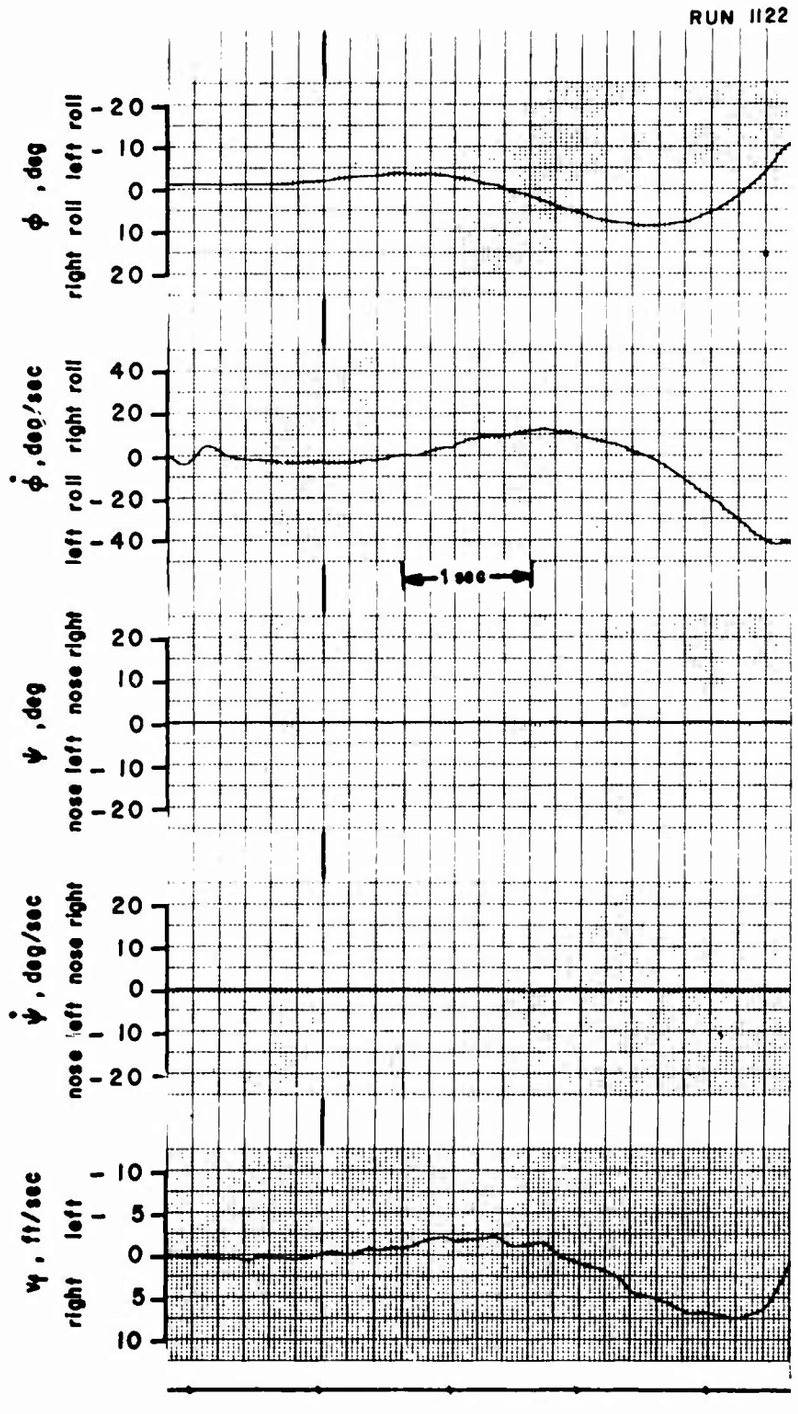

Figure 12. Lateral/Directional Transient Response. Two Degrees of Freedom, ϕ-v_f. $i_d = 80°$, $U_{o_f} = 10$ ft/sec, $\beta_{.75R} = 25.2°$, rpm = 6780, $\Delta\beta_o = 0.5°$, Large Vertical Tail.

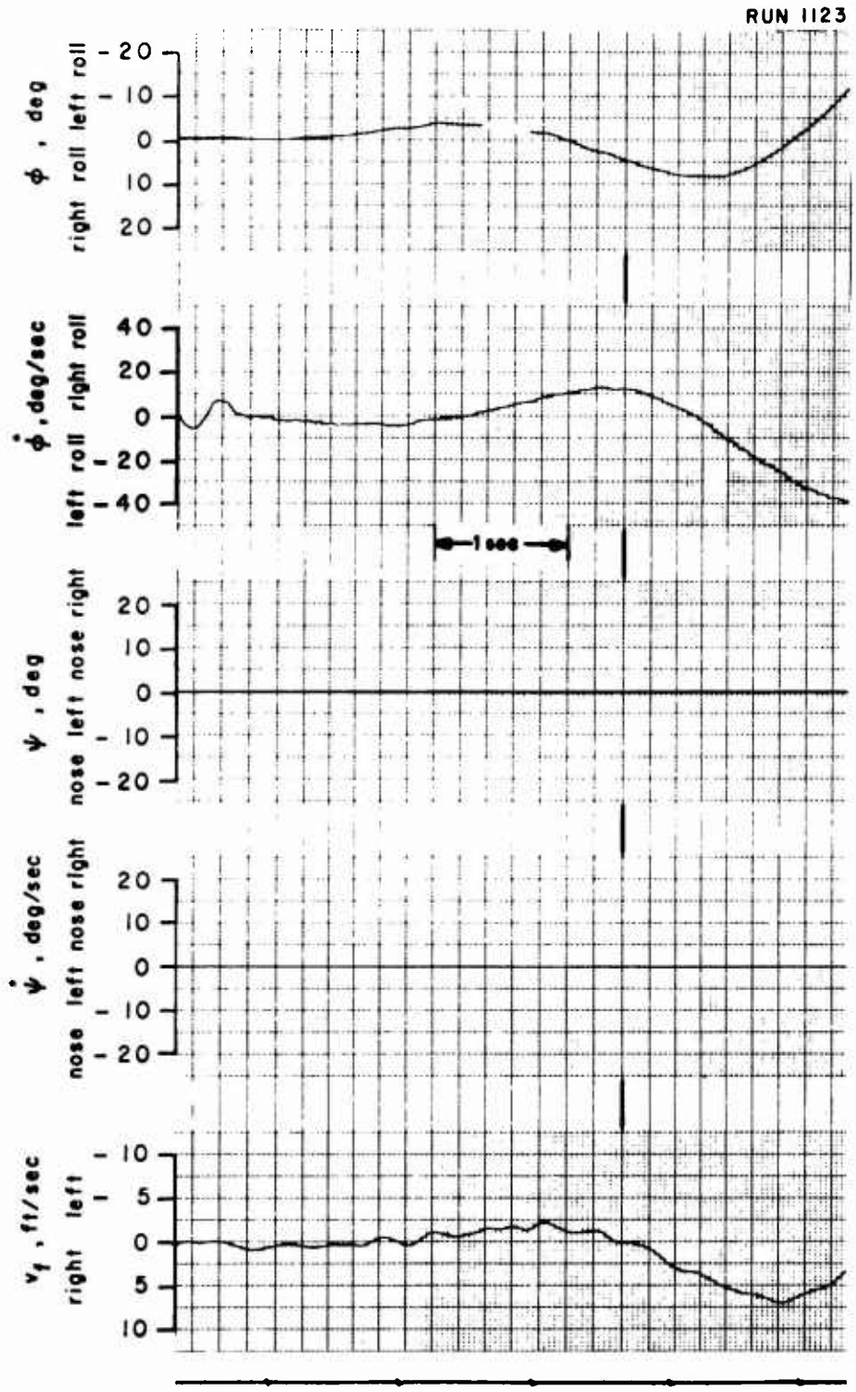

Figure 12. Lateral/Directional Transient Response. Two Degrees of Freedom, ϕ-v_f. $i_d = 80°$, U_{o_f} = 10 ft/sec, $\beta_{.75R} = 25.2°$, rpm = 6780, $\Delta\beta_o = 0.5°$, Large Vertical Tail.

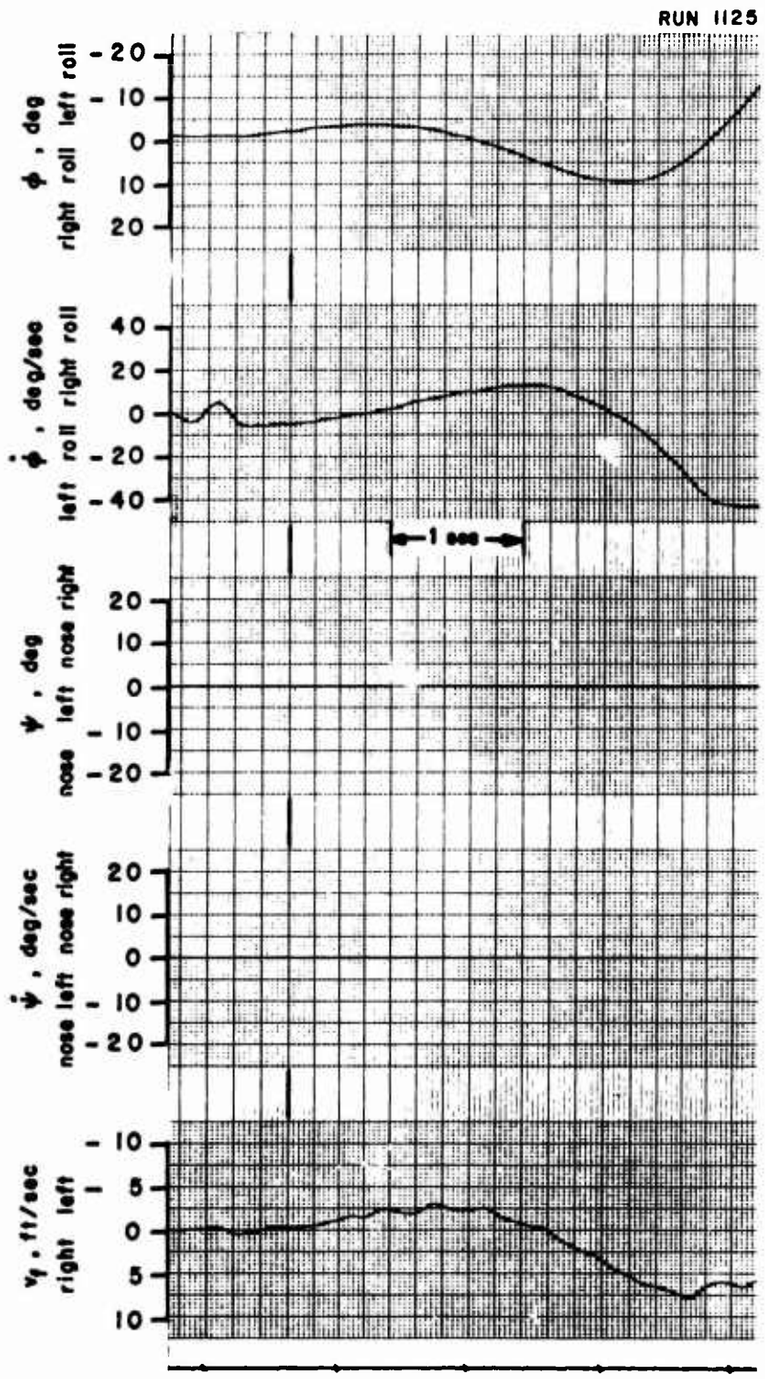

Figure 12. Lateral/Directional Transient Response. Two Degrees of Freedom, ϕ-v_f. $i_d = 80^\circ$, $U_{o_f} = 10$ ft/sec, $\beta_{.75} = 25.2^\circ$, rpm = 6780, $\Delta\beta_o = 0.5^\circ$, Large Vertical Tail.

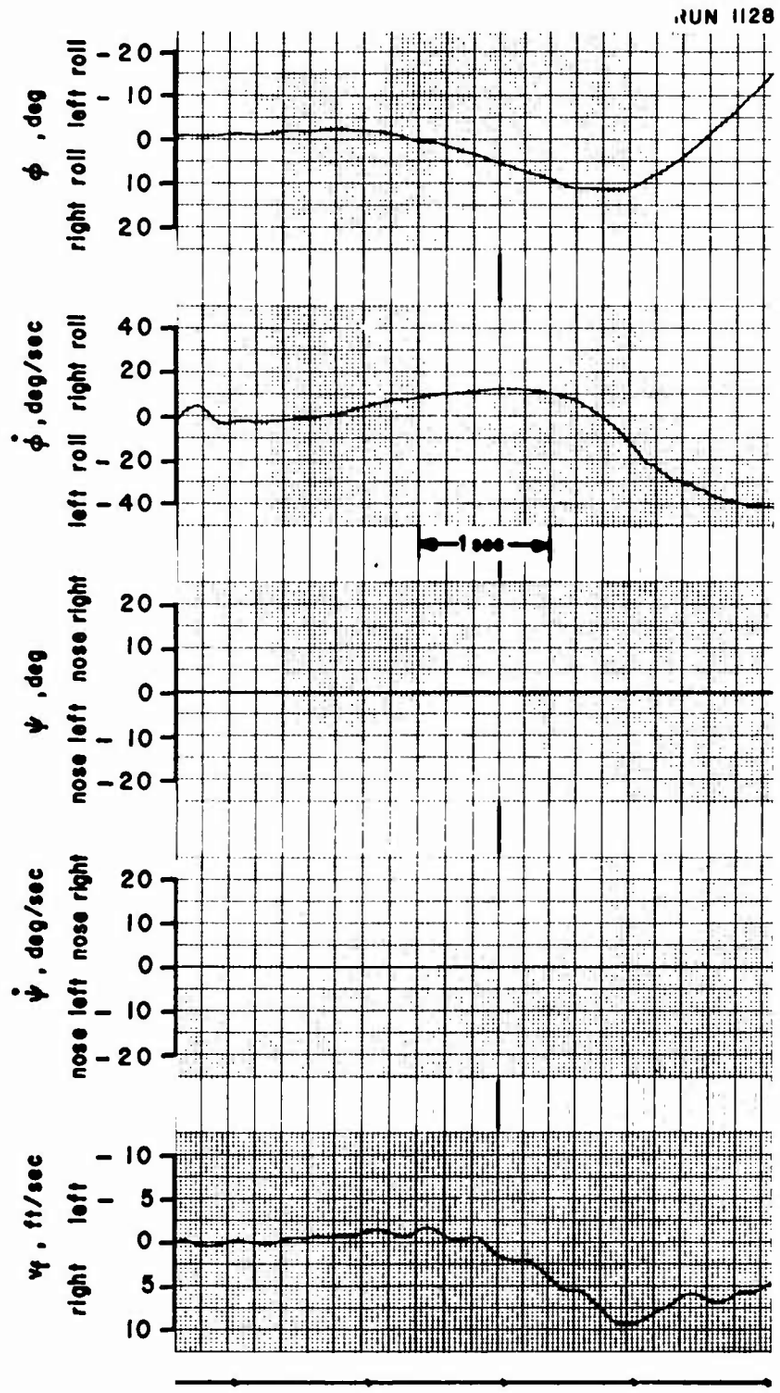

Figure 12. Lateral/Directional Transient Response. Two Degrees of Freedom, ϕ-v_f. $i_d = 80^\circ$, U_{o_f} = 10 ft/sec, $\beta_{.75R} = 25.2^\circ$, rpm = 6780, $\Delta\beta_o = 0.5^\circ$, Large Vertical Tail.

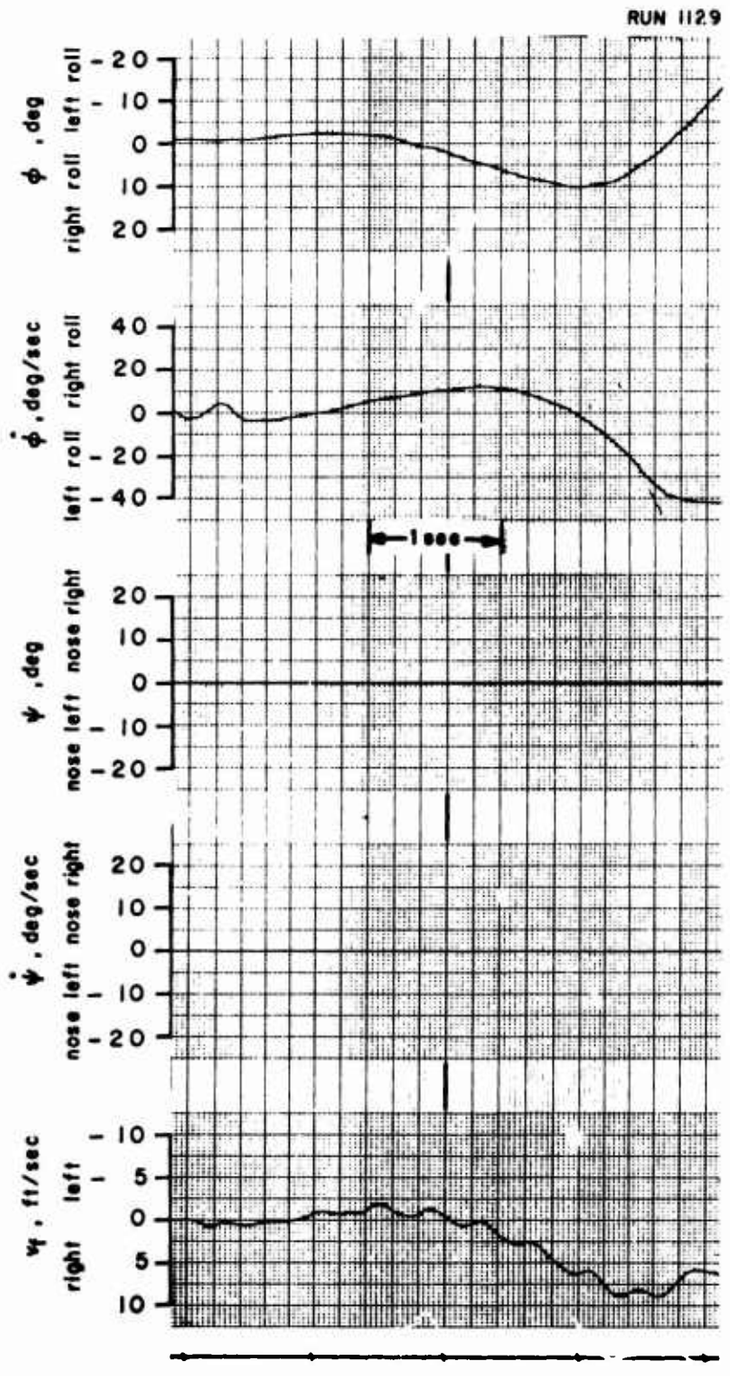

Figure 12. Lateral/Directional Transient Response. Two Degrees of Freedom, ϕ-v_f. $i_d = 80^\circ$, U_{o_f} = 10 ft/sec, $\beta_{.75R} = 25.2^\circ$, rpm = 6780, $\Delta\beta_o = 0.5^\circ$, Large Vertical Tail.

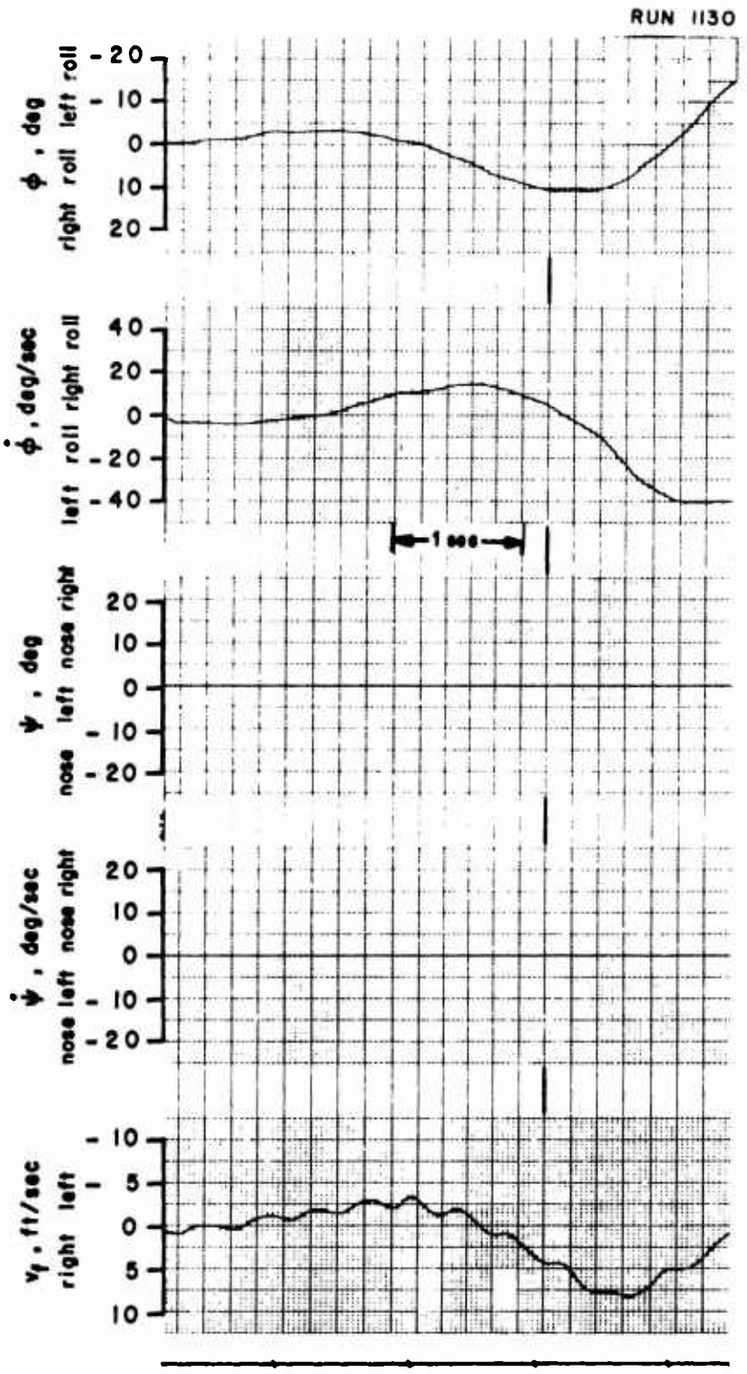

Figure 12. Lateral/Directional Transient Response. Two Degrees of Freedom, ϕ-v_f. $i_d = 80°$, $U_{o_f} = 10$ ft/sec, $\beta_{.75R} = 25.2°$, rpm = 6780, $\Delta\beta_o = 0.5°$, Large Vertical Tail.

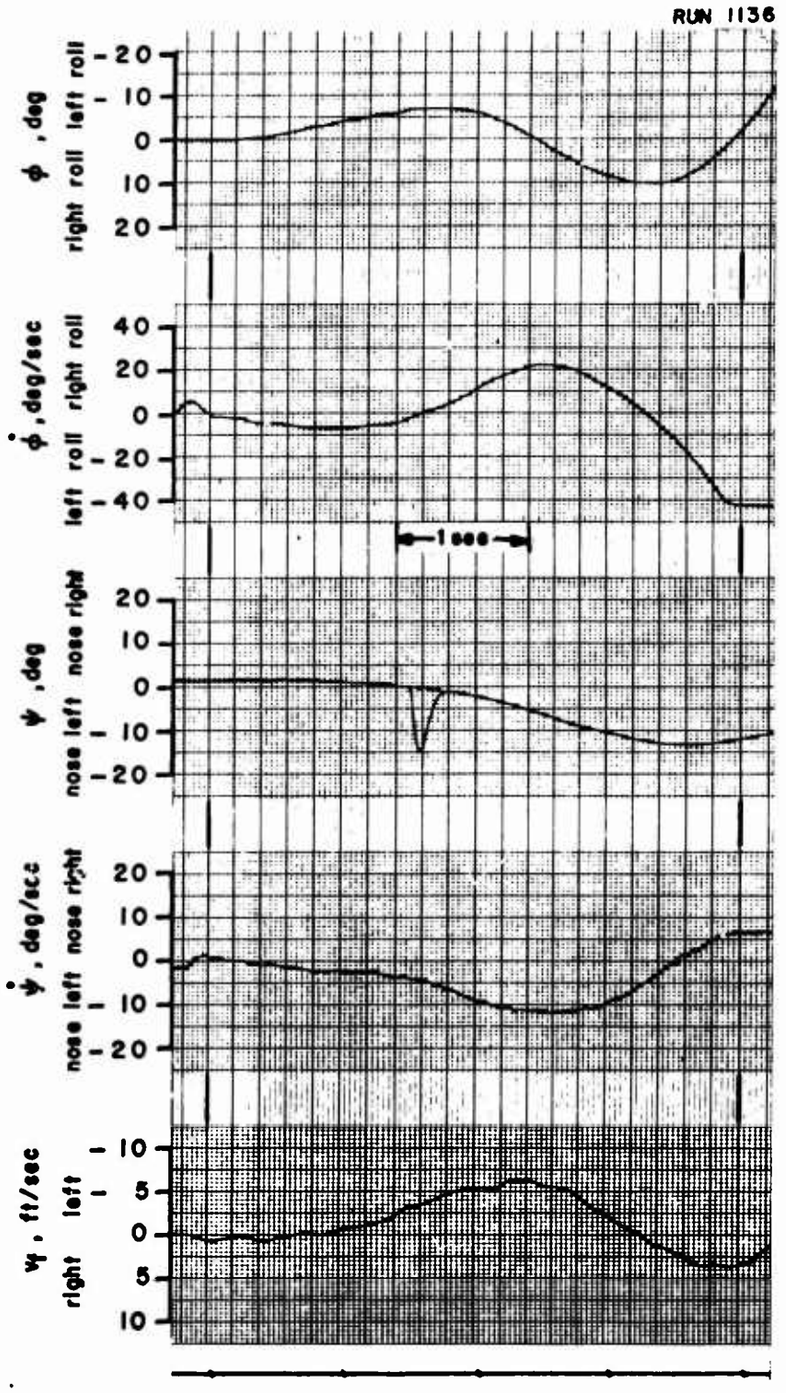

Figure 13. Lateral/Directional Transient Response. Three Degrees of Freedom, ϕ-Ψ-v_f. $i_d = 80^\circ$, $U_{o_f} = 10$ ft/sec, $\theta_{.75R} = 25.2^\circ$, rpm = 6780, $\Delta\beta_o = 0.5^\circ$, Large Vertical Tail.

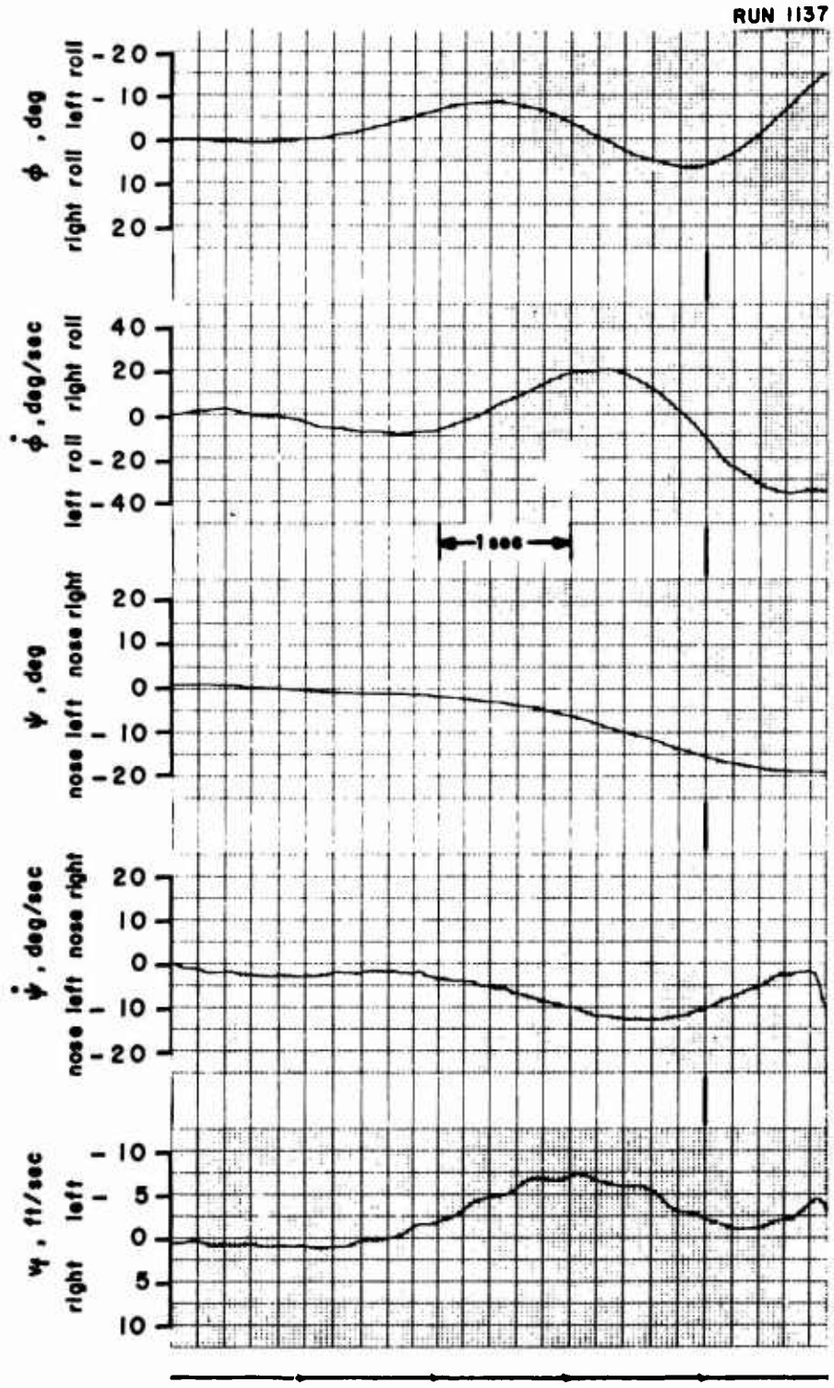

Figure 13. Lateral/Directional Transient Response. Three Degrees of Freedom, ϕ-Ψ-v_f. $i_d = 80°$, $U_{o_f} = 10$ ft/sec, $\beta_{.75R} = 25.2°$, rpm = 6780, $\Delta\beta_o = 0.5°$, Large Vertical Tail.

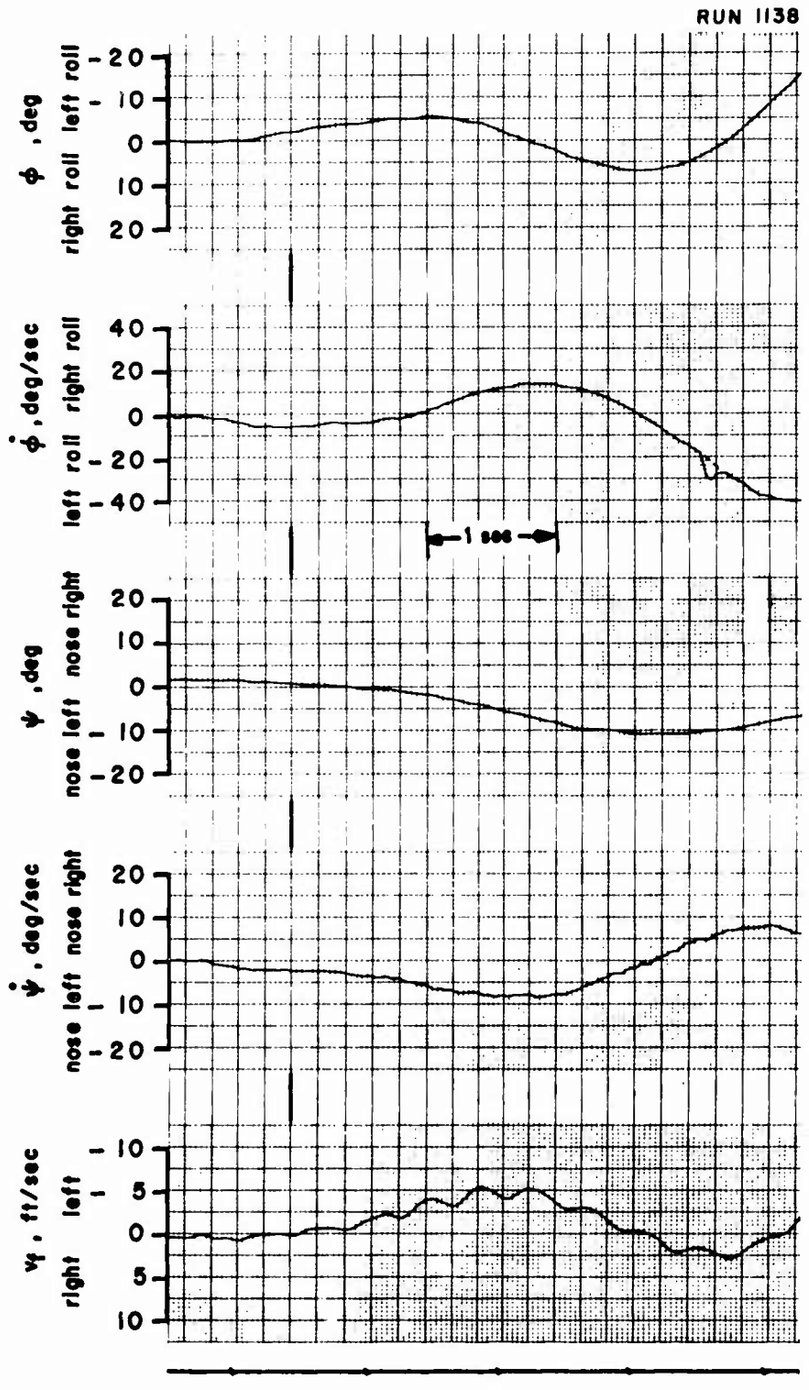

Figure 13. Lateral/Directional Transient Response. Three Degrees of Freedom, ϕ-Ψ-v_f. $i_d = 80°$, $U_{o_f} = 10$ ft/sec, $\beta_{.75R} = 25.2°$, rpm = 6780, $\Delta\beta_o = 0.5°$, Large Vertical Tail.

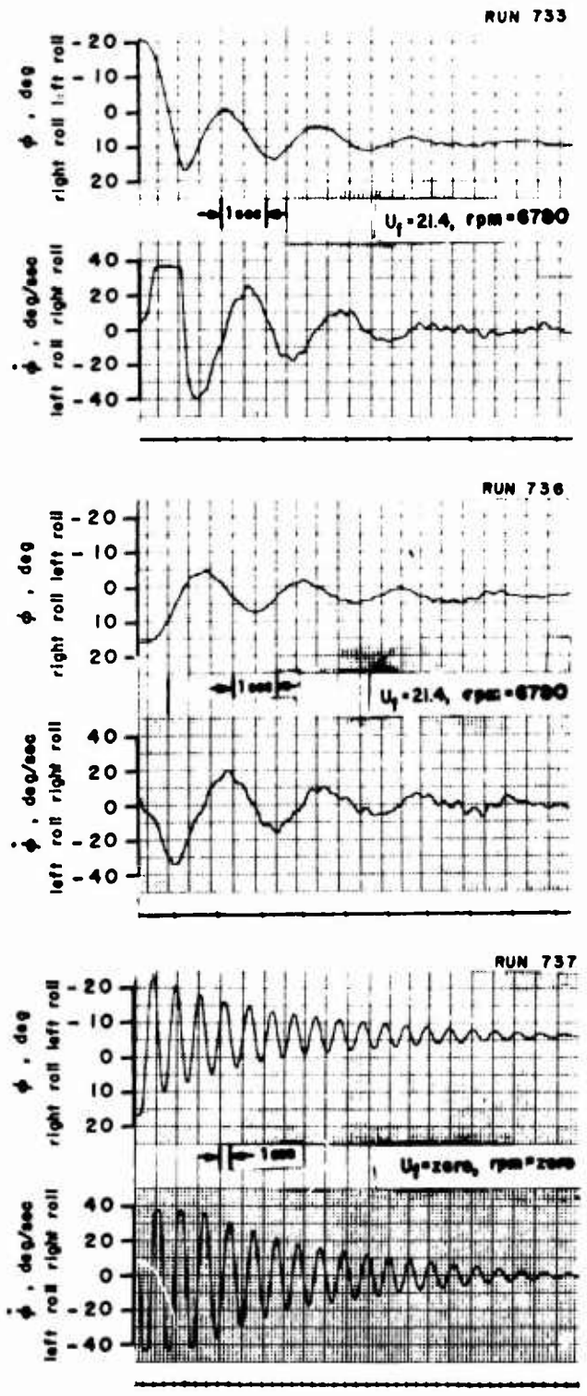

Figure 14. Lateral Transient Response. One Degree of Freedom, ϕ.
$i_d = 70°$, $B_{.75R} = 26.4°$, $\Delta B_o = 5.0°$,
Small Vertical Tail, Spring Restrained.

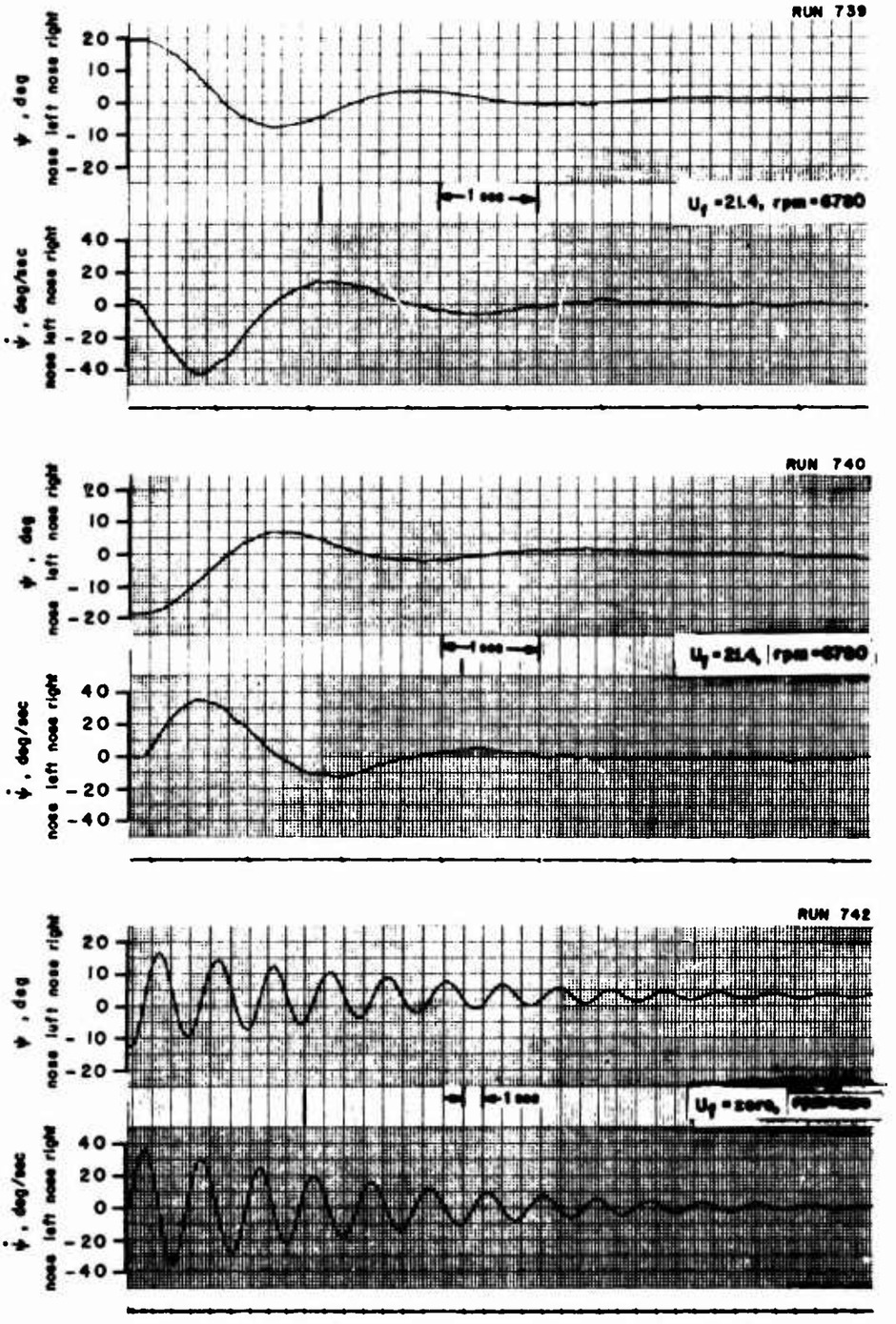

Figure 15. Directional Transient Response. One Degree of Freedom, Ψ.
$i_d = 70°$, $\beta_{.75R} = 26.4°$, $\Delta\beta_o = 5.0°$,
Small Vertical Tail, Spring Restrained.

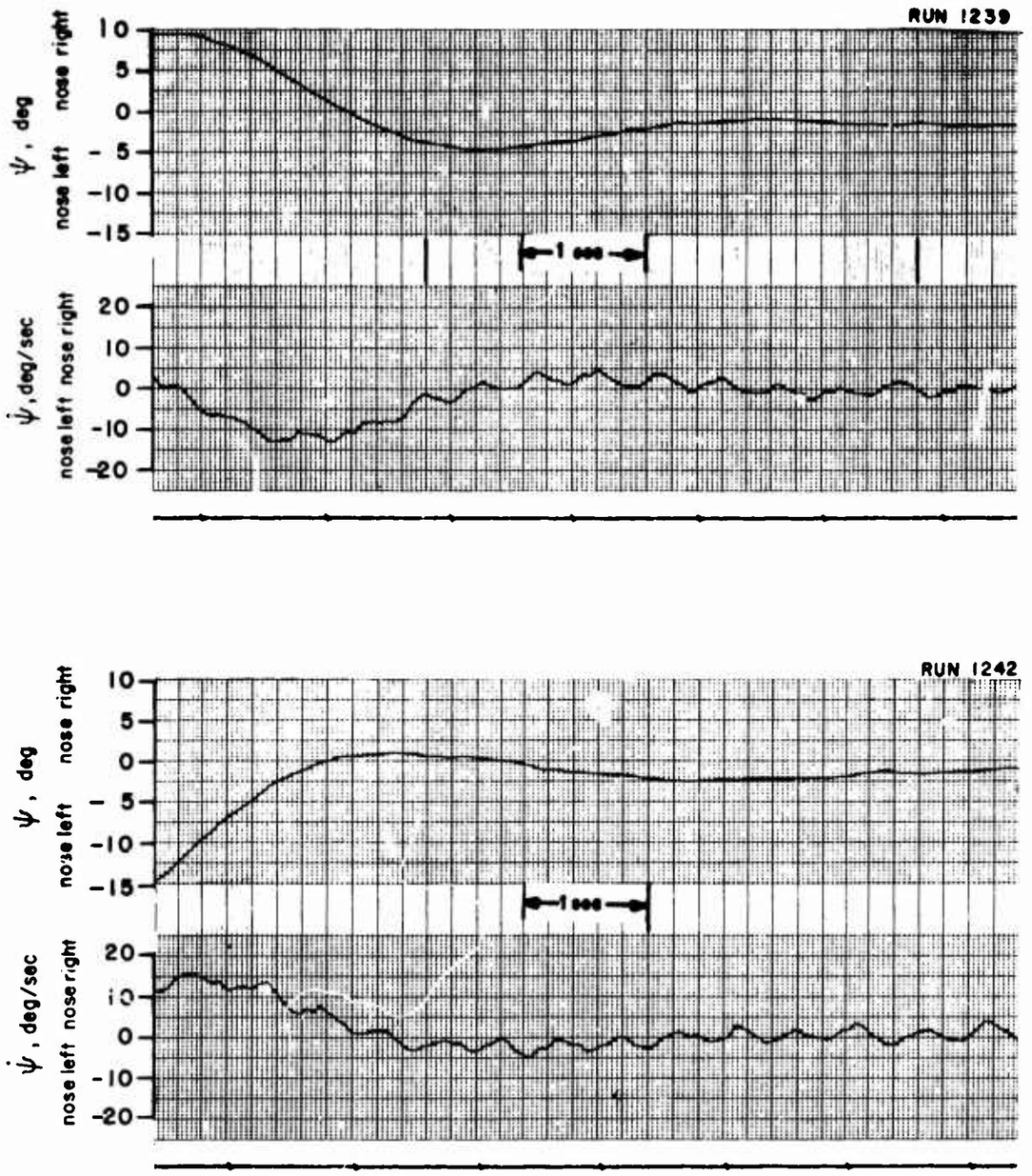

Figure 16. Lateral/Directional Transient Response. One Degree of Freedom, Ψ. $i_d = 70^\circ$, $U_{o_f} = 21$ ft/sec, $\beta_{.75R} = 25.6^\circ$, rpm = 6780, $\Delta\beta_o = 2.0^\circ$, Large Vertical Tail.

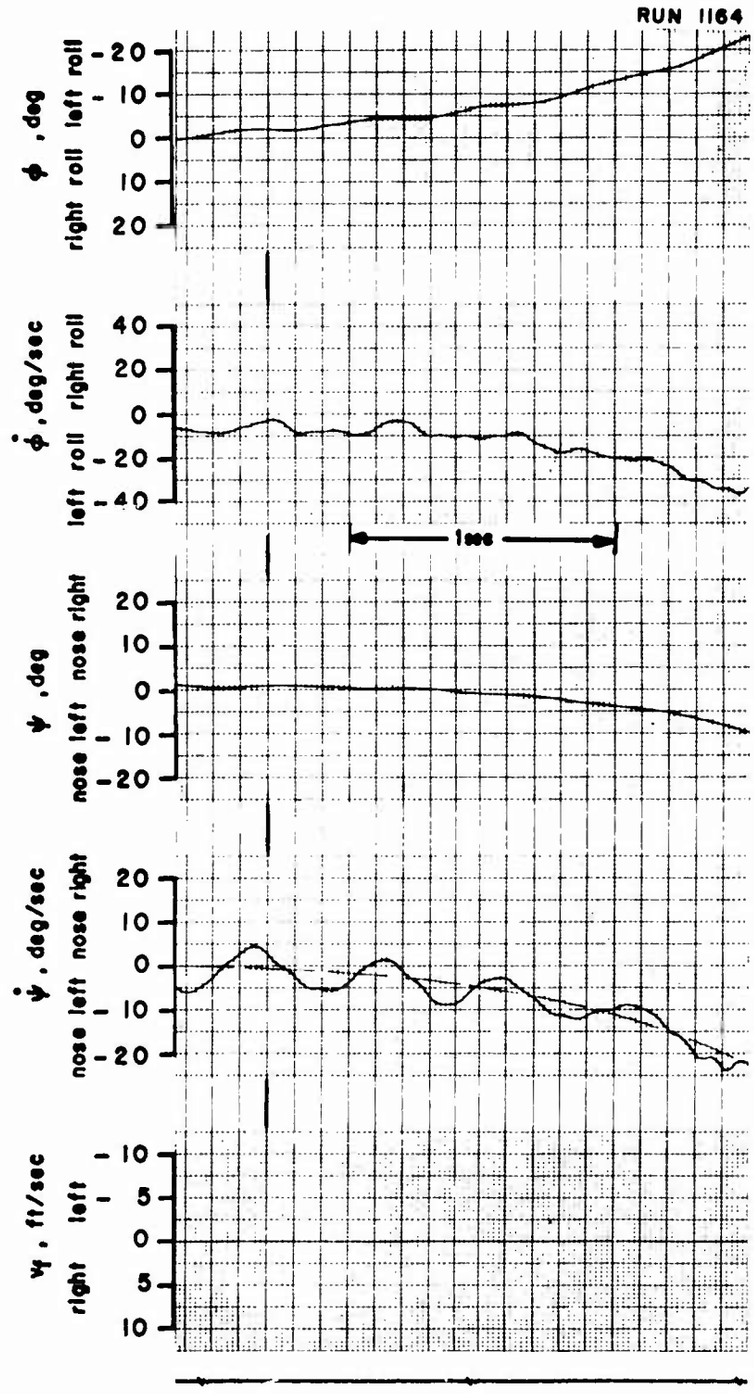

Figure 17. Lateral/Directional Transient Response. Two Degrees of Freedom, ϕ-Ψ. $i_d = 70^\circ$, $U_{O_f} = 21$ ft/sec, $\beta_{.75R} = 20.6^\circ$, rpm = 6780, $\Delta\beta_O = 2.0^\circ$, Large Vertical Tail.

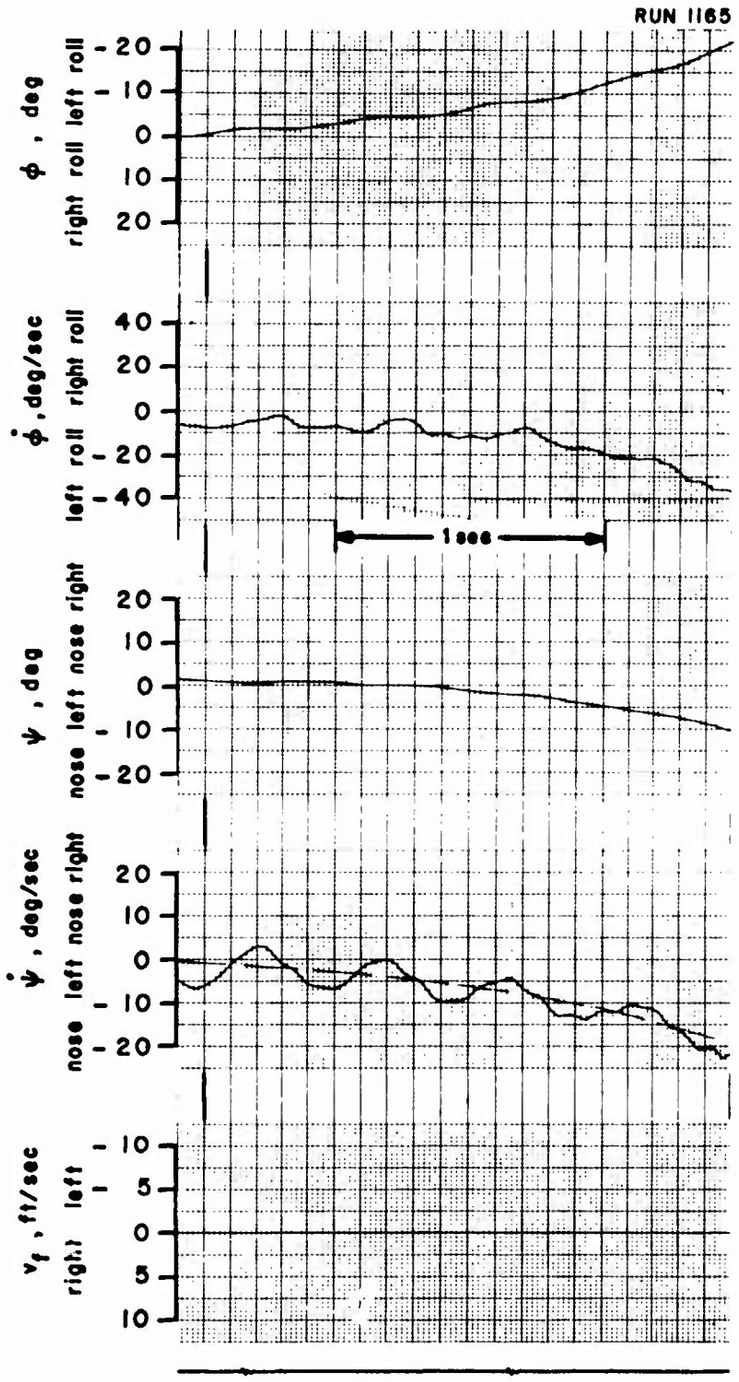

Figure 17. Lateral/Directional Transient Response. Two Degrees of Freedom, ϕ-Ψ. $i_d = 70°$, $U_{o_f} = 21$ ft/sec, $\beta_{.75R} = 25.6°$, rpm = 6780, $\Delta\beta_o = 2.0°$, Large Vertical Tail.

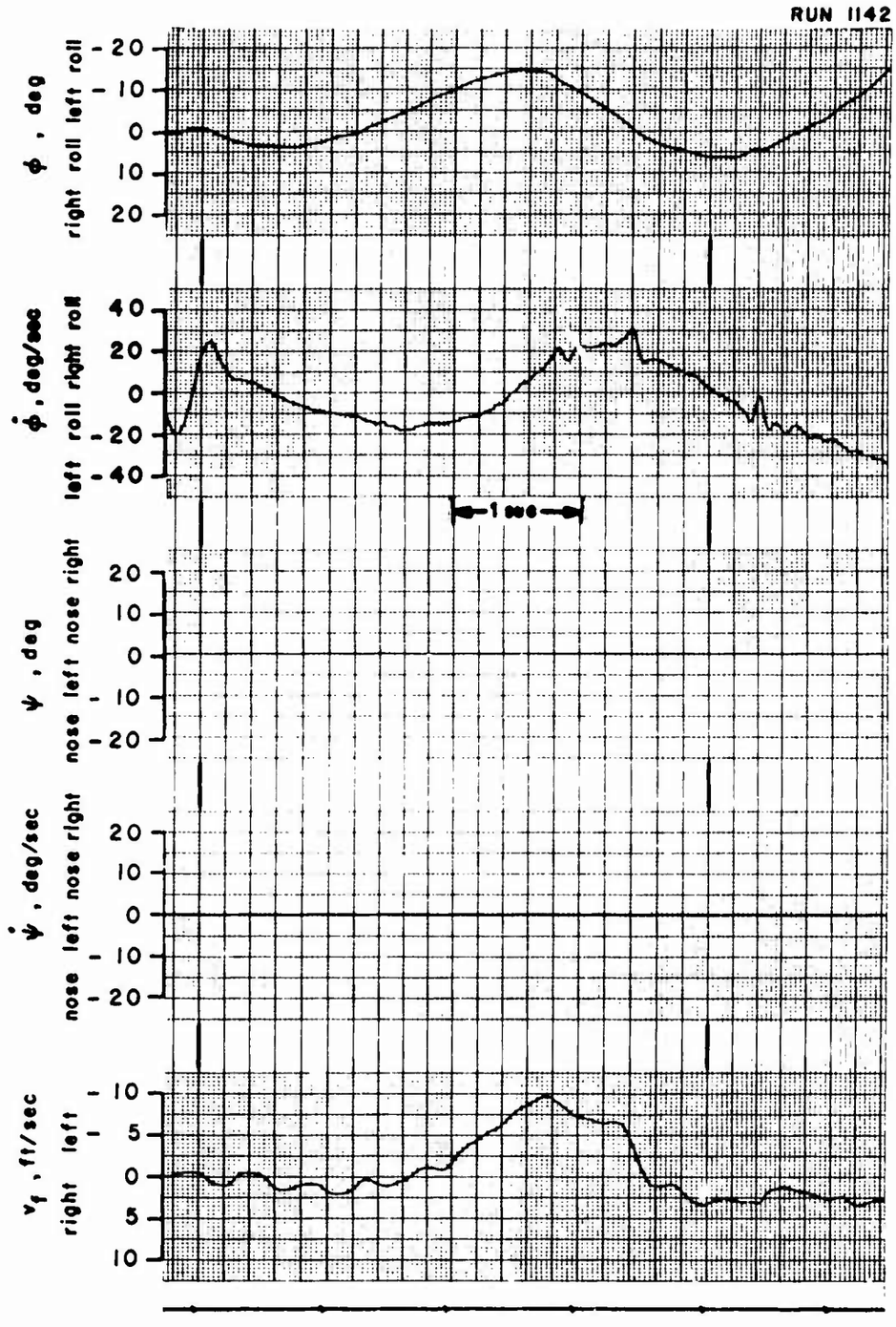

Figure 18. Lateral Transient Response. Two Degrees of Freedom, ϕ-v_f. $i_d = 70°$, $U_{o_f} = 21$ ft/sec, $\beta_{.75R} = 25.6°$, rpm = 6780, $\Delta\beta_o = 2.0°$, Large Vertical Tail.

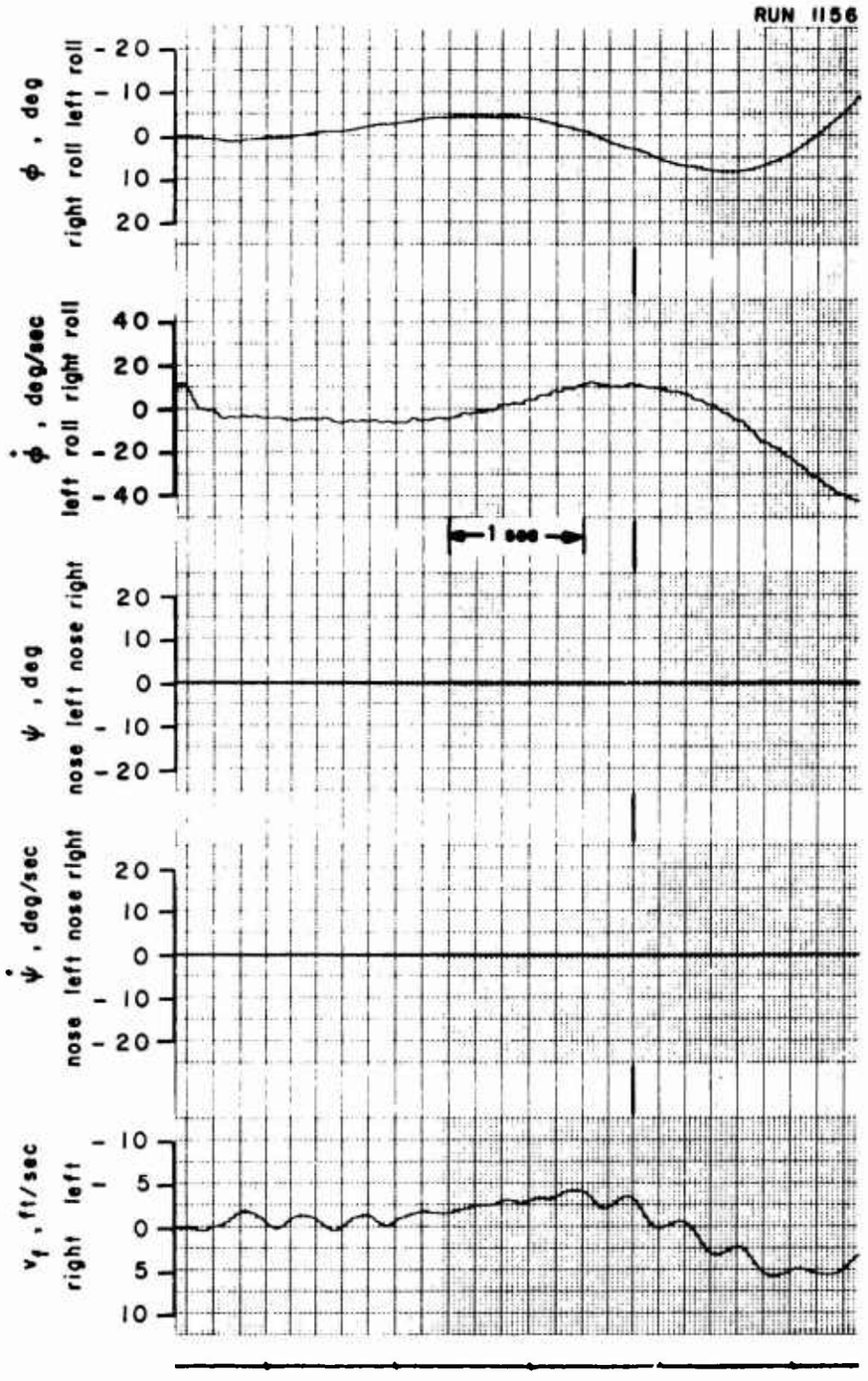

Figure 18. Lateral Transient Response. Two Degrees of Freedom, ϕ-v_f. $i_d = 70°$, U_{o_f} = 91 ft/sec, $\beta_{.75R} = 25.6°$, rpm = 6780, $\Delta\beta_o = 2.0°$, Large Vertical Tail.

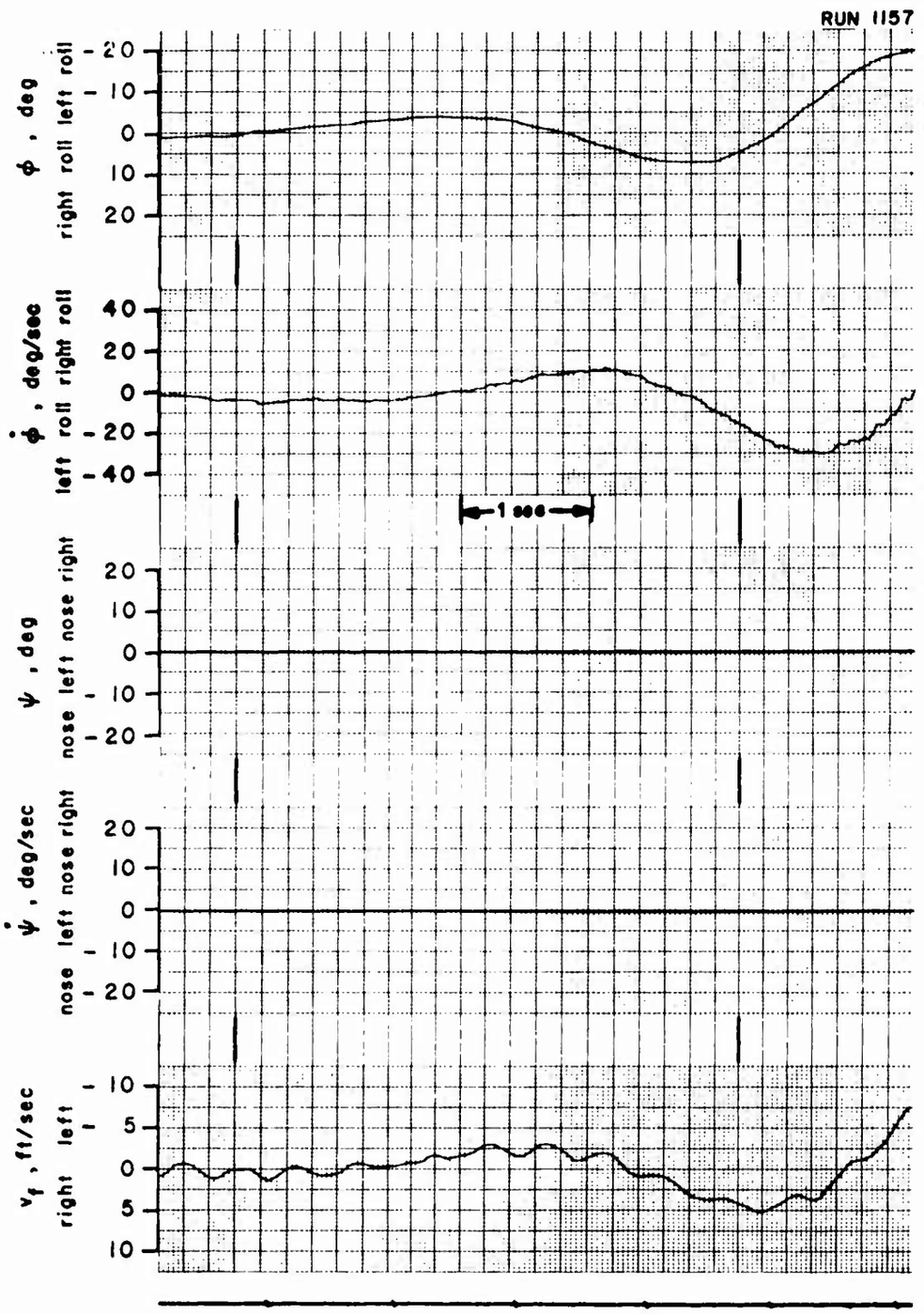

Figure 18. Lateral Transient Response. Two Degrees of Freedom, ϕ-v_f. $i_d = 70°$, $U_{o_f} = 21$ ft/sec, $\beta_{.75R} = 25.6°$, rpm = 6780 $\Delta\beta_o = 2.0°$, Large Vertical Tail.

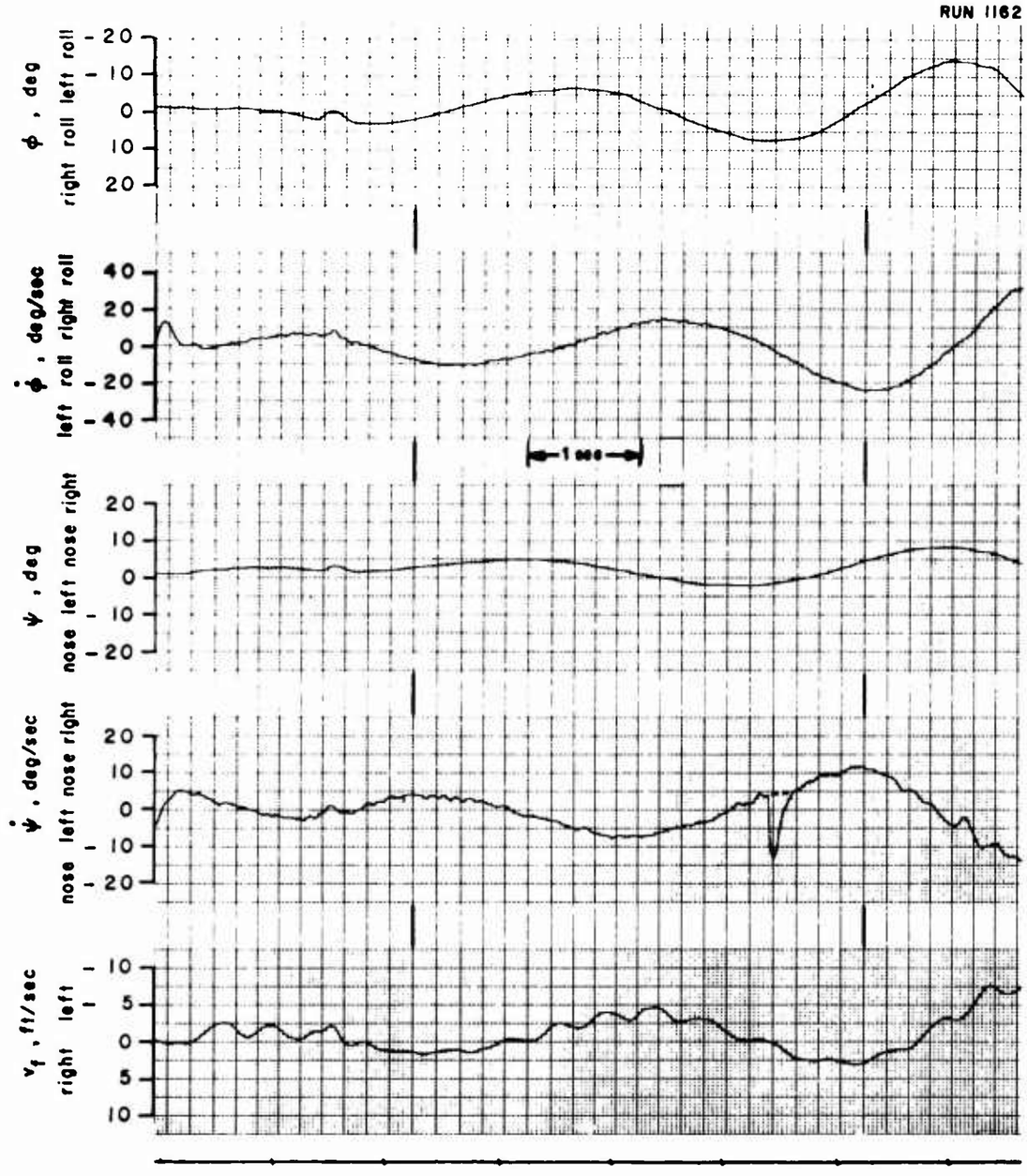

Figure 19. Lateral/Directional Transient Response. Three Degrees of Freedom, ϕ-Ψ-v_f. $i_d = 70^\circ$, U_{o_f} = 21 ft/sec, $\beta_{.75R} = 25.6^\circ$, rpm = 6780, $\Delta\beta_o = 2.0^\circ$, Large Vertical Tail.

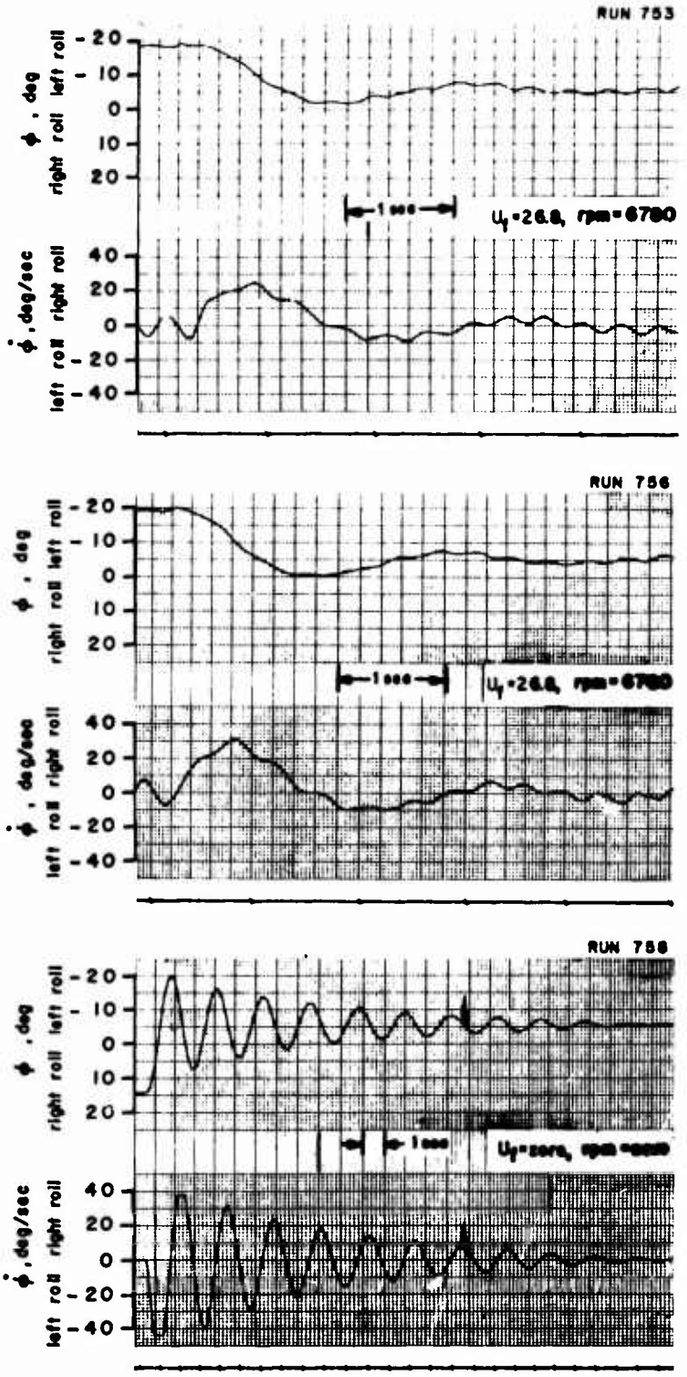

Figure 20. Lateral Transient Response. One Degree of Freedom, ϕ.
$i_d = 60°$, $\beta_{.75R} = 26.4°$, $\Delta\beta_o = 2.5°$,
Small Vertical Tail, Spring Restrained.

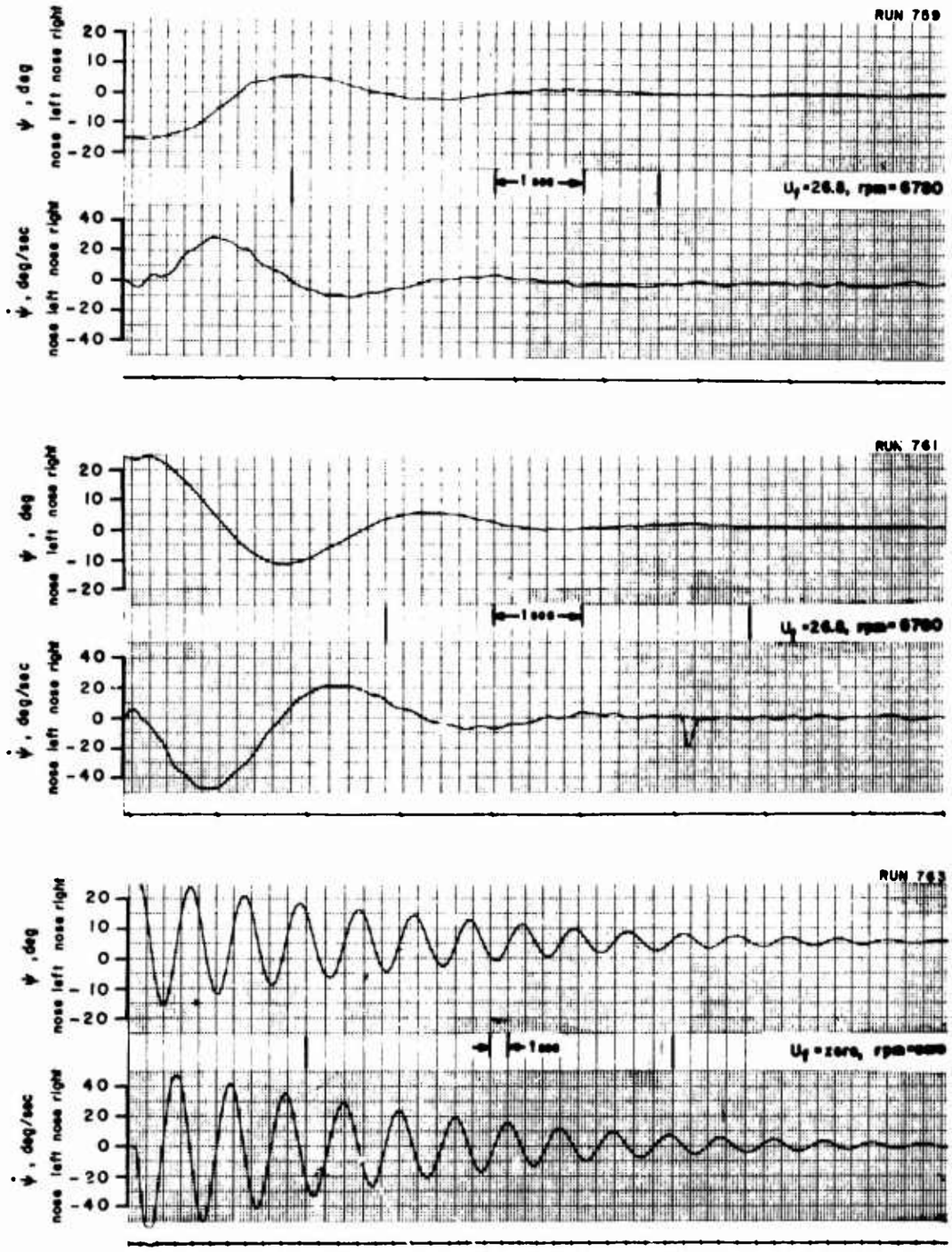

Figure 21. Directional Transient Response. One Degree of Freedom, Ψ.
$i_d = 60°$, $\beta_{.75R} = 26.4°$, $\Delta\beta_0 = 2.5°$,
Small Vertical Tail, Spring Restrained.

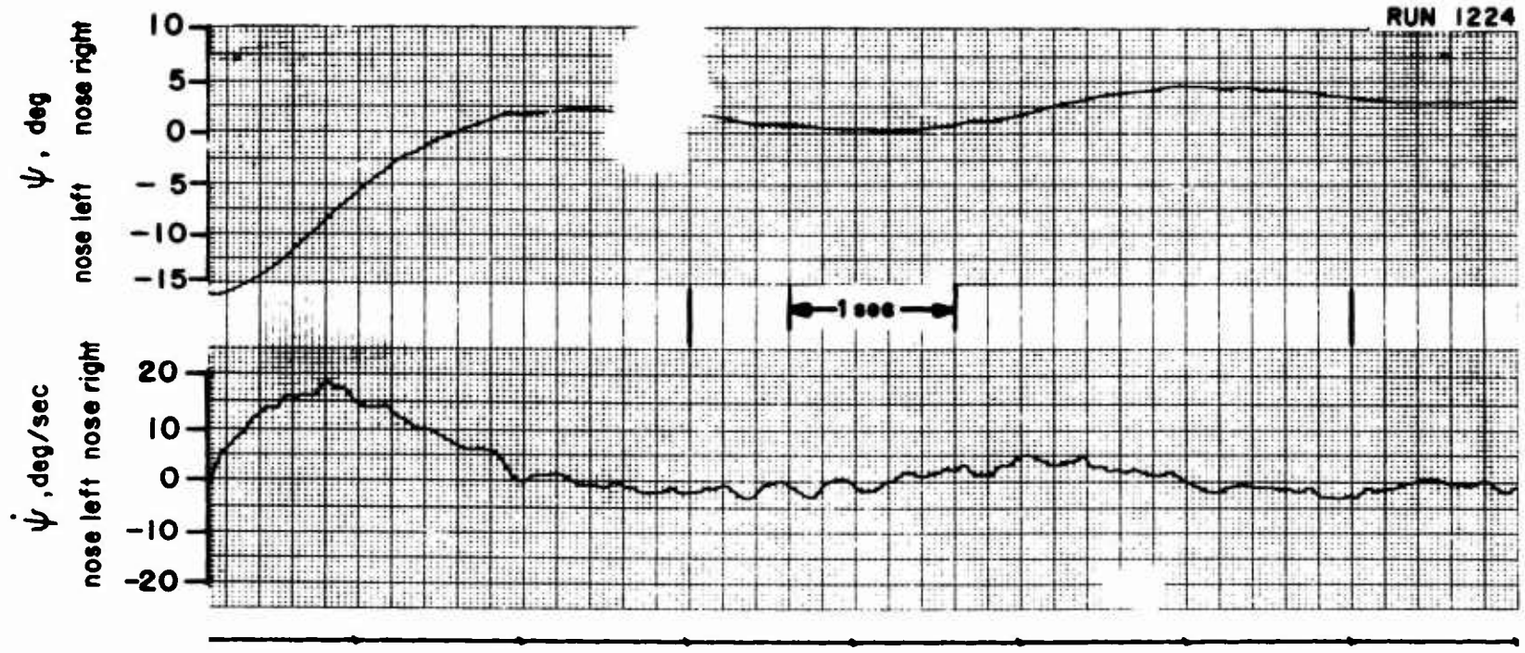

Figure 22. Directional Transient Response. One Degree of Freedom, Ψ. $i_d = 60°$, U_{c_f} = 2[illegible] ft/sec, $\theta_{.75R}$ = 2[illegible]°, rpm = 6780, $\Delta\theta_0 = 3.0°$, Large Vertical Tail.

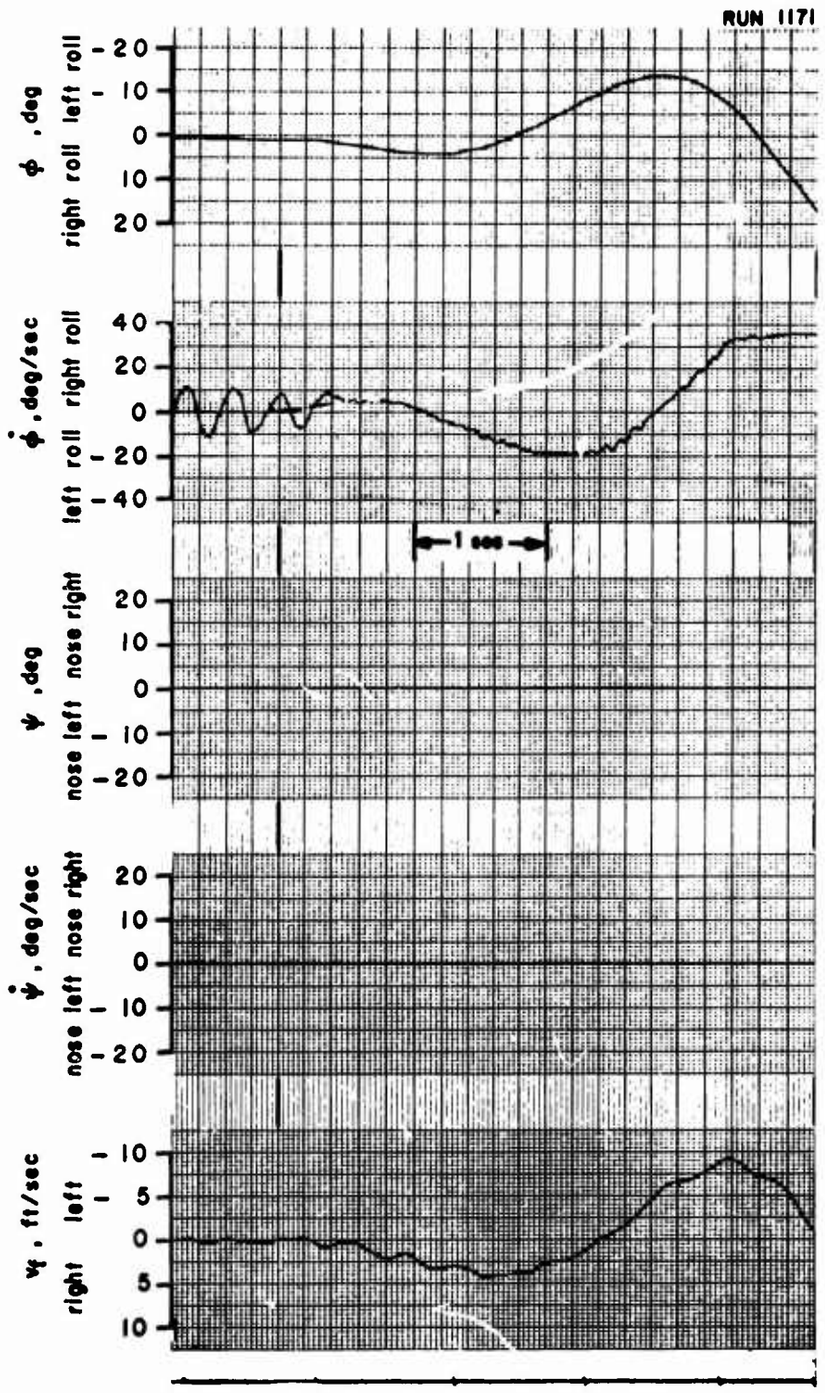

Figure 23. Lateral/Directional Transient Response. Two Degrees of Freedom, ϕ-v_f. $i_d = 60^\circ$, U_{o_f} = 29 ft/sec, $\beta_{.75R} = 25.5^\circ$, rpm = 6780, $\Delta\beta_o = 3.0^\circ$, Large Vertical Tail.

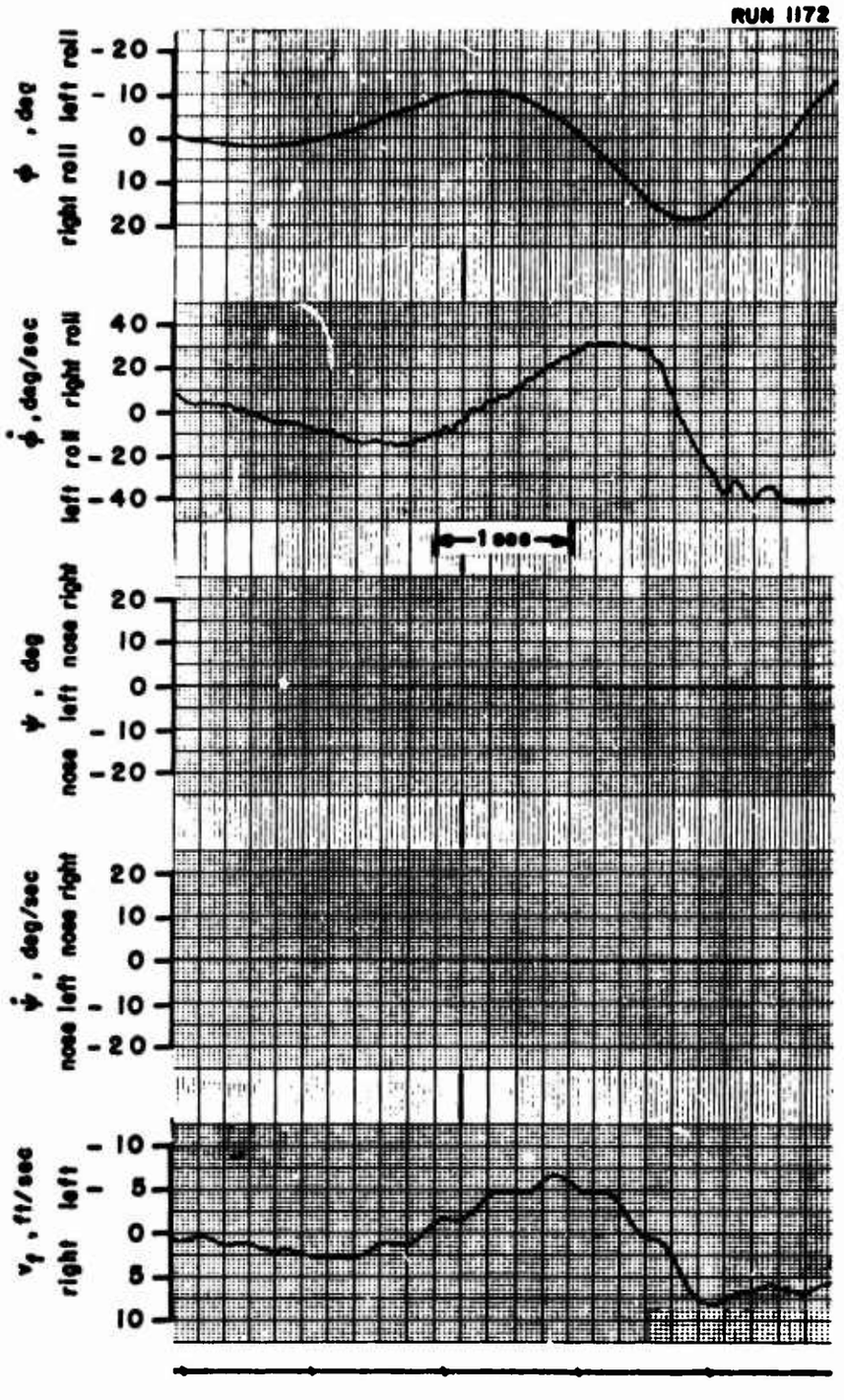

Figure 23. Lateral/Directional Transient Response. Two Degrees of Freedom, ϕ-v_f. $i_d = 60^\circ$, U_{o_f} = 29 ft/sec, $\beta_{.75R} = 25.5^\circ$, rpm = 6780, $\Delta\beta_o = 3.0^\circ$, Large Vertical Tail.

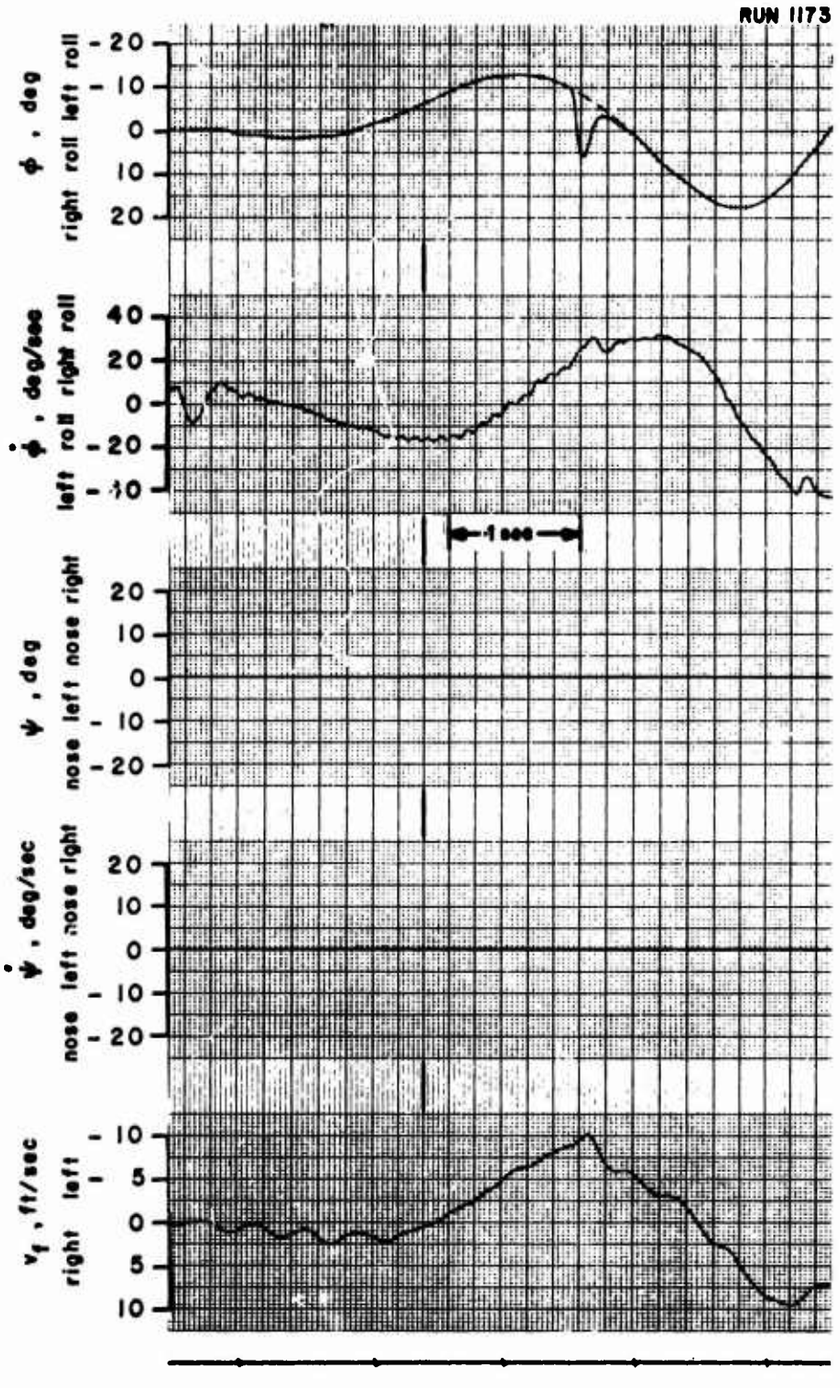

Figure 23. Lateral/Directional Transient Response. Two Degrees of Freedom, ϕ-v_f. $i_d = 60^\circ$, $U_{o_f} = 29$ ft/sec, $\beta_{.75R} = 25.5^\circ$, rpm = 6780, $\Delta\beta_o = 3.0^\circ$, Large Vertical Tail.

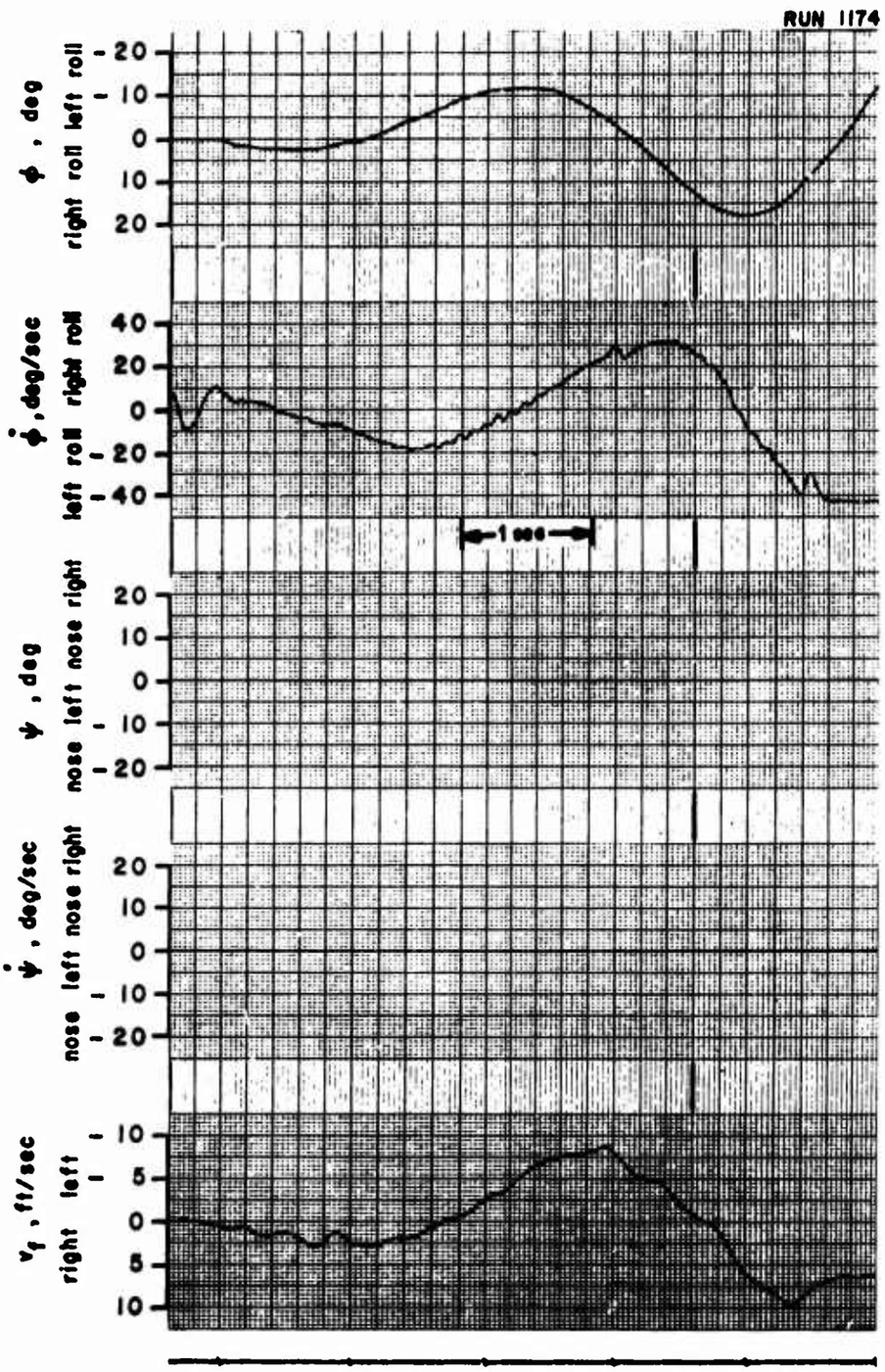

Figure 23. Lateral/Directional Transient Response. Two Degrees of Freedom, ϕ-v_f. $i_d = 60°$, $U_{o_f} = 29$ ft/sec, $\beta_{.75R} = 25.5°$, rpm = 6780, $\Delta\beta_o = 3.0°$, Large Vertical Tail.

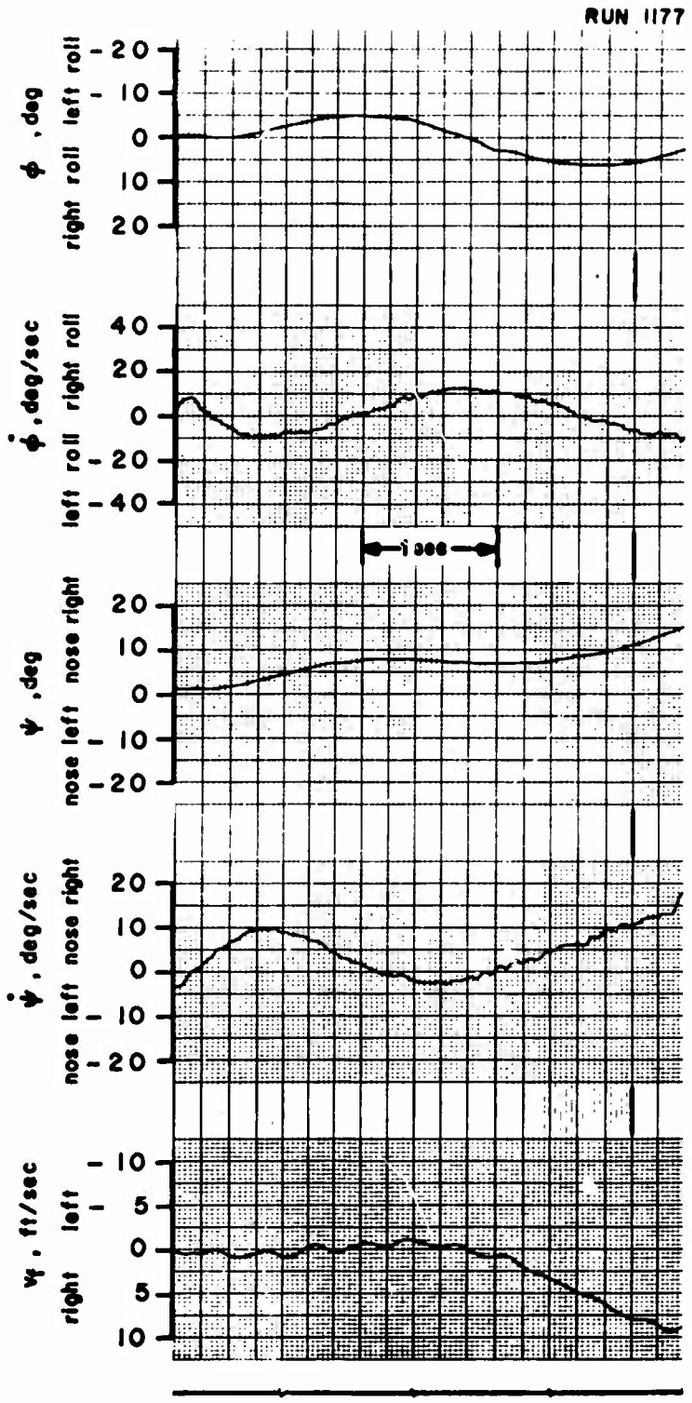

Figure 24. Lateral/Directional Transient Response. Three Degrees of Freedom, ϕ-Ψ-v_f. $i_d = 60°$, $U_{o_f} = 29$ ft/sec, $\beta_{.75R} = 25.5°$, rpm = 6780, $\Delta\beta_o = 3.0°$, Large Vertical Tail.

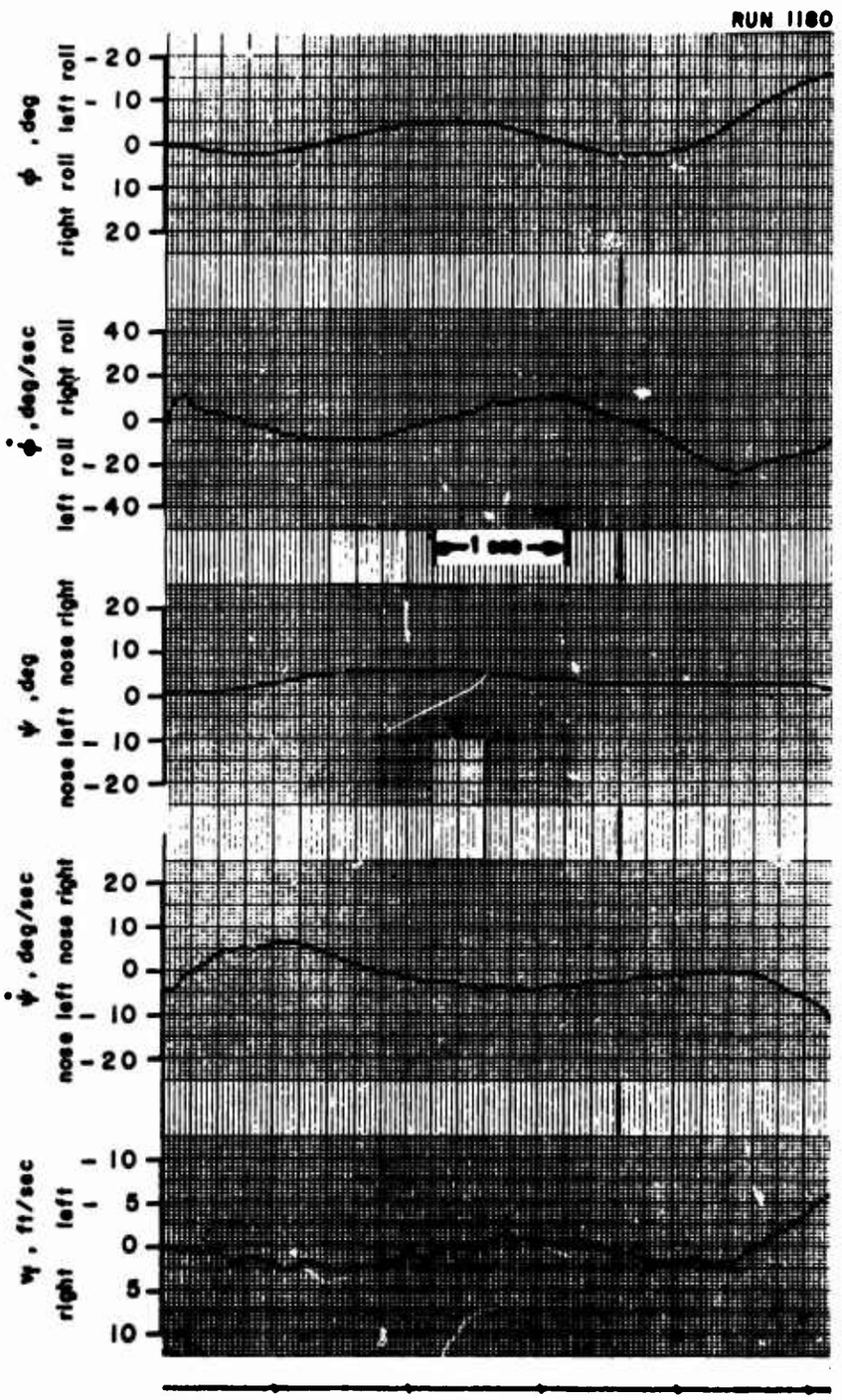

Figure 24. Lateral/Directional Transient Response. Three Degrees of Freedom, ϕ-Ψ-v_f. $i_d = 60°$, $U_{o_f} = 29$ ft/sec, $\beta_{.75R} = 25.5°$, rpm = 6780, $\Delta\beta_o = 3.0°$, Large Vertical Tail.

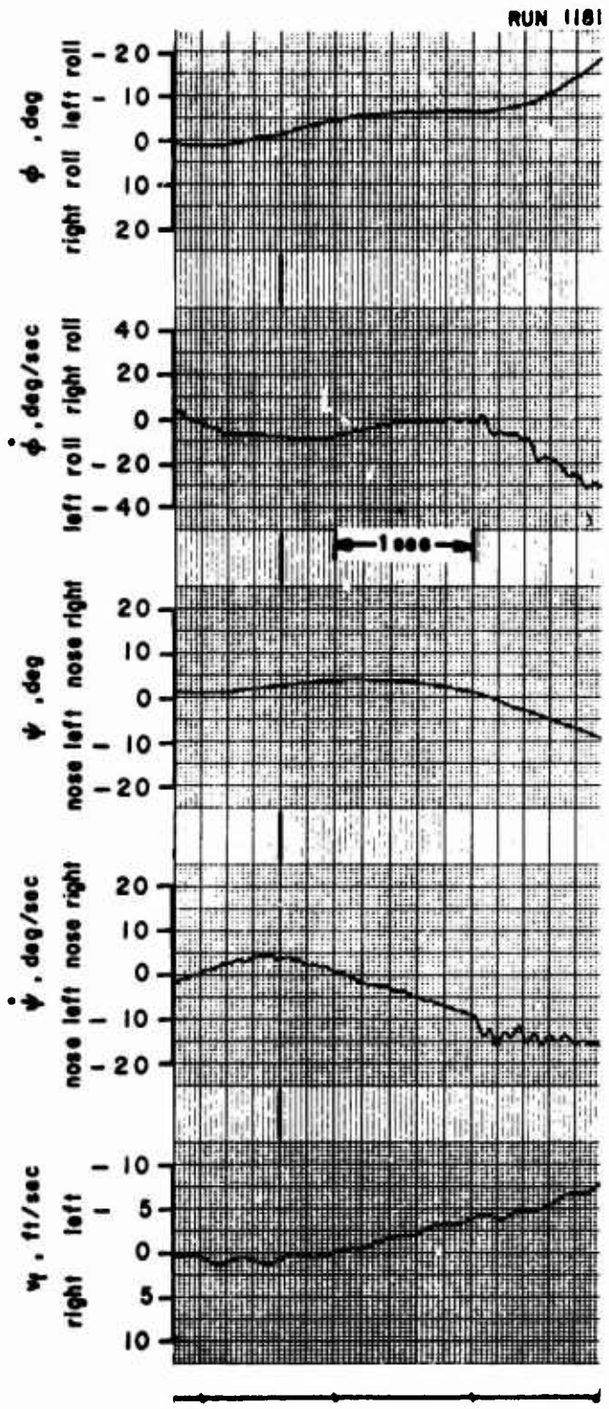

Figure 24. Lateral/Directional Transient Response. Three Degrees of Freedom, ϕ-Ψ-v_f. $i_d = 60°$, U_{o_f} = 29 ft/sec, $\beta_{.75} = 25.5°$, rpm = 6780, $\Delta\beta_o = 3.0°$, Large Vertical Tail.

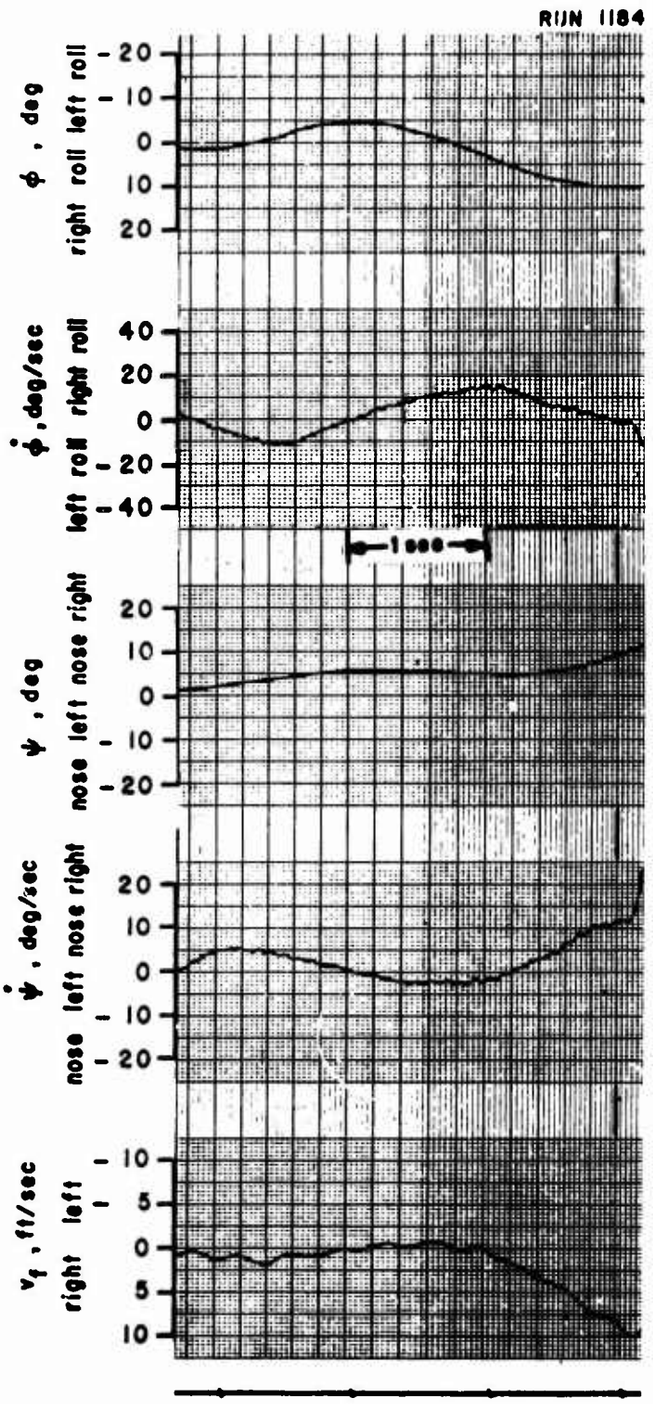

Figure 24. Lateral/Directional Transient Response. Three Degrees of Freedom, ϕ-Ψ-v_f. $i_d = 60°$, $U_{o_f} = 29$ ft/sec, $\beta_{.75R} = 25.5°$, rpm = 6780, $\Delta\beta_o = 3.0°$, Large Vertical Tail.

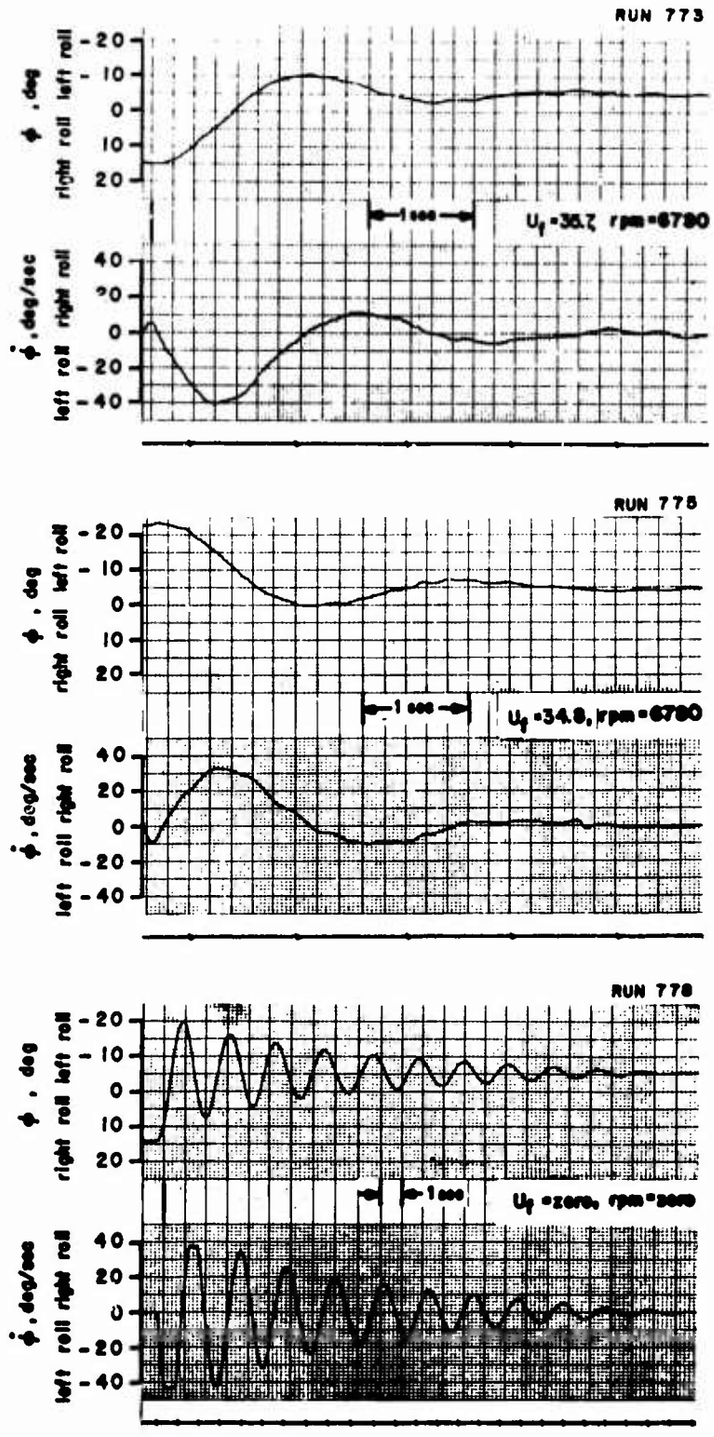

Figure 25. Lateral Transient Response. One Degree of Freedom, ϕ. $i_d = 50°$, $\beta_{.75R} = 26.4°$, $\Delta\beta_o = -0.5°$, Small Vertical Tail, Spring Restrained.

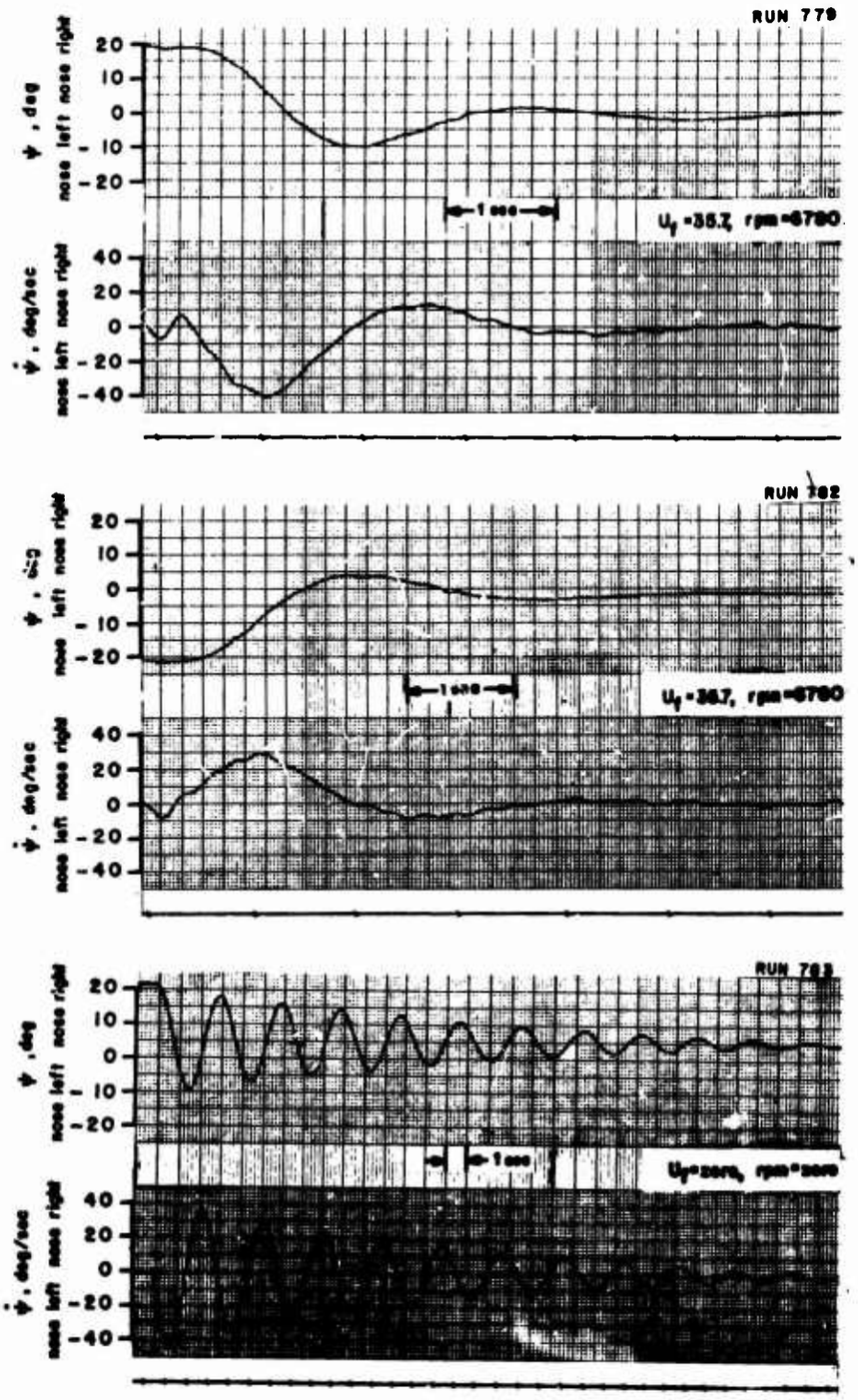

Figure 26. Directional Transient Response. One Degree of Freedom, Ψ. $i_d = 50°$, $\beta_{.75R} = 26.4°$, $\Delta\beta_o = -0.5°$, Small Vertical Tail, Spring Restrained.

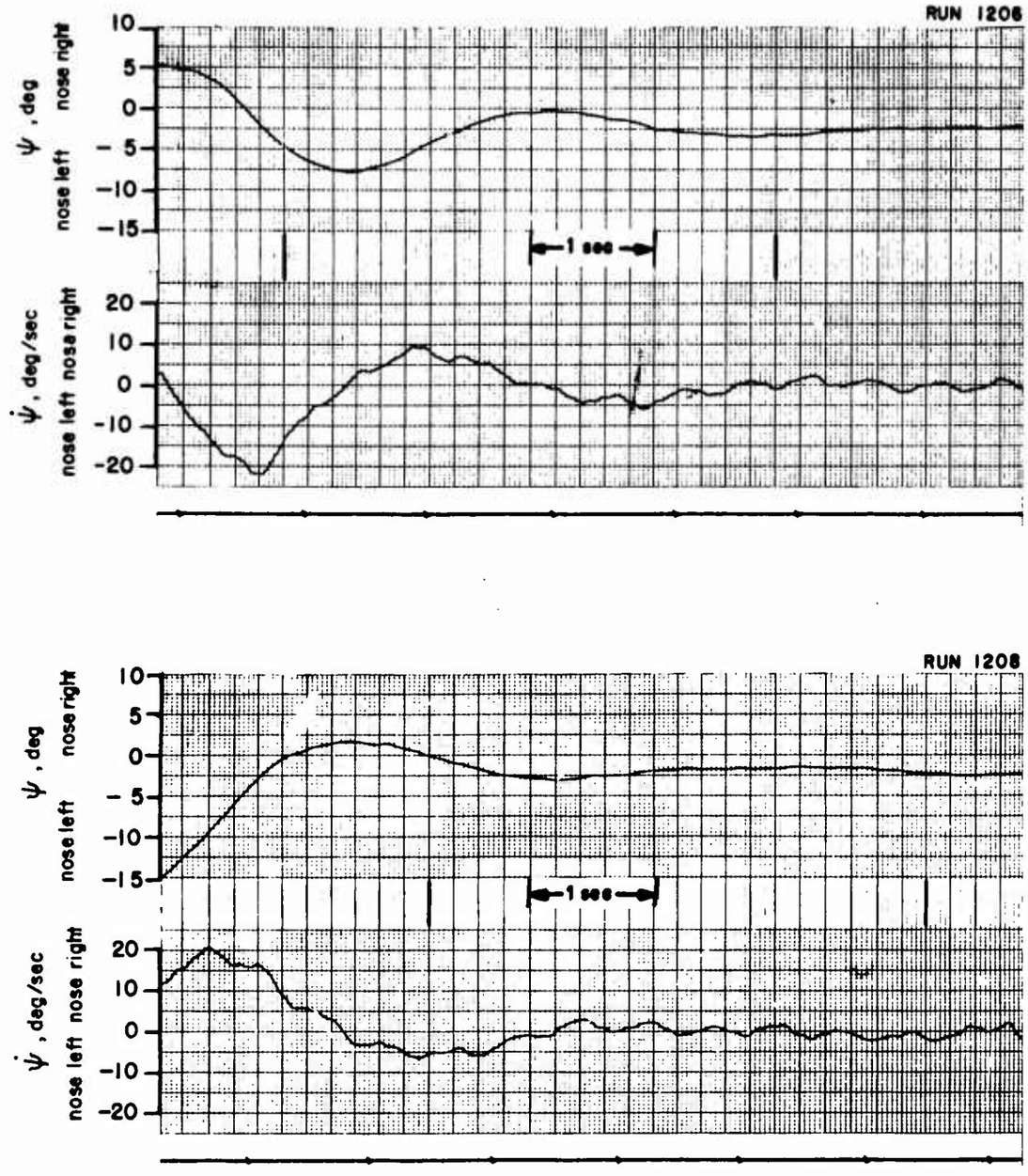

Figure 27. Directional Transient Response. One Degree of Freedom, Ψ. $i_d = 50°$, $U_{o_f} = 38$ ft/sec, $\theta_{.75R} = 24.8°$, rpm 6780, $\Delta\theta_o = 2.5°$, Large Vertical Tail.

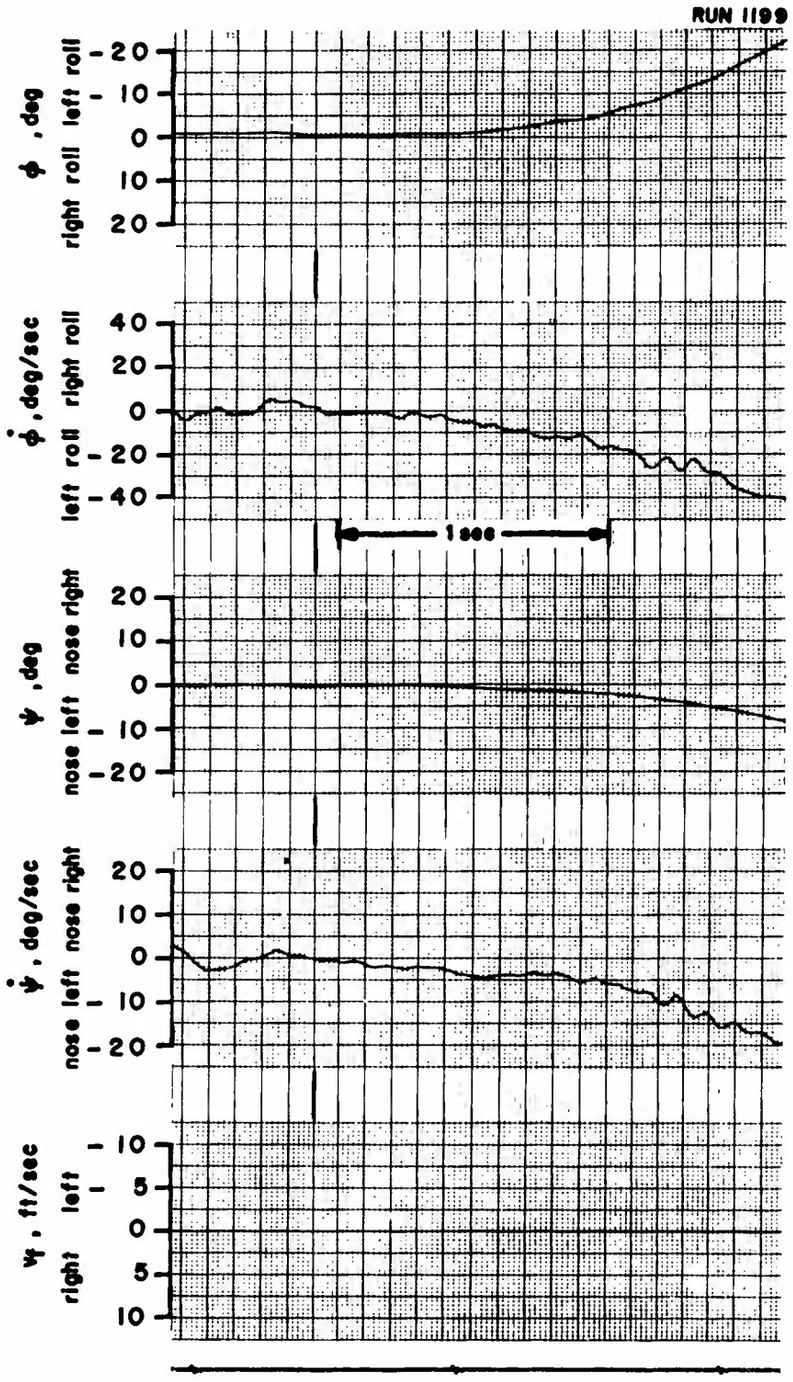

Figure 28. Lateral/Directional Transient Response. Two Degrees of Freedom, ϕ-Ψ. $i_d = 50^\circ$, $U_{O_f} = 38$ ft/sec, $\beta_{.75R} = 24.8^\circ$, rpm = 6780, $\Delta\beta_O = 2.5^\circ$, Large Vertical Tail.

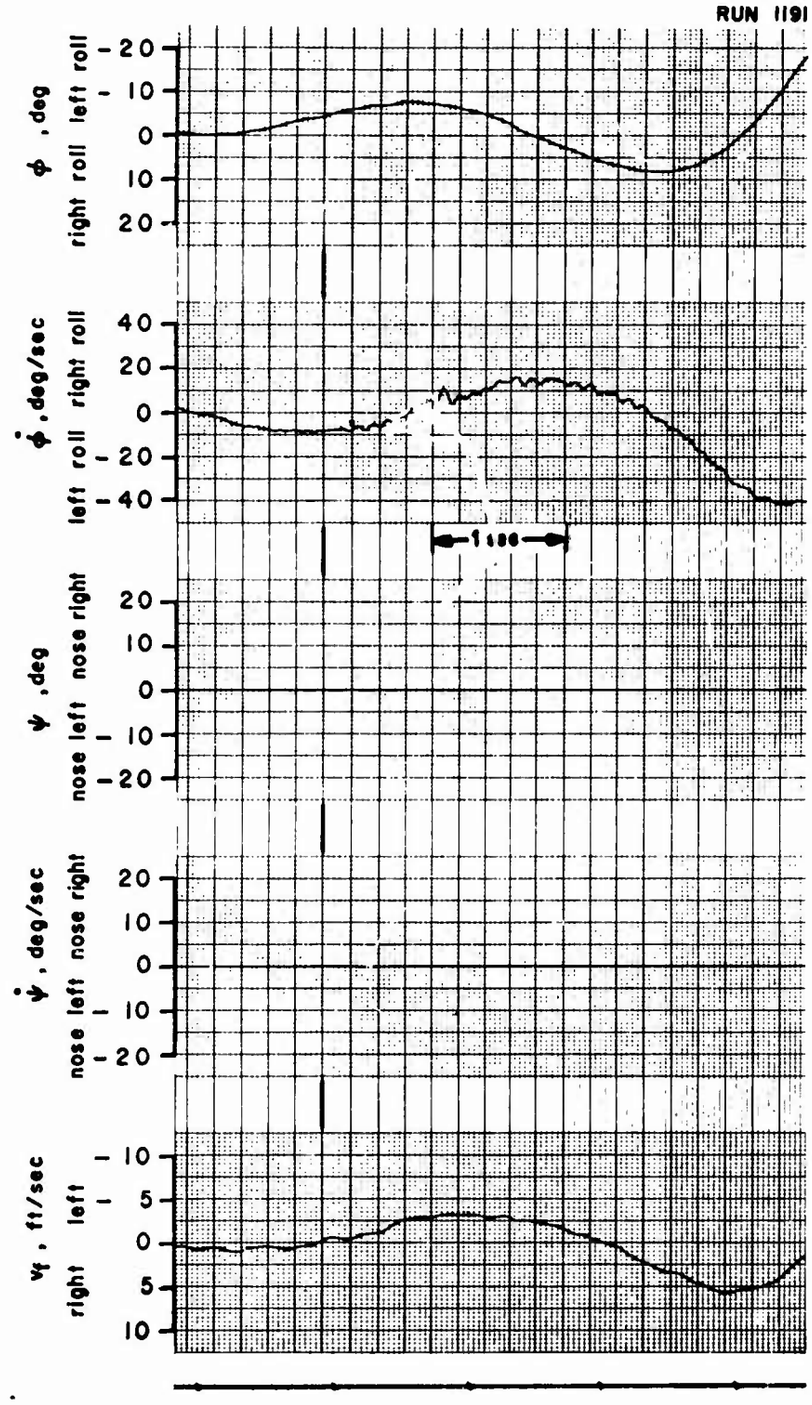

Figure 29. Lateral Transient Response. Two Degrees of Freedom, ϕ-v_f. $i_d = 50^\circ$, $U_{o_f} = 38$ ft/sec, $\beta_{.75R} = 24.8^\circ$, rpm = 6780, $\Delta\beta_o = 2.5^\circ$, Large Vertical Tail.

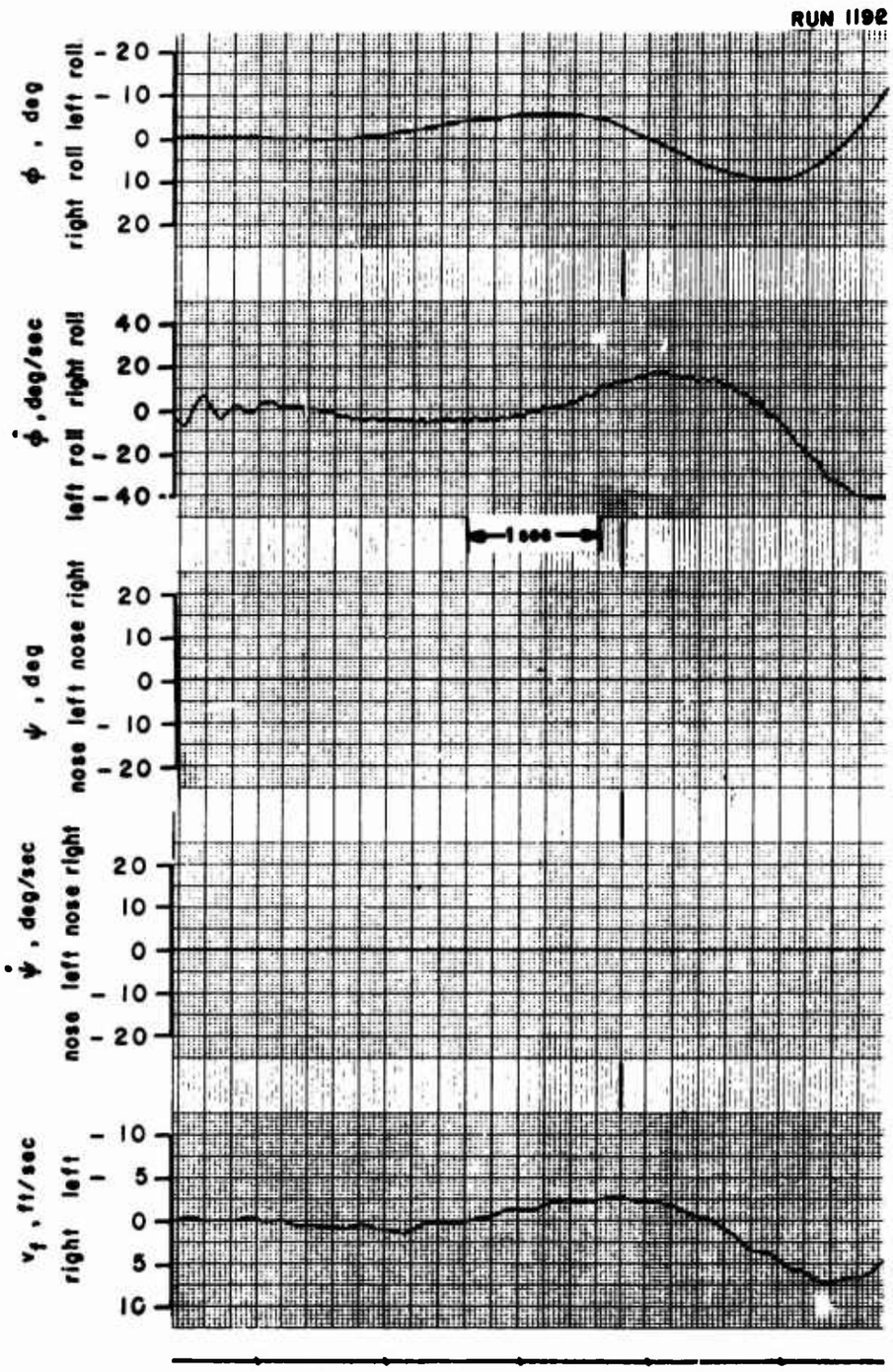

Figure 29. Lateral Transient Response. Two Degrees of Freedom, ϕ-v_f. $i_d = 50°$, U_{o_f} = 38 ft/sec, $\beta_{.75R} = 24.8°$, rpm = 6780, $\Delta\beta_o = 2.5°$, Large Vertical Tail.

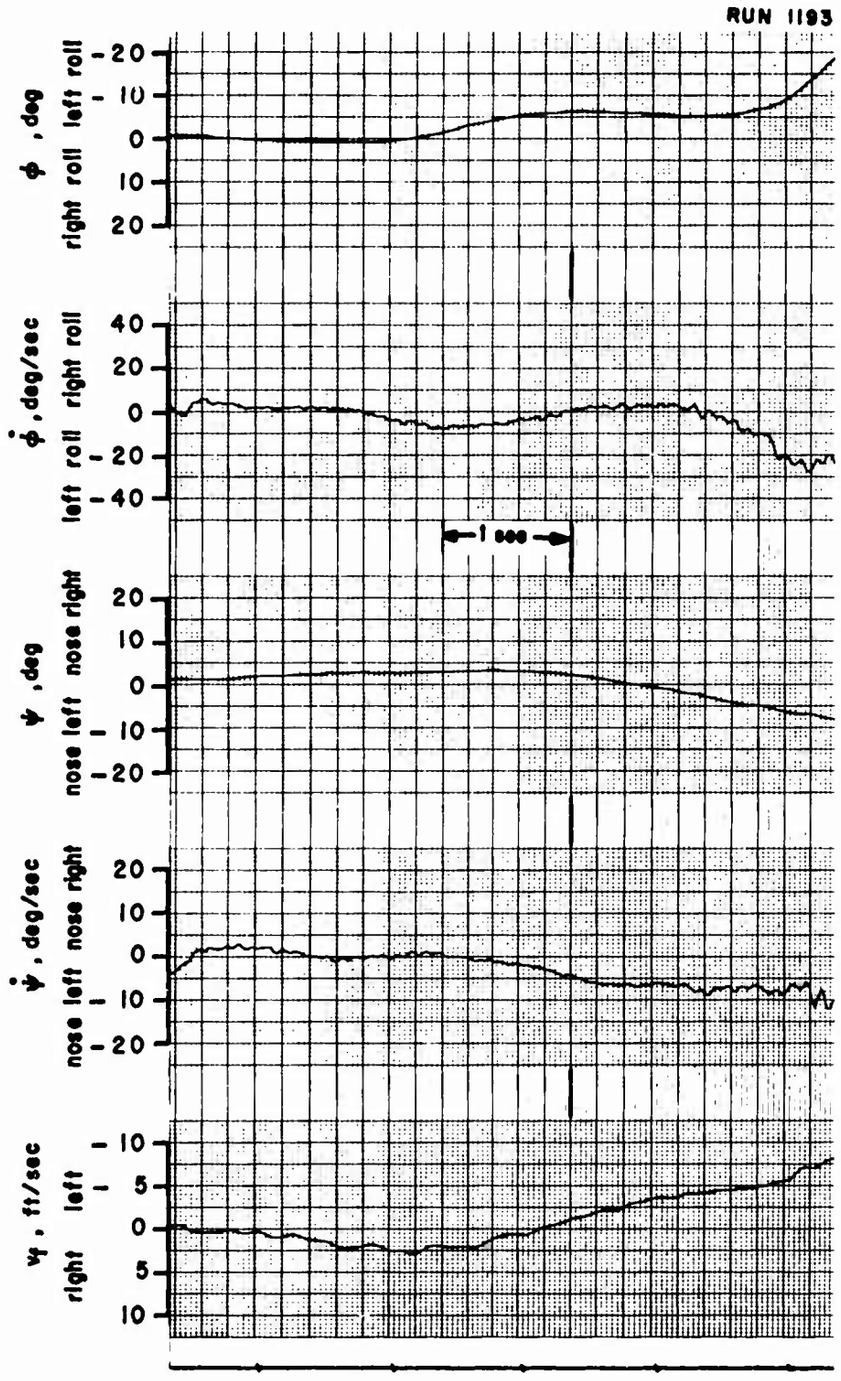

Figure 30. Lateral/Directional Transient Response. Three Degrees of Freedom, ϕ-Ψ-v_f. $i_d = 50°$, $U_{o_f} = 38$ ft/sec, $\theta_{.75R} = 24.8°$, rpm = 6780, $\Delta\beta_o = 2.5°$, Large Vertical Tail.

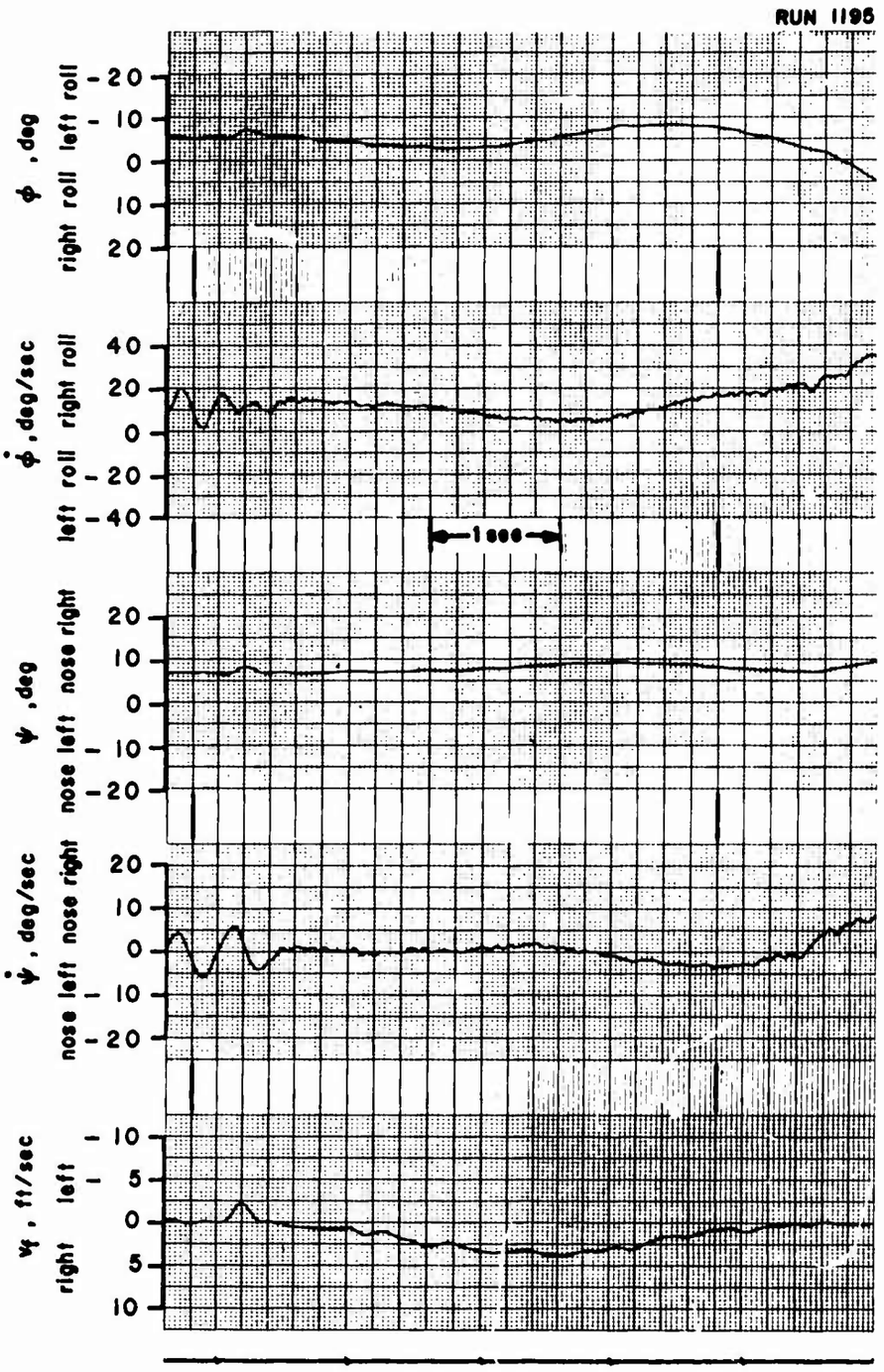

Figure 30. Lateral/Directional Transient Response. Three Degrees of Freedom, ϕ-Ψ-v_f. $i_d = 50°$, $U_{o_f} = 38$ ft/sec, $\beta_{.75R} = 24.8°$, rpm = 6780, $\Delta\beta_o = 2.5°$, Large Vertical Tail.

REFERENCES

1. Putman, W. F., Traybar, J. J., Curtiss, H. C., Jr., and Kukon, J. P., AN INVESTIGATION OF THE DYNAMIC STABILITY CHARACTERISTICS OF A QUAD CONFIGURATION, DUCTED-PROPELLER V/STOL MODEL, Princeton University; USAAVLABS Technical Report 68-49A, Phase I, Hovering Data Report, U. S. Army Aviation Materiel Laboratories, Fort Eustis, Virginia, September 1968.

2. Putman, W. F., Traybar, J. J., Curtiss, H. C., Jr., and Kukon, J. P., AN INVESTIGATION OF THE DYNAMIC STABILITY CHARACTERISTICS OF A QUAD CONFIGURATION, DUCTED-PROPELLER V/STOL MODEL, Phase II, Longitudinal Dynamics at High Duct Incidence Data Report, Princeton University; USAAVLABS Technical Report 68-49B, U. S. Army Aviation Materiel Laboratories, Fort Eustis, Virginia, August 1968.

3. Putman, W. F., SPECIFICATIONS FOR DESIGN OF A VARIABLE CONFIGURATION QUAD MODEL, Princeton University; Department of Aerospace and Mechanical Sciences Report 839, Princeton, New Jersey, October 1965.

4. Michaels, J. L., and Hesby, A. T., AERODYNAMIC STABILITY AND CONTROL AND FLYING QUALITIES, X-22A, Bell Aerosystems Company Report No. 2127-917003, Division of Bell Aerospace Corporation, Buffalo, New York, December 1962.

5. Curtiss, H. C., Jr., Putman, W. F., and Traybar, J. J., GENERAL DESCRIPTION OF THE PRINCETON DYNAMIC MODEL TRACK, Princeton University; USAAVLABS Technical Report 66-73, U. S. Army Aviation Materiel Laboratories, Fort Eustis, Virginia, November 1966, AD 645 883.

6. Boyden, Richmond P., and Curtiss, Howard C., Jr., INVESTIGATION OF THE LATERAL/DIRECTIONAL STABILITY CHARACTERISTICS OF A FOUR-PROPELLER TILT-WING VTOL MODEL, Princeton University; USAAVLABS Technical Report 68-19, U. S. Army Aviation Materiel Laboratories, Fort Eustis, Virginia, April 1968, AD 673 147.

7. Seckel, Edward, STABILITY AND CONTROL OF AIRPLANES AND HELICOPTERS, New York, Academic Press, 1964.

APPENDIX
EQUATIONS OF MOTION

Linearized equations of motion applicable to the analysis of various experimentally measured responses are presented in this appendix.

The lateral/directional equations of motion that describe the small perturbation motion of an aircraft from initially level flight are (Reference 7)

$$\begin{aligned} &\dot{v} - Y_v v + U_o r - g\phi - W_o p = 0 \\ &- L_v v - L_r r + \dot{p} - L_p p = 0 \\ &- N_v v + \dot{r} - N_r r - N_p p = 0 \end{aligned} \tag{1}$$

These equations are written with respect to principal axes, inclined nose down from the horizon by an angle η (Figure 4).

The gimbal mount supporting the model provides roll freedom about the principal body axis (X''), and yaw freedom about a space-fixed axis ($\bar{Z}_f$), as shown in Figure 31. It is not possible to provide body-axis freedom about the X'' and Z'' axes with a simple geometric linkage. For small disturbances from initially level flight, the difference between the equations of motion in principal axes (X'', Z'') and gimbal axes ($X'', \bar{Z}_f$) is of second order. Reference 6 may be consulted for further details. The relationships between the principal axis angular rates (p,r) and the gimbal axis rates ($\dot{\phi}, \dot{\Psi}$) are

$$\begin{aligned} p &= \dot{\phi} \\ r &= \dot{\Psi} \cos\phi \approx \dot{\Psi} \end{aligned} \tag{2}$$

It is convenient to transform the velocities to a space-fixed system to correspond to the manner in which the data are presented. The transformation equations for the linear velocities are, from Figure 32,

$$\begin{aligned} U &= U_f \cos\eta \cos\Psi + V_f \sin\Psi + W_f \sin\eta \cos\Psi \\ V &= -U_f (\cos\eta \sin\Psi \cos\phi + \sin\eta \sin\phi) \\ &\quad + V_f \cos\Psi \cos\phi + W_f (\cos\eta \sin\phi - \sin\eta \sin\Psi \cos\phi) \\ W &= U_f (\cos\eta \sin\Psi \sin\phi - \sin\eta \cos\phi) \\ &\quad - V_f (\cos\Psi \sin\phi) + W_f (\cos\eta \cos\phi + \sin\eta \sin\Psi \sin\phi) \end{aligned} \tag{3}$$

For small perturbations about a symmetrical level flight condition and neglecting second-order terms, these equations reduce to

$$U = U_f \cos \eta + w_f \sin \eta$$

$$v = - U_{o_f} [(\cos \eta)\, \psi + (\sin \eta)\, \phi] + v_f$$

$$W = - U_f \sin \eta + w_f \cos \eta \qquad (4)$$

Restricting the perturbation degrees of freedom to motions along the Y_f axis and about the X'' and $\bar{Z}_f$ axes (as considered in this report) and noting that U_{o_f} is finite, these expressions further reduce to

$$U = U_{o_f} \cos \eta = U_o$$

$$v = v_f - U_{o_f} [(\cos \eta)\, \psi + (\sin \eta)\, \phi]$$

$$W = - U_{o_f} \sin \eta = W_o \qquad (5)$$

Note that W_o is the same W_o that appears as the coefficient of p in the Y-force expression of equations (1).

Substituting the relations (2) and (5) into (1),

$$\dot{v}_f - Y_v v_f + Y_v U_{o_f} (\cos \eta)\, \psi - (g - Y_v U_{o_f} \sin \eta)\, \phi = 0$$

$$- L_v v_f - L_r \dot{\psi} + L_v U_{o_f} (\cos \eta)\, \psi + \ddot{\phi} - L_p \dot{\phi} + L_v U_{o_f} (\sin \eta)\, \phi = 0$$

$$- N_v v_f + \ddot{\psi} - N_r \dot{\psi} + N_v U_{o_f} (\cos \eta)\, \psi - N_p \dot{\phi} + N_v U_{o_f} (\sin \eta)\, \phi = 0 \qquad (6)$$

Because of certain features of the model and the apparatus, three modifications to these equations are necessary such that they will apply to all test conditions.

1. The linkage required to attach the model to the lateral servo carriage and mounting system used for this type of testing provides the lateral translational degree of freedom and contributes an additional mass m_ℓ that "flies" along with the model and, therefore, also must be accelerated by the model. The linkage is relatively small in weight compared to the "flying" weight of the model but nevertheless should be accounted for by additional mass terms in the equations of motion. If m_p is the

total mass of the model resting on the pivot axis, then the total accelerated mass in the lateral direction m_t is equal to $m_p + m_\ell$. This mass is larger than the trim vertical aerodynamic force on the model divided by the acceleration due to gravity. For analysis purposes the "flying" mass is considered to be the vertical aerodynamic force divided by the acceleration due to gravity. This value was set by the conditions of the longitudinal tests of Reference 2. This dynamic model-mount characteristic requires the modification of all terms in the side force equation, except the acceleration term, by a mass ratio defined as m/m_t and equal to 0.970 in value.

2. In certain of the test conditions as indicated in Table III, the center of gravity of the model was not located at the pivot axis of the model. Equations (6) may be considered to be written about the pivot axis of the model, which represents the full-scale center-of-gravity position about which the derivatives are determined. Additional terms are necessary in the equations of motion to account for the displacement of the model center of gravity. These are

$$\Delta L_{\dot{v}_{cg}} = + \frac{z_{cg}\, m_p}{I_x}$$

$$\Delta N_{\dot{v}_{cg}} = - \frac{x_{cg}\, m_p}{I_z}$$

$$\Delta L_{\phi_{cg}} = - \frac{W_p\, z_{cg}}{I_x} \qquad (7)$$

where m_p and W_p are the pivoting mass and pivoting weight of the model respectively.

3. Mechanical springs were added about the model roll axis and the model yaw axis to produce oscillatory motions in some single-degree-of-freedom tests. The following terms should be added for these tests:

$$\Delta L_{\phi_m} = - \frac{k_{\phi_m}}{I_x}$$

$$\Delta N_{\psi_m} = - \frac{k_{\psi_m}}{I_z} \qquad (8)$$

The values of the spring constants are given in Table III.

With these modifications, the equations of motion that apply to the experiments are

$$\dot{v}_f - \frac{m}{m_t} Y_v v_f + \frac{m}{m_t} Y_v U_{o_f} (\cos \eta) \Psi - \frac{m}{m_t} (g - Y_v U_{o_f} \sin \eta) \phi = 0$$

$$- \frac{z_{cg} m_p}{I_x} \dot{v}_f - L_v v_f - L_r \dot{\Psi} + L_v U_{o_f} (\cos \eta) \Psi + \ddot{\phi} - L_p \dot{\phi}$$

$$+ \left(\frac{k_{\phi_m}}{I_x} + L_v U_{o_f} \sin \eta + \frac{W_p z_{cg}}{I_x} \right) \phi = 0$$

$$\frac{x_{cg} m_p}{I_z} \dot{v}_f - N_v v_f + \ddot{\Psi} - N_r \dot{\Psi} + \left(N_v U_{o_f} \cos \eta + \frac{k_{\Psi_m}}{I_z} \right) \Psi$$

$$- N_p \dot{\phi} + N_v U_{o_f} (\sin \eta) \phi = 0 \qquad (9)$$

For the restricted degree-of-freedom tests, the following reduced sets of equations apply.

1. In two degrees of freedom, with $k_{\Psi_m} = k_{\phi_m} = 0$

   a. v_f, ϕ ($\Psi = 0$)

$$\dot{v}_f - \frac{m}{m_t} Y_v v_f - \frac{m}{m_t} (g - Y_v U_{o_f} \sin \eta) \phi = 0$$

$$- \frac{z_{cg} m_p}{I_x} \dot{v}_f - L_v v_f + \ddot{\phi} - L_p \dot{\phi} + \left(L_v U_{o_f} \sin \eta + \frac{W_p z_{cg}}{I_x} \right) \phi = 0 \qquad (10)$$

   b. ϕ, Ψ ($v_f = 0$)

$$- L_r \dot{\Psi} + L_v U_{o_f} (\cos \eta) \Psi + \ddot{\phi} - L_p \dot{\phi}$$

$$+ \left(L_v U_{o_f} \sin \eta + \frac{W_p z_{cg}}{I_x} \right) \phi = 0$$

$$\ddot{\Psi} - N_r \dot{\Psi} + N_v U_{o_f} (\cos \eta) \Psi - N_p \dot{\phi} + N_v U_{o_f} (\sin \eta) \phi = 0 \qquad (11)$$

2. In the single-degree-of-freedom experiments with mechanical springs, the equations of motion are

   a. ϕ ($\Psi = 0$, $v_f = 0$)

$$\ddot{\phi} - L_p \dot{\phi} + \left(\frac{k_{\phi_m}}{I_x} + L_v U_{o_f} \sin \eta + \frac{W_p z_{cg}}{I_x} \right) \phi = 0 \qquad (12)$$

   b. Ψ ($\phi = 0$, $v_f = 0$)

$$\ddot{\Psi} - N_r \dot{\Psi} + \left(N_v U_{o_f} \cos \eta + \frac{k_{\Psi_m}}{I_z} \right) \Psi = 0 \qquad (13)$$

3. In the single-degree-of-freedom tests without mechanical springs, the equation of motion is

   a. Ψ ($\phi = 0$, $v_f = 0$, $k_{\Psi_m} = 0$)

$$\ddot{\Psi} - N_r \dot{\Psi} + N_v U_{o_f} (\cos \eta) \Psi = 0 \qquad (14)$$

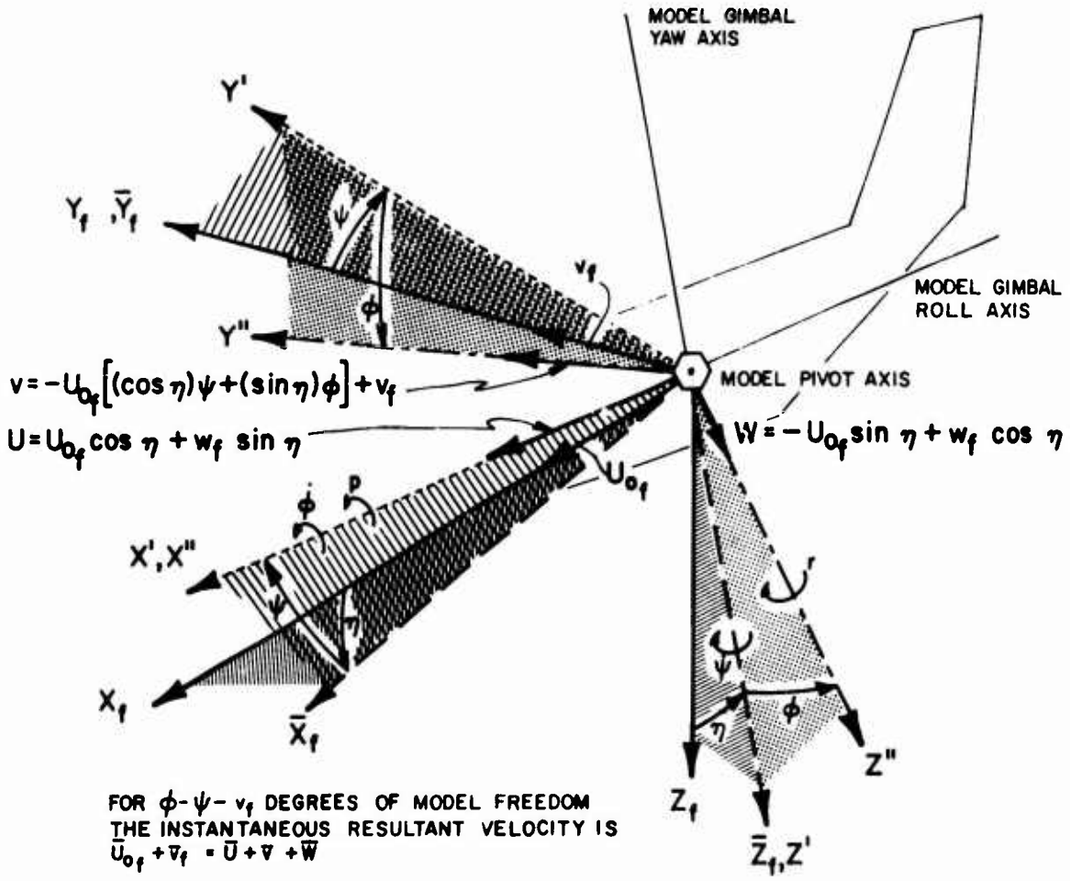

Notes:

$X_f - Y_f - Z_f$	are space fixed axes; $X_f - Y_f$ plane is horizontal.
$\bar{X}_f - \bar{Y}_f - \bar{Z}_f$	are space fixed axes, initially aligned with principal axis of vehicle.
$X'' - Y'' - Z''$	are principal axes of vehicle.
U, v and W	are for small perturbations about level symmetrical flight.

Figure 31. Model Axes Systems and Variables for Forward Flight Lateral/Directional Tests.

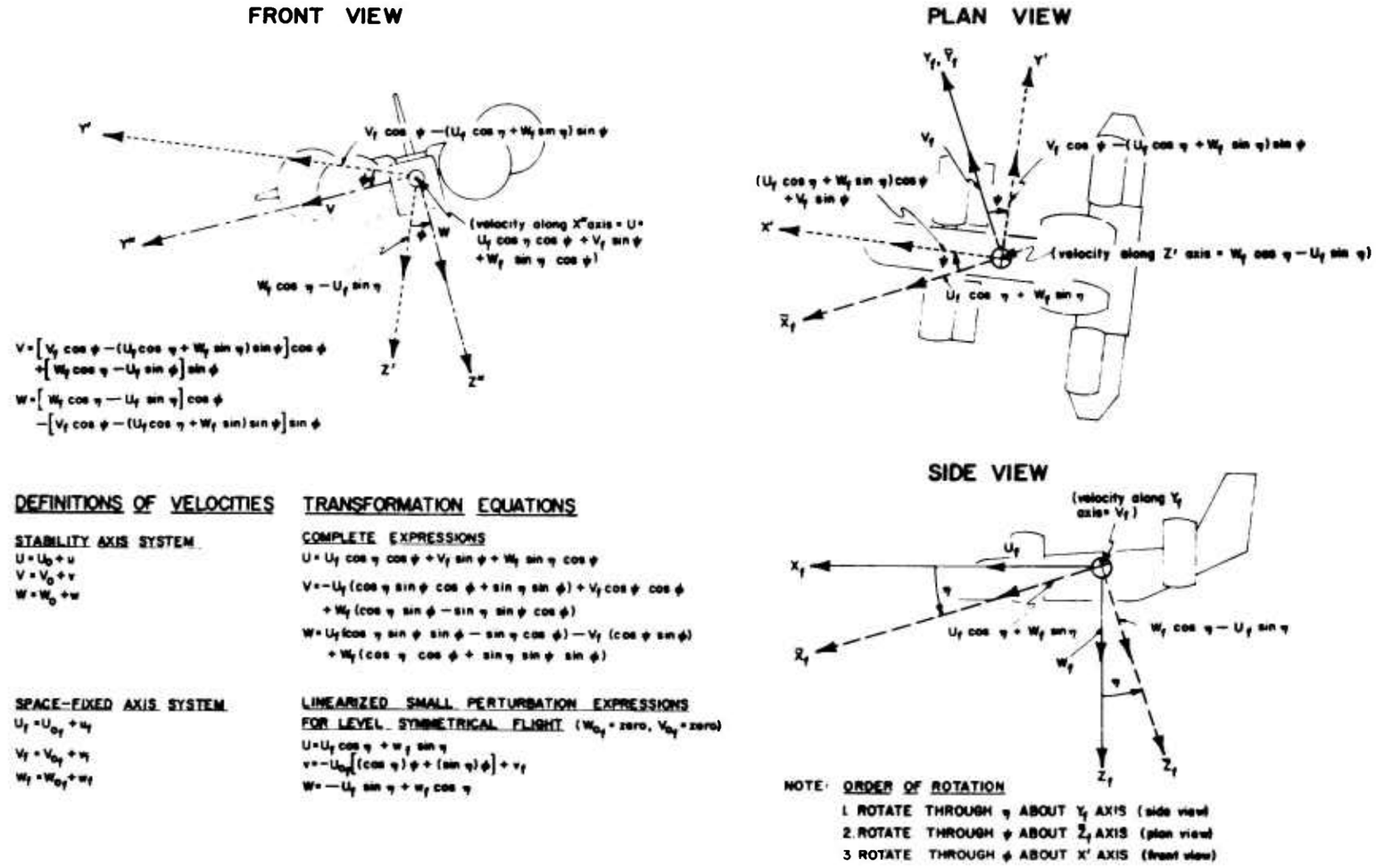

Figure 32. Transformation of Linear Velocities From Space-Fixed to Stability Axis System for Quad Model Gimbal Arrangement.

Unclassified

Security Classification

DOCUMENT CONTROL DATA - R & D

(Security classification of title, body of abstract and indexing annotation must be entered when the overall report is classified)

1. ORIGINATING ACTIVITY (Corporate author) Department of Aerospace and Mechanical Sciences Princeton University	2a. REPORT SECURITY CLASSIFICATION Unclassified 2b. GROUP -

3. REPORT TITLE

AN INVESTIGATION OF THE DYNAMIC STABILITY CHARACTERISTICS OF A QUAD CONFIGURATION, DUCTED-PROPELLER V/STOL MODEL
VOLUME III - PHASE III - LATERAL/DIRECTIONAL DYNAMICS AT HIGH DUCT INCIDENCES

4. DESCRIPTIVE NOTES (Type of report and inclusive dates)

Final Data Report

5. AUTHOR(S) (First name, middle initial, last name)

William F. Putman John P. Kukon
Joseph J. Traybar
Howard C. Curtiss, Jr.

6. REPORT DATE	7a. TOTAL NO. OF PAGES	7b. NO. OF REFS
November 1968	83	7

8a. CONTRACT OR GRANT NO.	9a. ORIGINATOR'S REPORT NUMBER(S)
DAAJ02-67-C-0025 b. PROJECT NO. 1F162204A14233 c. d.	USAAVLABS Technical Report 68-49C 9b. OTHER REPORT NO(S) (Any other numbers that may be assigned this report) Aerospace Sciences Report 847

10. DISTRIBUTION STATEMENT

This document has been approved for public release and sale; its distribution is unlimited.

11. SUPPLEMENTARY NOTES	12. SPONSORING MILITARY ACTIVITY
Volume III of a 4-volume report.	U.S. Army Aviation Materiel Laboratories Fort Eustis, Virginia

13. ABSTRACT

The results of experiments to determine the lateral/directional dynamic stability characteristics of a quad configuration, ducted-propeller V/STOL aircraft at four low-speed/high-duct-incidence trim conditions (i_d = 80°, 70°, 60°, and 50°,) are presented. Lateral/directional transient responses in various degrees of freedom were measured using a dynamic model on the Princeton Dynamic Model Track. The data presented include time histories of the model motions in various lateral/directional degrees of freedom that occur when the model is disturbed from trimmed flight.

The dynamic model employed in these experiments is a generalized research model arranged to represent closely the Bell X-22A V/STOL aircraft.

The data presented in this report comprise the third phase of a three-phase investigation of the dynamic stability characteristics of a quad configuration, ducted-propeller V/STOL aircraft at low speeds and high duct incidences. The other two phases pertain to the lateral and longitudinal hovering stability characteristics, presented in Reference 1, and the longitudinal characteristics at four low-speed/high-duct-incidence trim conditions presented in Reference 2.

DD FORM 1 NOV 68 1473 REPLACES DD FORM 1473, 1 JAN 64, WHICH IS OBSOLETE FOR ARMY USE.

Unclassified

Security Classification

14. KEY WORDS	LINK A		LINK B		LINK C	
	ROLE	WT	ROLE	WT	ROLE	WT
V/STOL Dynamics Stability Longitudinal Stability Transient Response Bell X-22A Hovering Characteristics Lateral Stability						